

Feature Article

Mechanisms of Foam Destruction by Oil-Based Antifoams

Nikolai D. Denkov

Laboratory of Chemical Physics & Engineering, Faculty of Chemistry, Sofia University,
1164 Sofia, Bulgaria

Received February 6, 2004. In Final Form: May 6, 2004

Oils and mixtures of oils with hydrophobic particles are widely used in various technologies and consumer products to control foaminess and foam stability. The aim of this review is to summarize our current understanding of the mechanisms of foam destruction by such substances, which are usually called antifoams or defoamers. The experimental results show that two types of antifoam can be distinguished (called for brevity “fast” and “slow”) which differ in the modes of their action. Fast antifoams are able to rupture the foam films at the early stages of film thinning. As a result, fast antifoams destroy completely the foam in less than a minute, in a typical foam-stability test. Microscopic observations have shown that the fast antifoams rupture the foam films by the so-called “bridging” mechanisms, which involve the formation of oil bridges between the two surfaces of the foam film. The stability/instability of these oil bridges is explained by using the theory of capillarity. In contrast, the oily globules of the slow antifoams are unable to enter the surfaces of the foam films and are first expelled into the Plateau borders (PBs). Only after being compressed by the narrowing walls of the PBs (due to water drainage from the foam), are the globules of the slow antifoams able to enter the solution surface and to destroy the adjacent foam films. Typically, the process of foam destruction by slow antifoams requires much longer time, minutes or tens of minutes, and a residual foam of well-defined height is observed in the foam tests. The experiments show that there is no direct relation between the magnitudes of the entry, E , spreading, S , and bridging, B , coefficients, on one side, and the antifoam efficiency, on the other side. The only requirement for having active antifoam, with respect to the bridging mechanisms, is that B should be positive. On the other hand, the barrier preventing the emergence of pre-emulsified antifoam globules on the solution surface (so-called “entry barrier”) is of crucial importance for the mode of foam destruction and for the antifoam efficiency. Measurements of the entry barrier with recently developed film trapping technique (FTT) showed that antifoams possessing low entry barriers act as fast antifoams, whereas high barriers correspond to slow or inactive antifoams, although E , S , and B coefficients could be strongly positive in the latter case. A good agreement between the magnitude of the entry barrier, measured by FTT, and the height of the residual foam, in the presence of slow antifoams, was experimentally established and theoretically explained. The importance of various factors, such as the size of antifoam globules, oil spreading, kinetics of surfactant adsorption, hydrophobicity of solid particles in mixed oil-solid antifoams, and the presence of amphiphilic additives (foam boosters), is discussed from the viewpoint of the mechanisms of antifoaming. The main experimental methods, used for studying the modes of antifoam action, are briefly described.

1. Introduction

1.1. Antifoams and Defoamers. Excessive foaming might create serious problems in many industrial processes. That is why various additives (usually called “antifoams” or “defoamers”) are widely used to reduce the volume of undesired foam in different technologies, such as pulp and paper production, food processing, textile dyeing, fermentation (e.g., in drug or food manufacturing), wastewater treatment, and oil industry.^{1–6} Antifoams are indispensable additives to various commercial prod-

ucts, like detergents for machine washing, paints, antidiarrhea and antiflatulence drugs.¹ Foam control is a very important factor in froth flotation of ores and other minerals, and the mechanisms of foam destruction in froth flotation are similar to those encountered in antifoam applications.¹

A typical antifoam or defoamer consists of oil, hydrophobic solid particles, or a mixture of both.^{1–7} Nonpolar oils (mineral oils, silicone oils) and polar oils (fatty alcohols and acids, alkylamines, alkylamides, tributyl phosphate, tioethers, and many others) have been successfully used. The solid particles could be inorganic (silica, Al_2O_3 , TiO_2), wax (e.g., Mg stearate), or polymeric (e.g., polyamide, polypropylene).¹

Following Wasan and Christiano,³ we term “antifoams” those substances which are predispersed in the foaming solution as solid particles, oil drops, or mixed oil–solid globules. Therefore, the main role of the antifoam is to prevent formation of excessive foam. A distinctive feature

(1) Garrett, P. R. The mode of action of antifoams. In *Defoaming: Theory and Industrial Applications*; Garrett, P. R., Ed.; Marcel Dekker: New York, 1993; Chapter 1.

(2) *Defoaming: Theory and Industrial Applications*; Garrett, P. R., Ed.; Marcel Dekker: New York, 1993.

(3) Wasan, D. T.; Christiano, S. P. Foams and Antifoams: A thin film approach. In *Handbook of Surface and Colloid Chemistry*; Birdi, K. S., Ed.; CRC Press: New York, 1997; Chapter 6.

(4) Kulkarni, R. D.; Goddard, E. D.; Chandar, P. Science and technology of silicone antifoams. In *Foams: Theory, Measurements and Applications*; Prud'homme, R. K., Khan, A., Eds.; Marcel Dekker: New York, 1996; Chapter 14.

(5) Ross, S.; Nishioka, G. Experimental researches on silicone antifoams. In *Emulsion, Latices, and Dispersions*; Becher, P., Yudenfreund, M. N., Eds.; Marcel Dekker: New York, 1978.

(6) Exerowa, D.; Kruglyakov, P. M. *Foams and Foam Films: Theory, Experiment, Application*; Elsevier: Amsterdam, 1998.

(7) Kralchevsky, P. A.; Nagayama, K. *Particles at Fluid Interfaces and Membranes*; Elsevier: Amsterdam, 2001; Chapter 14.

of antifoams is that their activity strongly depends on the so-called “entry barrier”, which indicates how difficult is for predispersed antifoam entities to pierce the air–water interface and to appear on a solution surface (see sections 2.3.2 and 6 below for a precise definition and discussion of entry barrier).

In contrast, defoamers are substances sprinkled over an already formed foam column, with the major aim to induce rapid foam collapse (“shock effect”). In this case, the entry barrier is less important, because the defoamer particles are introduced from the air phase and there is no barrier to prevent their emergence on the air–water interface. Note, however, that the foam destruction by defoamer is accompanied with its dispersal into the foaming solution. In this process, the defoamer is transformed into antifoam, and its further activity depends on the entry barrier of the dispersed globules.

1.2. Antifoam Compounds and Emulsions. It was found that mixtures of oil and hydrophobic solid particles (typically, 2–6 wt % solid) often have much higher antifoam efficiency, in comparison with each of the individual components (oil or solid particles) taken separately.^{1–6} Such mixtures of oil and particles are usually termed “antifoam compounds”. The reasons for the strong synergistic effect between oils and particles in compounds are discussed in section 5.4 below.

Many commercial antifoam compounds are sold in the form of oil-in-water emulsions, because the latter are more convenient for dosing during application. In many cases, emulsions are preferred, because the bulk compounds easily form a thick oily layer or large oily lenses on a solution surface. If such an oil layer or lenses are transferred onto the final product, this could compromise product quality (e.g., creation of oily spots on the paper in paper manufacturing). The fabrication of a stable antifoam emulsion is a serious technological challenge, because many factors that destabilize foams are known to destabilize emulsions as well. That is why only a few emulsifiers (such as PVA, and some nonsoluble surfactants, which make a shield of solid particles on the surface of the compound globules) have been found to stabilize efficiently the antifoam emulsions.

The optical observations show^{8–11} that two types of antifoam entities are usually present in the foaming solutions and play a role in foam destruction: (i) antifoam globules dispersed in the bulk, and (ii) lenses floating on solution surface, see Figure 1. Often, a layer of spread oil is present on the solution surface and could be also important for the antifoam action. The antifoam globules and lenses could destroy the foam by mechanisms explained in sections 3–5 below. For most of our consideration, there is no need to differentiate between the antifoam mechanisms of the dispersed globules and of the lenses, because an oil lens can be considered as an intermediate state between a dispersed antifoam globule and an oil bridge (which is the unstable configuration leading to foam film rupture, sections 3–5). Only on several occasions, we will distinguish explicitly between oil lenses

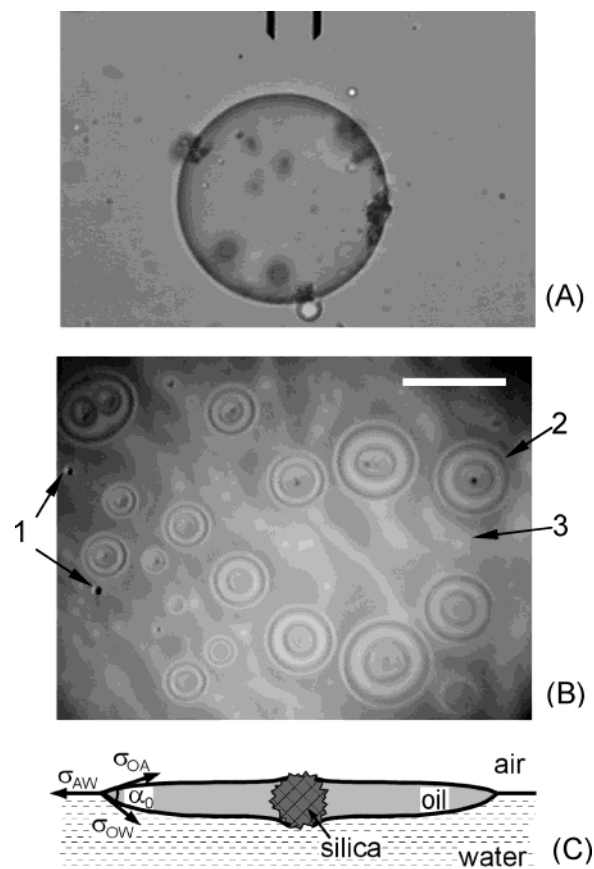


Figure 1. (A) Antifoam globule, containing silicone oil and silica particles (the dark objects of irregular shape, adsorbed on drop surface), as seen with an optical microscope in transmitted light, in the bulk surfactant solution. (B) Microscope image in reflected light of the surface of 10 mM AOT solution, containing 0.01 wt % silicone oil–silica emulsion: 1, antifoam globules, situated just below the solution surface; 2, flat oil lenses, floating on solution surface, most of these lenses contain silica agglomerates, seen as dark dots in the lens center; 3, bright areas between the lenses visualizing spread layer of silicone oil (bar 100 μm). (C) Schematic presentation of an oil lens on solution surface.

and dispersed globules. The role of the spread oil in foam destruction is different, and it is discussed in sections 6.4, 7.4, and 8.

In the case of antifoam emulsions, most of the antifoam is well predispersed in the foaming solution. Still, typically, there is some oil spread on the solution surface in coexistence with small oil lenses, but the amount of antifoam on the surface is usually a tiny fraction of the total antifoam dispersed in the solution.¹¹ In contrast, compounds are initially deposited on the solution surface as a big oily lens or as a thick spread layer. The dispersion of the compound is effected during agitation of the foaming solution and is greatly facilitated if the compound spreads well on the solution surface. If the compound is too viscous and/or does not spread well, its dispersion could be difficult and, as a result, its antifoam activity could be low.

The comparative studies of foam destruction by compounds and their emulsions showed^{8,9} that virtually the same mechanisms are operative for both types of antifoam. That is why, in the following consideration, we do not differentiate between a compound and its emulsion. Much more important, for the antifoam mechanisms and efficiency, is the difference between simple oils (free of solid particles) and compounds (oil–solid mixtures). The latter

(8) Denkov, N. D.; Tcholakova, S.; Marinova, K. G.; Christov, N.; Vankova, N.; Deruelle, M. Mechanisms and kinetics of exhaustion of mixed oil–silica antifoams. In preparation.

(9) Denkov, N. D.; Cooper, P.; Martin, J.-Y. Mechanisms of action of mixed solid–liquid antifoams. 1. Dynamics of foam film rupture. *Langmuir* **1999**, *15*, 8514.

(10) Denkov, N. D. Mechanisms of action of mixed solid–liquid antifoams. 2. Stability of oil bridges in foam films. *Langmuir* **1999**, *15*, 8530.

(11) Denkov, N. D.; Marinova, K.; Hristova, H.; Hadjiiski, A.; Cooper, P. Mechanisms of action of mixed solid–liquid antifoams. 3. Exhaustion and reactivation. *Langmuir* **2000**, *16*, 2515.

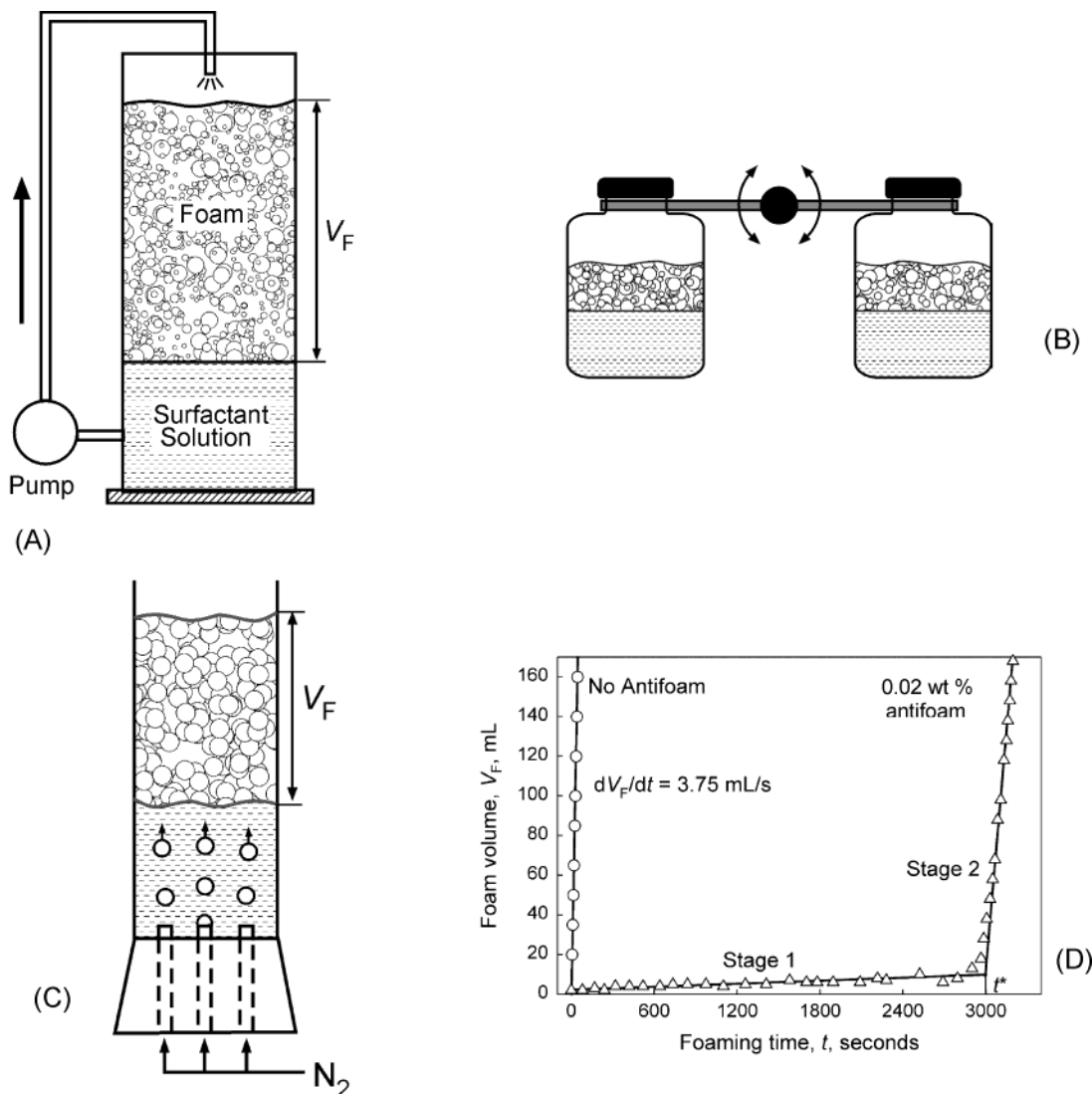


Figure 2. Schematic presentation of several foam tests, which are used for evaluation of antifoam efficiency: (A) Ross–Miles test; (B) automated shake test; (C) foam rise (bubbling) method. (D) Typical result from the foam rise method with 10 mM AOT solution, containing 0.02 wt % silicone oil–silica compound (fast antifoam).

two types of antifoam will be consistently compared throughout the paper. The same comparative studies^{8,9} showed that, usually, the emulsions are less efficient than the respective compounds at equivalent other conditions. This difference is naturally reflected in the recommendations for the typical antifoam concentration in practical applications. For example, in detergency, the typical concentration range for emulsions is about an order of magnitude higher (0.1–1 wt %), as compared to the respective compounds (0.01–0.1 wt %). Some of the reasons for this undesirable loss of antifoam efficiency, in the process of emulsion fabrication, are briefly discussed in section 5.5.

1.3. Antifoam Activity, Durability, and Efficiency.

In the current review we use several terms to characterize different aspects of the antifoam performance. The term *antifoam activity* characterizes the antifoam ability to prevent foam generation (during agitation) and/or the antifoam ability to destroy rapidly foam that is already generated (i.e., after stopping the agitation). Thus higher antifoam activity means less generated foam and/or faster foam destruction. *Antifoam exhaustion* is a process in which the antifoam loses its activity in the course of foam

destruction.^{3,8,11,12} The related term *antifoam durability* characterizes the antifoam ability to destroy a certain total amount of foam, before the antifoam activity is lost. More durable antifoams are able to destroy a larger total amount of foam or to maintain the instantaneous foam volume below a specified value (at given foam generation rate) for a longer time, before getting exhausted. The term *antifoam efficiency* is used throughout this review to characterize the antifoam performance in a vague, qualitative sense, with respect to both antifoam activity and durability.

The meaning of these terms is illustrated in Figure 2D with an example of foam evolution, in the presence of silicone oil–silica compound.¹² In the used Foam-Rise method, a controlled flux of nitrogen gas is blown through glass capillaries into 10 mM AOT solution, and the foam volume, V_F , is monitored as a function of time, t (see Figure 2C and section 2.1.4 for the used foam test). As seen from Figure 2D, the increase of foam volume is very fast in the absence of antifoam; in this experiment $dV_F/dt = 3.75$ mL/s, and 200 mL of the test cylinder is filled with foam

(12) Denkov, N. D.; Marinova, K.; Tcholakova, S.; Deruelle, M. Mechanism of foam destruction by emulsions of PDMS-silica mixtures. In *Proceedings 3rd World Congress on Emulsions*, 24–27 September, 2002, Lyon, France; paper 1-D-199.

for about 50 s. In contrast, when 0.02 wt % of oil–silica compound was predispersed in the foaming solution, the foam volume remained below 10 mL for about 3000 s (at the same foam generation rate), as a result of the rapid rupture of the foam bubbles by the antifoam. Note that the antifoam activity, which is related in this test to the instantaneous value of the foam volume,^{8,12} gradually decreases in the process of foam destruction, which is evidenced by the steady (though rather slow) increase of the foam volume during stage 1 in Figure 2D. After stage 1, whose duration is proportional to antifoam concentration,^{8,12} a sudden, almost complete loss of the antifoam activity is observed—see the rapid foam growth during stage 2 in Figure 2D. The sharp break in the curve $V_F(t)$, denoted by $t^* \approx 3000$ s, indicates the moment of antifoam exhaustion, when the process of bubble destruction becomes too slow to compensate for the bubble generation and, as a result, V_F starts increasing very rapidly with time. The total volume of the foam, destroyed before antifoam exhaustion, normalized by the amount of used antifoam (562 L/g in this particular experiment), is one possible measure of the antifoam durability.^{8,12}

Note that the appropriate quantitative characteristics of antifoam activity and durability (defoaming time, foam volume, etc.) depend on the foam test used. Furthermore, different characteristics might be more appropriate for fast and slow antifoams—see section 2.1.5 below for a further explanation.

1.4. Aim of the Current Review. The choice of particular oil or an oil–solid compound for a given application is still based on several semiempirical rules and “trial and error” methods, mainly because the actual mechanisms, by which the oil-based antifoams destroy foams, have remained obscure. As summarized by Garrett¹ in his landmark review on the various modes of antifoam action, “It is a feature of this subject that the mechanisms [proposed in the literature], although plausible, are often speculative. Thus unequivocal experimental evidence is often lacking ... In the main, all of this derives from the extreme complexity of the relevant phenomena.”

To a large extent, the above diagnosis¹ is still valid, though noticeable progress has been achieved during the past decade after Garrett’s review has appeared. Part of this progress has been summarized in more recent reviews by Wasan and Christiano,³ Exerowa and Kruglyakov,⁶ and Kralchevsky and Nagayama.⁷ During the last several years, new results were obtained in our Laboratory, which further clarified the previous concepts and suggested some new explanations of the studied phenomena. These results have been published in more than 15 original papers,^{9–25} which contain many experimental details (needed to prove

or reject certain hypotheses), so it is certainly difficult for a reader to grasp at a glance the relationships between various studies.

The current presentation is aimed to complement the aforementioned reviews^{1,3,6,7} by describing in a concise, coherent manner the main results obtained by our group in relation to the mechanisms of foam destruction by oil-based antifoams. Recent papers from several other research groups are also reviewed in the context of the mechanisms of antifoam action. The links between our conclusions and the results of the other authors are traced whenever possible. In addition, many important and still unresolved issues are highlighted throughout the text.

In the current review we consider mainly the mechanisms of foam destruction and the role of various factors affecting antifoam activity. A detailed discussion of the related process of antifoam exhaustion will be presented in a separate study.⁸

To make the paper easier for reading, several abbreviations are used throughout the text—an explanatory list is presented at the end of the paper, along with the notation used.

1.5. A Bridging–Dewetting Mechanism of Foam Film Rupture by Solid Particles. At the end of the Introduction, we briefly outline the mechanism considered in the literature as responsible for the foam destruction by solid particles.^{1,26–35} Some of the concepts introduced here are used in the subsequent consideration of oil-based antifoams.

The foam breaking efficiency of solid particles is mainly determined by their hydrophobicity, quantified by the value of the three-phase contact angle solid–water–air, α_{SA} . It was shown experimentally and theoretically that hydrophobic particles can rupture the foam films by the

(13) Basheva, E. S.; Ganchev, D.; Denkov, N. D.; Kasuga, K.; Satoh, N.; Tsujii, K. Role of betaine as foam booster in the presence of silicone oil drops. *Langmuir* **2000**, *16*, 1000.

(14) Basheva, E. S.; Stoyanov, S.; Denkov, N. D.; Kasuga, K.; Satoh, N.; Tsujii, K. Foam boosting by amphiphilic molecules in the presence of silicone oil. *Langmuir* **2001**, *17*, 969.

(15) Marinova, K. G.; Denkov, N. D. Foam destruction by mixed solid–liquid antifoams in solutions of alkyl glucoside: Electrostatic interactions and dynamic effects. *Langmuir* **2001**, *17*, 2426.

(16) Arnaudov, L.; Denkov, N. D.; Surcheva, I.; Durbut, P.; Broze, G.; Mehreteab, A. Effect of oily additives on the foamability and foam stability. 1. Role of interfacial properties. *Langmuir* **2001**, *17*, 6999.

(17) Hadjiiski, A.; Tcholakova, S.; Denkov, N. D.; Durbut, P.; Broze, G.; Mehreteab, A. Effect of oily additives on the foamability and foam stability. 2. Entry barriers. *Langmuir* **2001**, *17*, 7011.

(18) Marinova, K. G.; Denkov, N. D.; Branlard, P.; Giraud, Y.; Deruelle, M. Optimal hydrophobicity of silica in mixed oil–silica antifoams. *Langmuir* **2002**, *18*, 3399.

(19) Marinova, K. G.; Denkov, N. D.; Tcholakova, S.; Deruelle, M. Model studies of the effect of silica hydrophobicity on the efficiency of mixed oil–silica antifoams. *Langmuir* **2002**, *18*, 8761.

(20) Denkov, N. D.; Tcholakova, S.; Marinova, K. G.; Hadjiiski, A. Role of oil spreading for the efficiency of mixed oil–solid antifoams. *Langmuir* **2002**, *18*, 5810.

(21) Denkov, N. D.; Marinova, K. G. Antifoaming action of oils. In *Proceedings 3rd Eurofoam Conference*, June, 2000, Delft, The Netherlands; Verlag MIT Publishing: Bremen, 2000; p 199.

(22) Hadjiiski, A.; Denkov, N. D.; Tcholakova, S.; Ivanov, I. B. Role of entry barriers in the foam destruction by oil drops. In *Adsorption and Aggregation of Surfactants in Solution*; Mittal, K., Shah, D., Eds.; Marcel Dekker: New York, 2002; Chapter 23, p 465.

(23) Marinova, K. G.; Tcholakova, S.; Denkov, N. D.; Roussev, S.; Deruelle, M. Model studies on the mechanism of deactivation (exhaustion) of mixed oil–silica antifoams. *Langmuir* **2003**, *19*, 3084.

(24) Kralchevsky, P. A.; Danov, K. D.; Denkov, N. D. Chemical physics of colloid systems and interfaces. In *Handbook of Surface and Colloid Chemistry*; Second Expanded and Updated Edition; Birdi, K. S., Ed.; CRC Press: New York, 2002; Chapter 5.

(25) Christova, D.; Marinova, K. G.; Denkov, N. D.; Deruelle, M. Hydrophobization of glass surface by silicone oils. In preparation.

(26) Roberts, K.; Axberg, C.; Österlund, R. The effect of spontaneous emulsification of defoamer on foam prevention. *J. Colloid Interface Sci.* **1977**, *62*, 264.

(27) Garrett, P. R. Preliminary considerations concerning the stability of a liquid heterogeneity in a plane-parallel liquid film. *J. Colloid Interface Sci.* **1980**, *76*, 587.

(28) Dippenaar, A. The destabilization of froth by solids. I. The mechanism of film rupture. *Int. J. Mineral Process.* **1982**, *9*, 1.

(29) Garrett, P. R.; Davis, J.; Rendall, H. M. An experimental study of the antifoam behaviour of mixtures of a hydrocarbon oil and hydrophobic particles. *Colloids Surfaces, A* **1994**, *85*, 159.

(30) Aveyard, R.; Cooper, P.; Fletcher, P. D.; Rutherford, C. E. Foam breakdown by hydrophobic particles and nonpolar oil. *Langmuir* **1993**, *9*, 604.

(31) Aveyard, R.; Binks, B. P.; Fletcher, P. D. I.; Peck, T. G.; Rutherford, C. E. Aspects of aqueous foam stability in the presence of hydrocarbon oils and solid particles. *Adv. Colloid Interface Sci.* **1994**, *48*, 93.

(32) Aveyard, R.; Clint, J. H. Liquid droplets and solid particles at surfactant solution interfaces. *J. Chem. Soc., Faraday Trans.* **1995**, *91*, 2681.

(33) Aveyard, R.; Beake, B. D.; Clint, J. H. Wettability of spherical particles at liquid surfaces. *J. Chem. Soc., Faraday Trans.* **1996**, *92*, 4271.

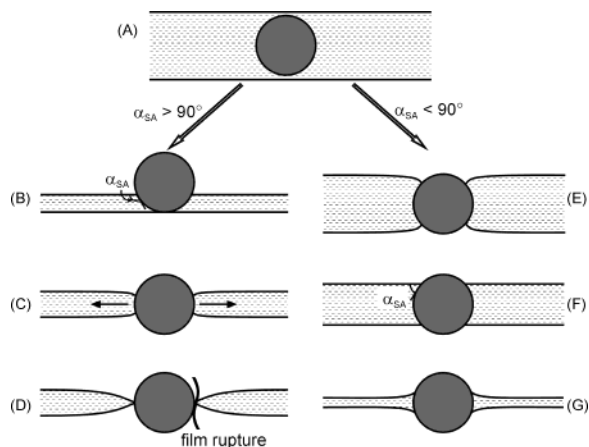


Figure 3. Schematic presentation of the bridging of foam film surfaces by a spherical solid particle. When the particle is sufficiently hydrophobic ($\alpha_{SA} > 90^\circ$), it is dewetted by the liquid and the three-phase contact lines eventually come in direct contact with each other—the foam film gets perforated at the particle surface (B–D). If the contact angle $\alpha_{SA} < 90^\circ$, the particle is not dewetted and the foam film remains stable (E–G).

so-called “bridging–dewetting” mechanism.^{1,26–35} This mechanism implies that, first, the solid particle comes in contact with the two opposite surfaces of the foam film, forming a “solid bridge” between them; see Figure 3. If the particle is sufficiently hydrophobic (α_{SA} is larger than a certain critical value), it is dewetted by the liquid and the three-phase contact lines eventually come in direct contact with each other—the foam film gets perforated at the particle surface.

Various theoretical and experimental studies^{1,27,28,30–35} showed that the critical contact angle is 90° for complete dewetting of solid particles, which have smooth convex surface, such as spheres, ellipsoids, disks, and rods. Particles of contact angle $\alpha_{SA} > 90^\circ$ induce foam film rupture and foam collapse. Less hydrophobic smooth particles ($\alpha_{SA} < 90^\circ$) do not cause foam film rupture—they can even stabilize the foam by blocking the Plateau channels and reducing the rate of water drainage from the foam. Interestingly, some experiments showed that foam film rupture can be induced by less hydrophobic particles (α_{SA} well below 90°) if the latter have sharp edges and are properly oriented in the foam film.^{1,28} Theoretical analysis of the role of shape, size, and contact angle of solid particles, for their antifoam activity, was presented by Garrett,¹ Frye and Berg,^{35,36} and Aveyard et al.^{30–34}

One should note that, in detergency and many other applications (where “strong”, i.e., very active surfactants of concentration above the cmc, are typically used), the solid particles are inefficient foam breakers—the surfactant molecules adsorb on particle surface and render it too hydrophilic for having a pronounced antifoam effect.^{30–34} That is why the antifoam effect of solid particles is of interest mainly in relation to froth flotation, in which no “strong” surfactants are used. In the presence of strong surfactants, oil-based compounds and their emulsions are much more efficient foam breakers and have found a wide application in practice.^{1,3,31,34}

(34) Aveyard, R.; Binks, B. P.; Clint, J. H.; Fletcher, P. D. I. Foams and emulsions: Their stability and breakdown by solid particles and liquid droplets. The colloid chemistry of a dog's breakfast. In *Foams and Emulsions*; Sadoc J. F., Rivier, N., Eds.; Kluwer Academic Publishers: Dordrecht, 1999; Chapter 2.

(35) Frye, G. C.; Berg, J. C. Antifoam action by solid particles. *J. Colloid Interface Sci.* **1989**, *127*, 222.

(36) Frye, G. C.; Berg, J. C. Mechanisms for the synergistic antifoam action by hydrophobic solid particles in insoluble liquids. *J. Colloid Interface Sci.* **1989**, *130*, 54.

2. Main Experimental Methods Used To Study the Mechanisms of Antifoaming

2.1. Foam Tests. Four types of foam tests are mainly used to characterize antifoam activity and durability. The particular experimental conditions differ in the various laboratories. Below, we briefly describe these tests, as used in our studies to obtain the results presented in the current review.^{8–25} Other methods are sometimes used, depending on the particular application (see, e.g., refs 3–6, 31, and 37).

2.1.1. Ross–Miles Test (Figure 2A). This test is widely used in research and application laboratories for characterization of (1) foamability of surfactant solutions and (2) foam stability in the presence of antifoams. In our experiments, a certain amount of antifoam (typically between 0.01 and 0.1 wt %, depending on antifoam activity) was pre-emulsified in 300 mL of surfactant solution by stirring for 10 min on a magnetic stirrer. The obtained emulsion was additionally homogenized by several hand-shakes before placing it into the glass cylinder of the Ross–Miles test (volume 1 L, internal diameter 37 mm). The solution was circulated for 20 s, with a flux of 125 mL/s, through an orifice (7 mm diameter), which was placed at 23 cm above the level of the liquid. The initial foam volume (after stopping the circulation) is a measure of solution foaminess. The further change of the foam volume with time, $V_F(t)$, characterizes the foam stability. The accuracy in the foam volume determination is ± 2 mL (determined mainly by the irregular upper boundary of the foam), whereas the reproducibility in separate experiments is typically ± 5 mL. From the internal diameter of the cylinder one can easily calculate the conversion factor from the foam volume to foam height (10.75 mL per 1 cm) and vice versa.

The method can be equally well applied for studying antifoams (predispersed in the foaming solution) and defoamers (added on the top of a preformed foam column). In the second case, the antifoam can rapidly destroy preaccumulated voluminous foam (shock effect). The method is rather convenient for studying the activity and durability of both fast and slow antifoams.

When fast antifoams are studied, the Ross–Miles method is often run in continuous mode—the solution is continuously circulated and the time evolution of the upper boundary of the foam is monitored. From research viewpoint, a disadvantage of this continuous mode of operation is that one cannot separate the effect of antifoam on solution foaminess from the effect on foam stability.

2.1.2. Bartsch Method. In this simple and useful method, the foam is produced by 10 hand-shakes of a 300 mL glass cylinder, containing 100 mL of surfactant solution and antifoam. The initial foam volume and the further evolution of the foam with time are used to characterize the foaminess and foam stability, respectively. Since the lower boundary of the foam column is often diffuse (especially soon after stopping the cylinder shaking), it is more convenient to measure only the position of the upper foam boundary, which is well-defined. Then, one can subtract the volume of the surfactant solution from the total volume (solution plus air bubbles) to calculate the volume of trapped air with a very good precision.

By this method one can study both fast and slow antifoams. It is convenient also for studying the defoamer activity—in this case, the defoamer is introduced (spread or sprinkled) at the top of a preformed foam column.

(37) Tsuge, H.; Ushida, J.; Hibino, S.-I. Measurement of film-breaking ability of antifoaming agents. *J. Colloid Interface Sci.* **1984**, *100*, 175.

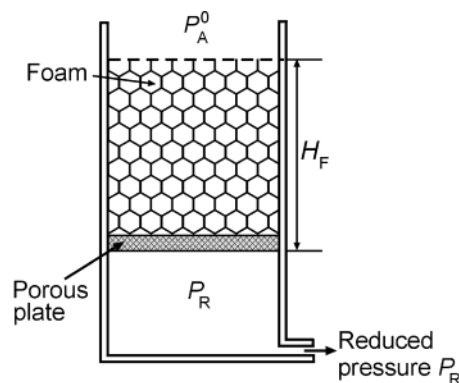
2.1.3. Automated Shake Test, AST (Figure 2B). This method is convenient for studying the activity and durability of fast antifoams. Briefly, 100 mL of foaming solution is placed in a standard 250 mL glass bottle and a certain amount of antifoam (typically 0.01 vol. %) is introduced into this sample. The bottle is then mechanically agitated in a series of consecutive shake cycles. After each cycle of agitation for 10 s, the solution remains quiescent for another 60 s, and the defoaming time, t_D , is measured (defined as the time for appearance of a clean water–air interface, not covered with bubbles). Shorter defoaming time (taken as an average from the first three to five cycles) corresponds to higher antifoam activity and vice versa. These cycles are repeated until t_D exceeds 60 s, which is considered as the moment of antifoam exhaustion. The number of cycles before exhaustion is a measure of antifoam durability. The method can be fully automated.³⁸

2.1.4. Foam-Rise Method (also Called “Bikerman Test” or “Bubbling Method”, Figure 2C). In this method, the foam is generated by blowing gas through an array of capillaries or through porous glass. The method is particularly appropriate for research purposes, because the size of the bubbles (which could be very monodisperse, if capillaries of equal diameter are used) and the foam generation rate can be controlled and are exactly known. This allows the researcher to compare quantitatively the activity and durability of various antifoams.^{8,12} It can be used for studying both fast antifoams ($V_F(t)$ is monitored under continuous bubbling) and slow antifoams ($V_F(t)$ is monitored after stopping bubble generation).

In our experiments for studying antifoam durability,^{8,12} 100 mL of surfactant solution is poured in a 500 mL glass cylinder of 37 mm internal diameter. A bunch of glass capillaries (27, internal diameter 0.13 mm) is mounted at the bottom of the cylinder. The bubbles are generated by blowing nitrogen, at constant flow rate, through these capillaries. The foam volume is measured as a function of time in the absence of antifoam (to determine the foam generation rate) and in the presence of antifoam (to determine the antifoam activity and durability, see Figure 2D). The bubble size is determined in the experiments without antifoam by using optical microscopy.⁸

Another method, developed by Kruglyakov, Exerowa, and Khristov^{6,39,40} for studying foam stability, Figure 4, could be useful for comparing the activity of slow antifoams. In this method, the aqueous phase is forcibly sucked out from a foam column, by using a semipermeable membrane. The foam stability is evaluated by measuring the pressure leading to foam collapse, which is expected to be lower in the presence of antifoam. To the best of our knowledge, this method has not been used so far for studying the antifoam effect.

2.1.5. Measures of Foam Stability in the Presence of Antifoam. Different measures of foam stability are used in the literature to characterize antifoam activity. We briefly define some of these measures here, because qualitatively different, and even opposite conclusions, can be sometimes drawn from the same results if different measures are used—an illustrative example is given by the end of section 4.4 below. The appropriate choice of



$$\text{Capillary pressure } P_C^{PB} = P_A^0 - P_R + \rho g H_F$$

Figure 4. Schematic presentation of the setup developed by Khristov et al.^{39,40} for studying foam stability.

measures depends on several factors, such as the foam test used, the rate of foam destruction, which might vary many orders of magnitude for different antifoams, and the time-scale of interest, which is usually determined by the particular application behind the antifoam study.

The antifoam effect on *foamability* is usually characterized by the ratio of the foam volumes produced in the presence and in the absence of antifoam, under fixed conditions, e.g., after certain duration of solution circulation in the Ross–Miles test or after a certain number of shakes in the Bartsch method.^{14,16,30,31,35,36} The result can strongly depend on the particular experimental conditions: antifoam concentration (section 4.1 and ref 16), size of the predispersed antifoam globules (section 4.3 and ref 13), duration and intensity of agitation,¹³ and foam test used. That is why experiments at several different conditions might be performed to draw more reliable conclusions.

The most widely used measures for *foam stability* fall into two groups: (1) characteristic times and (2) foam volumes. Most often, the time for reducing the initially produced foam by half (the so-called “half-time”), $t_{1/2}$, is used.^{3,6,31} This characteristic time is equally well applied to both fast and slow antifoams (see sections 3–5 for definition and discussion of these different types of antifoam). Another characteristic time often used for fast antifoams is the so-called “defoaming time”, t_D , which corresponds to the appearance of solution surface, free of bubbles, in the foam test after agitation.^{9,11,38} Note that t_D is inappropriate for characterization of slow antifoams, because long-standing residual foam remains in the latter case (section 4.1, Figures 12 and 14). In ref 14, the time for beginning of the foam destruction process, t_{ON} , was discussed for slow antifoams, because the ratio between t_{ON} and the time scale of the experiment/application determines whether the foamability or the foam stability is more important (section 4.4). Note that t_{ON} cannot be measured for fast antifoams, because there is no period of stable foam, as is often the case with slow antifoams (cf. the results from the foam tests shown in Figures 12 and 14 with those in Figure 43).

Alternatively, the antifoam effect on foam stability can be characterized by the ratio of the foam volume after a certain time and the initial foam volume, $V_F(t)/V_F(0)$.^{1,13,14,16,29} Note that $V_F(0)$ can be taken for solution with or without antifoam, and the results might be very different between these two cases if the antifoam affects strongly the solution foamability (which is often the case). If $V_F(0)$ is taken for solution *without* antifoam, then the ratio $V_F(t)/V_F(0)$ evaluates the antifoam effect on both

(38) Pouchelon, A.; Araud, C. Silicone defoamers: The performance, but how do they act. *J. Dispersion Sci. Technol.* **1993**, *14*, 447.

(39) Khristov, K. I.; Exerowa, D. R.; Kruglyakov, P. Determination of foam stability at constant pressure in the Plateau–Gibbs borders of the foam. *J. Colloid Interface Sci.* **1981**, *79*, 584.

(40) Khristov, K. I.; Exerowa, D. R.; Minkov, G. Critical capillary pressure for destruction of single foam films and foam: effect of foam film size. *Colloids Surf., A* **2002**, *210*, 159.

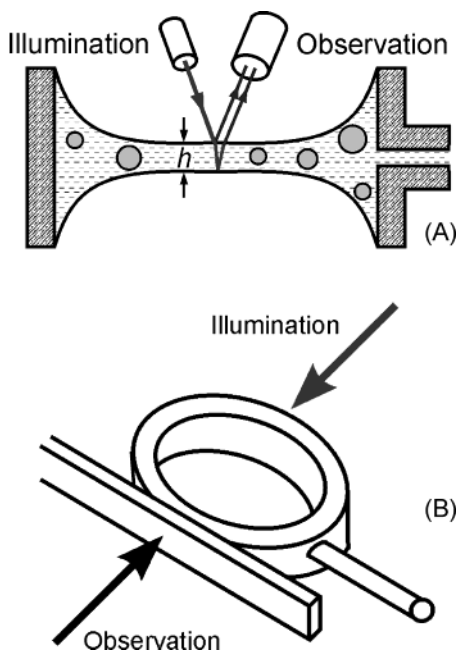


Figure 5. Sketch of the cells used for observation of thin aqueous films with antifoam particles in reflected (A) and in transmitted (B) light.

foamability and foam stability. In contrast, if $V_F(0)$ is for solution *with* antifoam, then this ratio characterizes the antifoam effect on foam stability only. The choice of the appropriate time, t , for constructing these ratios is very important, because qualitatively different results can be obtained for the same system at $t \leq t_{ON}$ and at $t \geq t_{ON}$. For slow antifoams, the dependence $V_F(t)$ is better determined with still foams. For fast antifoams, $V_F(t)$ is better determined during continuous foam generation (circulation in the Ross–Miles test or bubbling in the foam rise method).⁴

Other measures of antifoam activity, which might be more appropriate in detailed antifoam studies, can be found in refs 4, 6, 8, and 12.

2.2. Methods for Studying Single Foam Films and Plateau Channels. **2.2.1. Microscopic Foam Films in a Capillary Cell.** This method was proposed by Scheludko and Exerowa^{41,42} and has been widely used^{6,41–48} for studying the stability of foam films and the rate of film thinning. A foam film is formed from a biconcave drop, placed in a short capillary (2.5 mm i.d., 4 mm height in our experiments), by sucking out liquid through a side orifice; see Figure 5A. The film is illuminated and observed in monochromatic reflected light. The interference of the light, reflected from the upper and lower surfaces of the foam film, leads to appearance of dark and bright interference fringes, each of them corresponding to a certain film thickness (similarly to the contours in

topographic map). The difference, Δh , in the film thickness between two neighboring dark (or two neighboring bright) fringes is equal to⁴⁹

$$\Delta h = \lambda/2n \approx 203 \text{ nm} \quad (1)$$

where λ is the wavelength of the illuminating light (540 nm in our experiments) and n is the refractive index of the surfactant solution ($n \approx 1.33$ for not-very-concentrated solutions). One can easily distinguish changes in the film brightness of the order of $\Delta h/4$ (bright to gray, gray to dark, and so on). Therefore, changes in the film thickness of the order of 50 nm can be easily detected in this way, without the necessity of using special interferometric techniques. More refined procedures of light intensity detection can be used,^{41–47} if the film thickness has to be measured with high precision (usually not necessary in the antifoam studies, because the foam films rupture at relatively large thickness, $h \geq 1 \mu\text{m}$). The capillary is closed in an insulating box, with optically clean windows, to eliminate air convection and water evaporation from the film.

Technical details about the microscope requirements and about the light illumination and detection can be found in the original papers (e.g., refs 41–47). The method can be combined with a high-speed video camera, which allows the researcher to observe the entry of antifoam globules at the film surfaces, as well as the processes that precede the foam film rupture.⁹

A major advantage of the capillary cell is that experiments can be performed with actual antifoam substances, dispersed into micrometer-sized globules or lenses, just as in the case for practical antifoams.^{9,48} Thus, the films in the capillary cell closely mimic the behavior of relatively small films (diameter around 1 mm) in real foams.

In our experiments,^{9,11,13,15,22} we used this method mainly to (1) characterize the dynamics of foam film thinning by measuring the duration of the various stages of film thinning and the respective film thickness, (2) observe the process of entrapment of antifoam globules in the foam films, and (3) observe the entry of antifoam globules and the events preceding foam film rupture by a high-speed camera; see sections 4.2 and 5.1 below.

The capillary cell was used by Dippenaar²⁸ for observation of the process of foam film destruction by hydrophobic solid particles. However, instead of observing the foam film in reflected light, Dippenaar²⁸ observed the foam lamella and the solid particles in transmitted light, through the wall of the glass capillary; see Figure 5B. These experiments provided convincing proof for the bridging–dewetting mechanism of foam film rupture by solid particles. In addition, the effects of particle hydrophobicity and shape were studied.²⁸ In our experiments,⁹ we used the Dippenaar technique to observe the evolution of an oil bridge, formed when a drop of antifoam compound bridges the two opposite surfaces of a foam lamella, section 5.1. The main advantage of this method is that it allows one to directly observe the shape of the oil bridge. However, such observations are possible only when the bridge is rather large (dimensions above ca. 100 μm). Therefore, the conclusions, drawn from such observations, should be tested with other experimental methods, because the

(41) Scheludko, A.; Exerowa, D. Device for interferometric determination of the thickness of microscopic foam films. *Commun. Dep. Chem. (Bulg. Acad. Sci.)* **1959**, *7*, 123.

(42) Scheludko, A. Thin liquid films. *Adv. Colloid Interface Sci.* **1967**, *1*, 391.

(43) Kolarov, T.; Scheludko, A.; Exerowa, D. Contact angle between black film and bulk liquid. *Tans. Faraday Soc.* **1968**, *64*, 2864.

(44) Traykov, T. T.; Manev, E. D.; Ivanov, I. B. Hydrodynamics of thin liquid films. Experimental investigation of the effect of surfactants on the drainage of emulsion films. *Int. J. Multiphase Flow* **1977**, *3*, 485.

(45) Rao, A. A.; Wasan, D. T.; Manev, E. D. Foam stability—effect of surfactant composition on the drainage of microscopic aqueous films. *Chem. Eng. Commun.* **1982**, *15*, 63.

(46) Radoev, B. P.; Scheludko, A. D.; Manev, E. D. Critical thickness of thin liquid films: Theory and experiment. *J. Colloid Interface Sci.* **1983**, *95*, 254.

(47) Nikolov, A. D.; Wasan, D. T.; Kralchevsky, P. A.; Ivanov, I. B. Ordered micelle structuring in thin films formed from anionic surfactant solutions. *J. Colloid Interface Sci.* **1989**, *133*, 1 and 13.

(48) Aronson, M. Influence of hydrophobic particles on the foaming of aqueous surfactant solutions. *Langmuir* **1986**, *2*, 653.

(49) Born, M.; Wolf, E. *Principles of Optics*; Pergamon: Oxford, 1980.

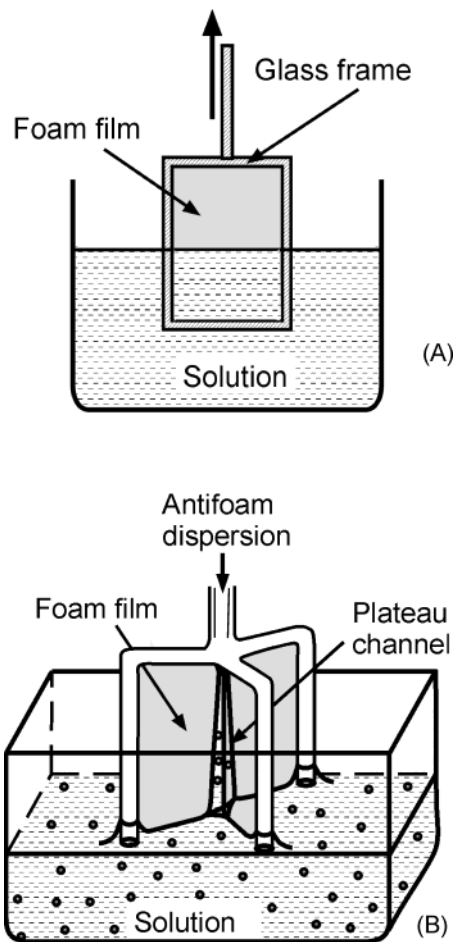


Figure 6. Sketch of the glass frames used for formation and observation of vertical foam films (A and B) and of a single Plateau channel, which is formed between three vertical foam films (B).

actual antifoam entities are typically 1–2 orders of magnitude smaller.⁹

2.2.2. Large Vertical Films and Plateau Channels Suspended on a Frame. This method of film formation and observation allows one to study relatively large foam films (up to several centimeters in size). Hence, it complements the capillary method, described in section 2.2.1, because the size of the foam films in actual foams can cover the range between 0.01 and several centimeters.

In our experiments,^{9,13–15} a rectangular glass frame (2 × 3 cm or 5 × 5 mm) was attached to a specially designed sliding mechanism, Figure 6A. The latter was driven by a powerful elastic spring, which ensured reproducible rapid withdrawal of the frame from the surfactant solution (for 40–50 ms). The mechanical shock, which could break the newly formed foam film at the end of the withdrawal process, was minimized by using a mechanical buffer to decelerate the frame just before it stops. The surfactant solution and the frame were kept in a closed glass container (to reduce water evaporation from the film) with optically clean front and rear walls. The vertical films were observed in reflected light, which allowed us (1) to detect the position of film rupture by antifoam globules, a high-speed video camera and stroboscope illumination were used for this observation, (2) to measure the thickness at which the film ruptures, monochromatic laser light was used in these observations to create sharp interference pattern, and (3) to measure the film lifetime, which could be as short as a fraction of second, in the presence of fast antifoam. With all studied systems, reference experiments were performed

with surfactant solutions deprived of antifoam, to check the foam films stability. Thus we verified that the observed film rupture events, in the presence of antifoam, were not caused by artifacts.

In some of the experiments¹³ we used a different glass frame, with a design suggested by Koczo and Racz.⁵⁰ It consists of three vertical legs (1.0 cm long) which meet at 120°, at the tip of a central capillary, Figure 6B. Three foam films are simultaneously formed, with a Plateau channel between them, when the frame is withdrawn from the surfactant solution. The antifoam globules can be injected directly into the Plateau channel through the central capillary. Alternatively, the antifoam globules can be predispersed in the surfactant solution. In this way, one can study the effect of antifoam globules on the stability of Plateau channels.

2.3. Methods for Studying Asymmetric Oil–Water–Air Films. 2.3.1. Optical Observation of Asymmetric Oil–Water–Air Films. Asymmetric oil–water–air film appears when an oily antifoam globule approaches the surface of a foam film or Plateau channel. As explained in sections 3.2, 4.3, and 6.2–6.5 below, the stability of this asymmetric film determines how easily the oil globules appear on the air–water interface which, in turn, has important consequences for the mode of foam destruction and for antifoam efficiency.

For model studies, asymmetric films of millimeter size can be formed by pressing a drop of oil or compound against the solution surface, from below. The drop can be released from a capillary and allowed to float up, under the action of buoyancy, or can stay attached to the tip of the capillary; see Figure 7A.^{15,51,52} In the latter case, the capillary is mounted on an XYZ stage, which allows one to adjust the drop position. A syringe, filled by oil and driven by a micrometer screw, is connected to the capillary and is used to control the drop radius. The experimental cell is covered by an optically clean glass shield to suppress water evaporation from the asymmetric film. These films are observed from above, in reflected light, by using a microscope. By this technique, one can observe the process of film rupture by the solid particles, which protrude from the compound globule into the aqueous film, and evaluate the film thickness in the moment of rupture.¹⁵

Bergeron et al.⁵² used a pressure transducer, connected to the capillary with the oil phase, to measure the capillary pressure at which the asymmetric film ruptures. By using a somewhat different configuration, Koczo et al.⁵³ were also able to measure the rupture pressure of the asymmetric film, which is formed on the surface of an oil (compound) drop, blown from a capillary; see Figure 7B.

2.3.2. Film Trapping Technique (FTT). FTT has been intensively used in our laboratory for quantification of the entry barrier of oil drops and compound globules, in relation to their antifoam activity.^{11,15,17–23,54} With some modifications, this method was applied to measure the coalescence pressure of micrometer-sized oil drops with oil macrophase (in relation to coalescence stability of

(50) Koczo, K.; Racz, G. Flow in a plateau border. *Colloids Surf.* **1987**, *22*, 97.

(51) Kruglyakov, P. M.; Koretskaya, T. A. Suppression of black spots formation and stability of asymmetric water films. *Izv. Sib. Otd. AN USSR* **1973**, *2*, 12.

(52) Bergeron, V.; Cooper, P.; Fischer, C.; Giermanska-Kahn, J.; Langevin, D.; Pouchelon, A. Poly(dimethylsiloxane) (PDMS)-based antifoams. *Colloids Surf., A* **1997**, *122*, 103.

(53) Koczo, K.; Koczona, J. K.; Wasan, D. Mechanisms for antifoaming action in aqueous systems by hydrophobic particles and insoluble liquids. *J. Colloid Interface Sci.* **1994**, *166*, 225.

(54) Hadjiiski, A.; Tcholakova, S.; Ivanov, I. B.; Gurkov, T. D.; Leonard, E. F. Gentle film trapping technique with application to drop entry measurements. *Langmuir* **2002**, *18*, 127.

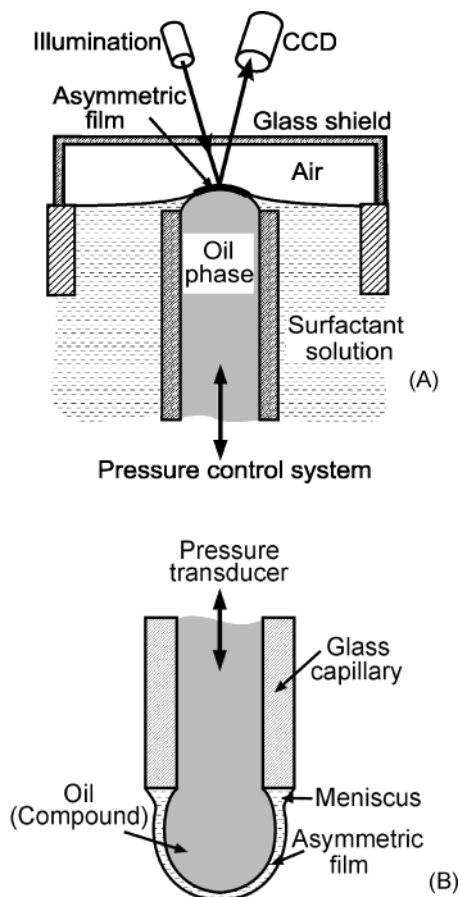


Figure 7. (A) Schematic presentation of a setup for observation of asymmetric oil–water–air film, formed by pressing a drop of oil (or compound) underneath the solution surface.^{15,52} (B) Sketch of the setup used by Koczó et al.⁵³ to measure the rupture pressure of the asymmetric film formed on the surface of an oil (compound) drop, blown from a capillary.

emulsions),⁵⁵ three-phase contact angle of micrometer-sized latex spheres,⁵⁶ and the adhesion energy of biological cells to adsorption layers of bioactive molecules.⁵⁷

The principle of the method and the measuring procedure are as follows (see Figure 8): A vertical glass capillary, a few millimeters in radius and several centimeters long, is positioned at a small distance above the flat bottom of glass vessel. The lower end of the capillary is immersed in the surfactant solution, which contains dispersed antifoam globules. The capillary is connected to a pressure control system that allows one to vary and to measure the difference, ΔP_A , between the air pressure in the capillary, P_A , and the ambient atmospheric pressure, P_A^0 . The data acquisition equipment includes a pressure transducer and digital multimeter, connected to a computer.

When P_A increases, the air–water meniscus in the capillary is pushed against the glass substrate and a wetting film is formed, which traps some of the antifoam globules (Figure 8B). These globules remain sandwiched between the air–water meniscus and the glass substrate. The capillary pressure of the air–water meniscus around the trapped drops is $P_C \equiv P_A - P_W$, where $P_W = (P_A^0 + \rho gZ)$ is the pressure in the liquid around the drops. P_W can be

calculated from the liquid depth, Z ; ρ is the water mass density; and g is the gravity acceleration. Therefore, the relationship between the capillary pressure, P_C , and the measured pressure difference, $\Delta P_A = (P_A - P_A^0)$, is

$$P_C = \Delta P_A - \rho gZ \quad (2)$$

The liquid depth, Z , is measured by a micrometer translator, during the submersion of the capillary into the solution.

During an experiment, one increases the pressure in the capillary, P_A , by small increments. After each step of pressure increase, one waits for liquid drainage from the wetting film around the trapped antifoam globules and for reaching mechanical equilibrium. The changes of the meniscus shape around the trapped drops (caused by liquid drainage) are observed by an optical microscope in reflected monochromatic light—the light interference pattern changes with time until the liquid drains from the wetting film. The equatorial diameter of the trapped globules, $2R_E$, is measured microscopically (in white transmitted light).

The experiments show that the trapped globules enter (pierce) the surface of the wetting film at a certain, critical capillary pressure, P_C^{CR} ; see Figure 8C. The moment of drop entry, which is accompanied by significant local change in the shape of the air–water meniscus, is clearly seen in both reflected and transmitted light. Therefore, the equipment allows one to measure P_C^{CR} as function of solution composition and drop radius. In our studies,^{9–25} we refer to P_C^{CR} as a quantitative measure of the barrier to drop entry (see section 6.2 for further explanations). Larger values of P_C^{CR} correspond to higher entry barriers (viz., more difficult drop entry) and vice versa.

The experimental setup, shown in Figure 8B, allows one to measure entry barriers, which are higher than ca. 20 Pa. This lower limit is determined by the capillary pressure of the initial air–water meniscus, which is formed in the capillary when starting the experiment. This meniscus has a radius of curvature approximately equal to the radius of the used capillary, and the corresponding capillary pressure is ≈ 20 Pa. The entry barriers of fast antifoams are lower than 20 Pa, and another modification of the method (called gentle FTT, see Figure 8D) was used for these systems.^{22,54}

The main idea of the gentle FTT is to create a virtually flat air–water interface in the capillary, with $P_C \approx 0$, before trapping the drops. For this purpose, a sapphire disk of special design is attached to the lower end of the capillary. The disk has an opening with a wedgelike shape (Figure 8D), which ensures stable attachment of the air–water interface to the sapphire upper edge. Additionally, a substrate with a small stub, cut out onto a glass plate, is used in these experiments. This glass plate is placed on the bottom of the solution container, so that the stub is projected upward into the opening of the sapphire disk. One can position precisely the capillary and juxtapose the flat fluid interface with the glass stub. Thus one can achieve trapping of drops by flat interface with $P_C \approx 0$, followed by a gentle increase of P_C until P_C^{CR} is reached. A detailed description of the FTT can be found in ref 54. A comprehensive review of the results obtained so far by this method in relation to antifoaming is presented in ref 22.

(55) Tcholakova, S.; Denkov, N. D.; Ivanov, I. B.; Campbell, B. Coalescence in β -lactoglobulin stabilized emulsions: Effects of protein adsorption and drop size. *Langmuir* **2002**, *18*, 8960.

(56) Hadjiiski, A.; Dimova, R.; Denkov, N. D.; Ivanov, I. B.; Borwankar, R. Film trapping technique: Precise method for three-phase contact angle determination. *Langmuir* **1996**, *12*, 6665.

(57) Ivanov, I. B.; Hadjiiski, A.; Denkov, N. D.; Gurkov, T. D.; Kralchevsky, P. A.; Koyasu, S. Energy of adhesion of human T cells to adsorption layers of monoclonal antibodies measured by a film trapping technique. *Biophys. J.* **1998**, *75*, 545.

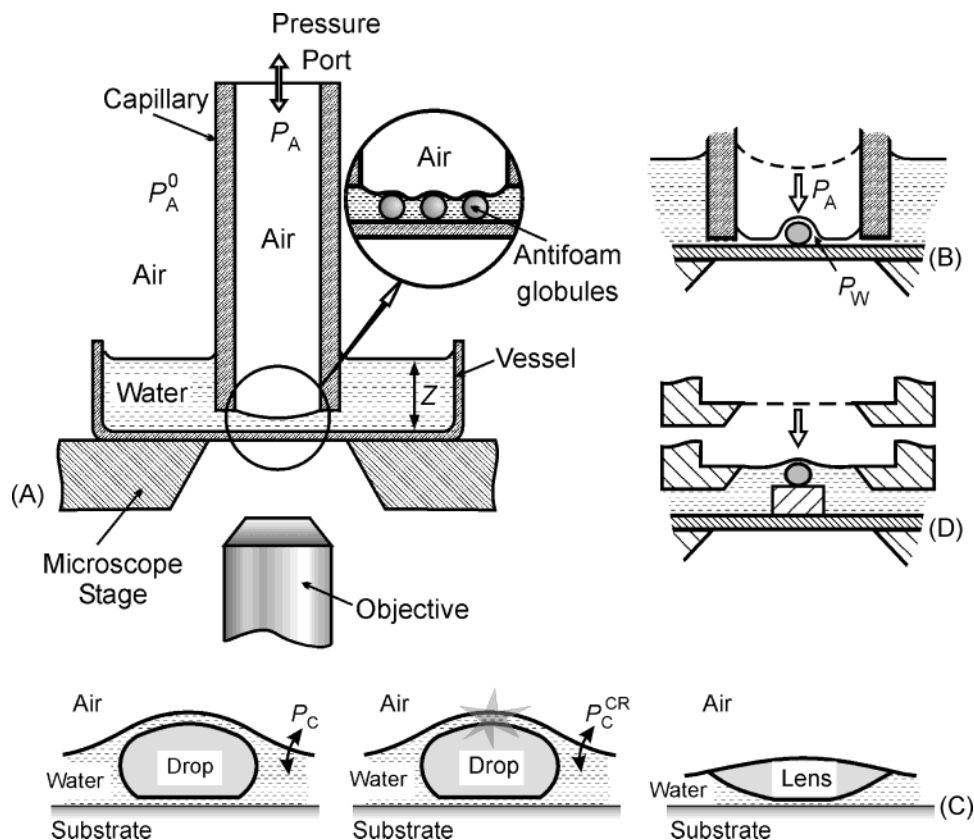


Figure 8. Scheme of the experimental setup and the basic principle of operation of the film trapping technique (FTT). (A, B) A vertical capillary, partially immersed in surfactant solution containing oil drops, is held close above the bottom of the experimental vessel. The air pressure inside the capillary, P_A , is increased, and the water–air meniscus in the capillary is pressed against the glass substrate. Some of the oil drops remain trapped in the wetting glass–water–air film and are compressed by the meniscus. (C) At a certain critical capillary pressure, $P_C^{CR} = (P_A - P_W)$, the asymmetric film formed between an oil drop and the solution surface ruptures. (D) Another modification, called “gentle FTT”, is used for measuring low entry barriers—a flat meniscus is formed first, which allows entrapment of oil drops at virtually zero capillary pressure.

Optical observations of the antifoam globule entry, in similar configuration (globules trapped in wetting film on solid substrate) were made by Tamura et al.,⁵⁸ by using a scanning laser microscope. No quantitative characterization of the entry barrier was attempted in ref 58.

2.4. Methods for Studying Oil Spreading. 2.4.1.

Rate of Spreading. The spreading rate can be measured by using trace particles to visualize the front of spreading oil.^{11,15,18,19,52,59,60} Briefly, a glass Petri dish of diameter 20 cm and depth 2 cm is filled with surfactant solution, and trace particles (hydrophobized silica or small grinded PTFE chips) are evenly sprinkled over the solution surface. A thin glass rod, whose tip has been soaked by the tested oil or compound, is gently placed in contact with the solution surface, by using a micrometer drive device. The radial motion of the trace particles, indicating the front of a spreading precursor oil film, is observed and recorded by means of a CCD camera connected to a video recorder. The video records are afterward processed, and the spreading rate is measured.⁶⁰ Alternatively, the time period needed for oil spreading up to 5 cm radial distance from the oil source can be used for comparison of various oils and compounds.^{11,15,18,19}

2.4.2. Ellipsometry. Ellipsometry is particularly suitable for measuring the thickness of the layer of oil (compound) spread on the surface of the solution, which is used in the foam test.^{18–20,23,61,62} Ellipsometry can be used also for measuring the thickness of the precursor (molecularly thin) oil layer, which spreads upon deposition of oil or compound on the solution surface.¹¹ In our experiments, we used ellipsometry to determine (1) how the thickness of the layer of spread oil changes in the course of antifoam exhaustion²³ and (2) how the thickness of the spreading oil is affected by the viscosity of silicone oils⁸ or by the concentration and hydrophobicity of silica particles, included in the antifoam compound.¹⁹

We used a commercial null-type ellipsometer (LEF 3M, Novosibirsk, Russia), which was upgraded by introducing an additional rotating analyzer in the optical system to achieve a higher time resolution.⁶³ The light source was a He–Ne laser ($\lambda = 632.8$ nm), and the angle of incidence was 50° (close to Brewster angle for water). The experimental setup was driven by computer, and the raw ellipsometric data were instantaneously recomputed to provide the values of the so-called ellipsometric angles, ψ and Δ , which were stored in 0.1 s intervals. The

(58) Tamura, T.; Kageyama, M.; Kaneko, Y.; Kishino, T.; Nikaido, M. Direct observation of foam film rupture by several types of antifoams using a scanning laser microscope. *J. Colloid Interface Sci.* **1999**, *213*, 179.

(59) Davies, J. T.; Rideal, E. K. In *Interfacial Phenomena*; Academic Press: New York, 1963.

(60) Bergeron, V.; Langevin, D. Monolayer spreading of poly(dimethylsiloxane) oil on surfactant solutions. *Phys. Rev. Lett.* **1996**, *76*, 3152.

(61) Mann, E. K.; Langevin, D. Poly(dimethylsiloxane) molecular layers at the surface of water and of aqueous surfactant solutions. *Langmuir* **1991**, *7*, 1112.

(62) Lee, L. T.; Mann, E. K.; Langevin, D.; Farnoux, B. Neutron reflectivity and ellipsometry of a polymer molecular layer spread on the water surface. *Langmuir* **1991**, *7*, 3076.

(63) Russev, S. C.; Argirov, T. V. Rotating analyzer-fixed analyzer ellipsometer based on null type ellipsometer. *Rev. Sci. Instrum.* **1999**, *70*, 3077.

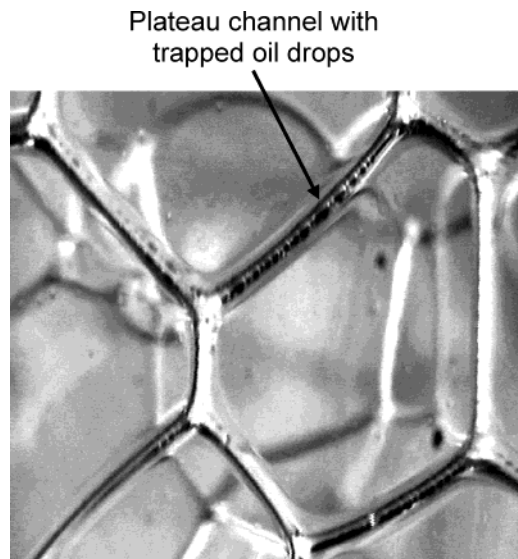


Figure 9. Photograph of foam cells in real foam, produced from 0.1 M SDP3S solution, containing silicone oil (0.1 wt %). The Plateau channels are densely populated with trains of trapped oil drops, which is evidenced by the wavy appearance of the Plateau channel walls (adapted from ref 14).

variations of ψ and Δ were analyzed after the experiment, and the thickness of the spread oil layer was determined as a function of time. For details in the measuring procedures, see refs 19 and 23.

2.5. Methods for Determination of Size Distribution and Morphology of Antifoam Globules. Several methods are used to determine the size distribution of antifoam globules. Most appropriate seems to be the laser diffraction method, which covers simultaneously a wide range of sizes (ca. from 0.3 to 100 μm).^{24,52} A combination of optical microscopy and dynamic light scattering was used in ref 11 to cover the ranges above and below 2 μm , respectively. The optical microscopy has the advantage to provide also information about the globule shape and, in some cases, about the location of the solid particles in mixed oil–solid globules.^{11,21} Electron microscopy was applied^{11,29} to investigate the location of silica particles in the antifoam globules of fresh and exhausted compounds.

3. Fast and Slow Antifoams

3.1. Location of Antifoam Globule Entry and Activity—“Fast” and “Slow” Antifoams. A very important component of any mechanism of antifoam action is the location, where the antifoam globules enter the air–water interface and cause foam destruction. Most of the researchers have assumed that the antifoam globules enter the surfaces of the foam films and destroy these films soon after globule entry (see, e.g., the review in ref 1). In contrast, Koczko et al.⁵³ suggested that the antifoam globules first escape from the foam films into the neighboring Plateau borders (PBs) and get trapped there. According to the latter mechanism, the antifoam globules are compressed by the walls of the shrinking PBs (as a result of water drainage from the foam) and eventually the globules enter the walls of the PBs, causing rupture of the neighboring foam films.^{3,53}

Our optical observations^{9–17,22} showed that both scenarios may occur in practical systems: In the case of oil drops deprived of solid particles, the foam destruction typically occurs through an initial accumulation of drops in the PBs, as suggested by Koczko et al.⁵³ See for example Figure 9, which shows a photograph of oil drops trapped in the PBs of actual foam.¹³ No antifoam drops are present

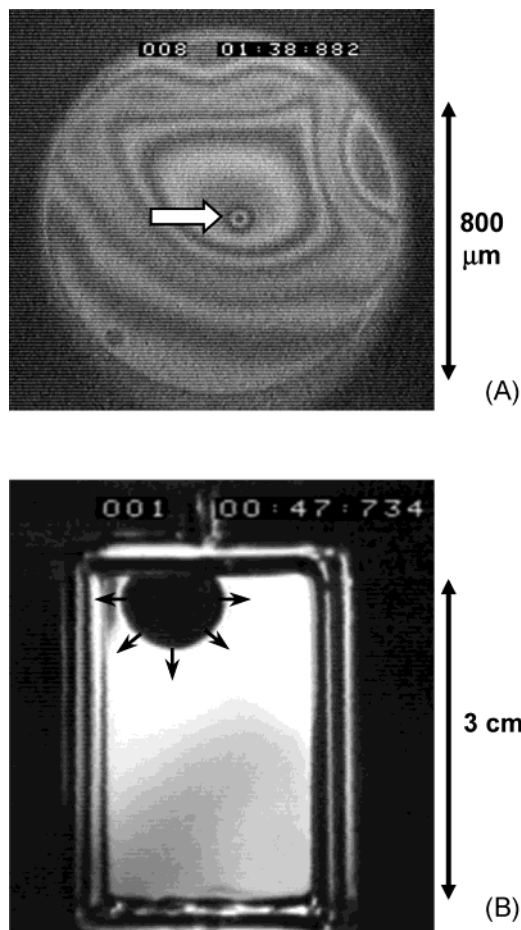


Figure 10. Images of (A) small horizontal and (B) large vertical foam films made from 10 mM AOT solution, containing 0.01 wt % of silicone oil–silica emulsion (fast antifoam). (A) A characteristic interference pattern, called “fisheye” (pointed by white arrow), is seen at high magnification, just before film rupture. (B) By using a high-speed camera, one can observe the formation of a hole in the foam film, which expands (the black arrows) and eventually leads to film rupture (adapted from ref 9).

in the foam films at this stage of foam evolution (see section 4 for further explanations). Various experiments unambiguously showed that the foam destruction in such systems (oil drops accumulated in PBs) necessarily requires a compression of the trapped drops by the shrinking walls of the PBs.^{13,14} On the other hand, mixed globules of appropriately formulated oil–solid compounds are often (though not always) able to enter the surfaces of the foam films and to rupture these films very soon after film formation. As an illustration, Figure 10 shows the moments of foam film rupture, as captured by a high-speed video camera, about a second after the foam films were formed.⁹

These two different modes of foam destruction exhibit a remarkable difference in their characteristic time scales. The mechanism involving foam film rupture usually leads to complete foam destruction within seconds, whereas the foam destruction through compression of the antifoam globules in the PBs usually requires many minutes or hours, because the water drainage from the foam (needed for compression of the trapped drops) is relatively slow; see Figures 11, 12, and 14 below for examples. Furthermore, in the case of slow foam destruction, one usually observes residual foam, one to several centimeters high, which may remain stable for many hours; see Figures 12 and 14. Although the defoaming time may depend on the used foam test and antifoam concentration, the large gap

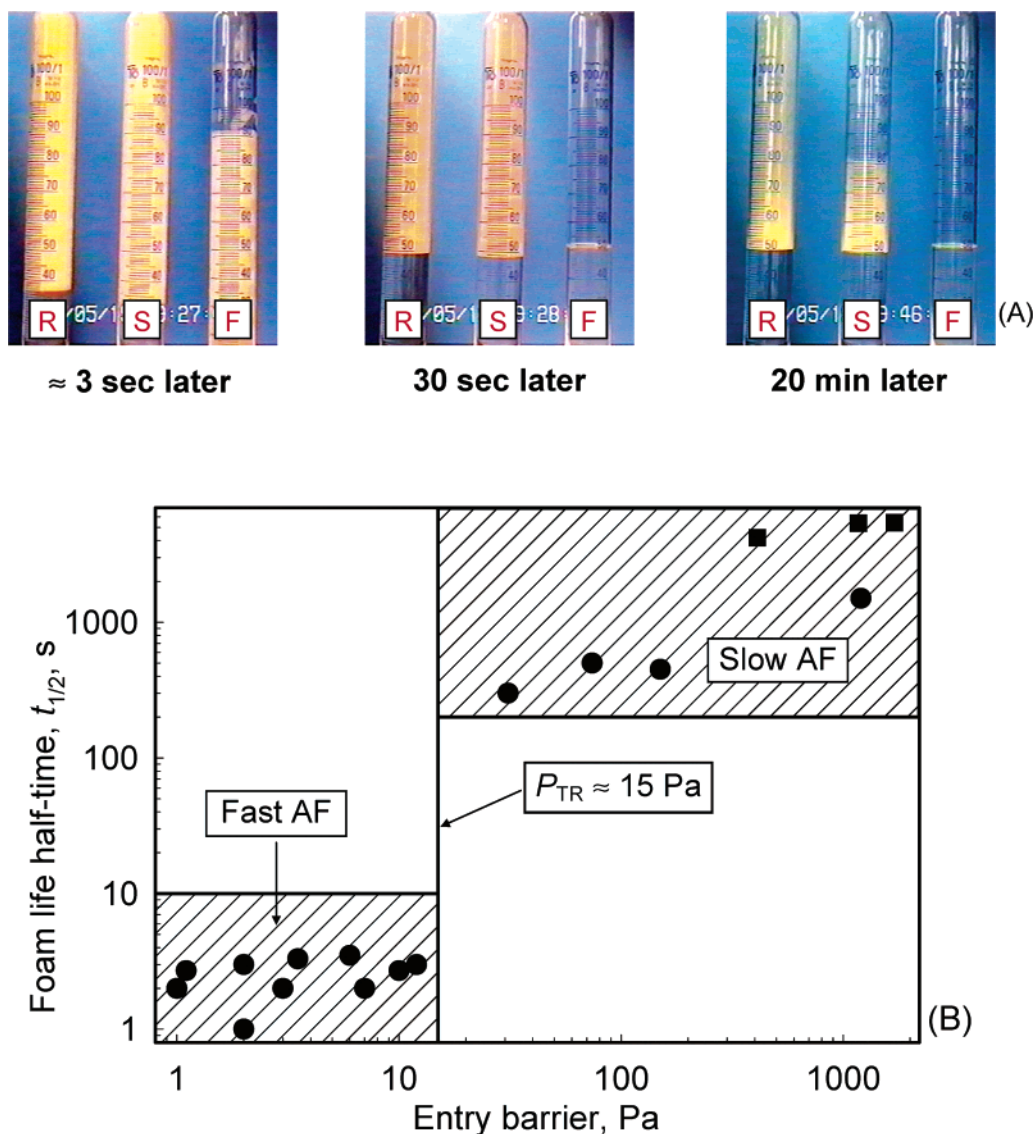


Figure 11. (A) Photographs of cylinders from Bartsch test: R, reference surfactant solution without antifoam; S, same solution with 0.1 wt % silicone oil, acting as slow antifoam; F, same solution with 0.01 wt % silicone oil–silica compound, acting as fast antifoam. The photographs show different moments after foam formation. (B) The full circles show the foam half-time, $t_{1/2}$, as a function of drop entry barrier for different surfactant–antifoam pairs (see ref 22 for sample description). The squares denote samples, for which $H_{RES} > H_{IN}/2$, and $t_{1/2}$ is not defined; the onset of stage IV is used to plot these data; see Figure 12. Note the logarithmic scale on the axes.

between the foam lifetimes, for these two different modes of foam destruction, was always observed in our experiments.

For these reasons, we introduced the term “fast antifoams” to denote the antifoams whose globules are able to enter the surfaces of the foam films and to destroy these films in the early stages of film thinning.²¹ The term “slow antifoams” was suggested²¹ for antifoams whose globules first leave the foam films and destroy the foam after entering the walls of the PBs, as in the mechanism suggested by Koczo et al.⁵³ The detailed mechanisms of foam destruction by the slow and fast antifoams are considered in sections 4 and 5, respectively.

Note that the problem about the location of antifoam action has important practical implications, because the PBs are much larger in size (cross sections of tens to hundreds of micrometers) as compared to the film thickness, which typically becomes $\approx 1 \mu\text{m}$ within several seconds after film formation (see section 4.2 for illustrative results). Therefore, the optimal size of the antifoam globules, which should correspond to the characteristic

size of the structural element, in which the drop entry occurs (foam film or PB), would be different in these two cases.⁹ This problem is discussed in sections 4.3 and 5.5 below.

3.2. Critical Entry Barrier Separating Fast from Slow Antifoams. Parallel foam tests, FTT experiments, and microscope observations of foam films, with a variety of antifoam–surfactant systems, showed that one of the main factors that determines whether a given antifoam would behave as “fast” or “slow” is the barrier to drop entry.^{19–22} In Figure 11 we show summarized results for the foam half-time as a function of entry barrier for 17 different systems. Each experimental point corresponds to a different surfactant–antifoam pair. One sees that the data fall into two distinct regions: (1) systems where the foam is destroyed in less than 10 s (fast antifoams), for all these systems, the entry barrier is below 15 Pa; (2) systems where the foam half-time is longer than 5 min (slow antifoams), for which the entry barrier is above 20 Pa. One can conclude that there is a well-defined threshold value of the entry barrier, P_{TR} , somewhere between 15

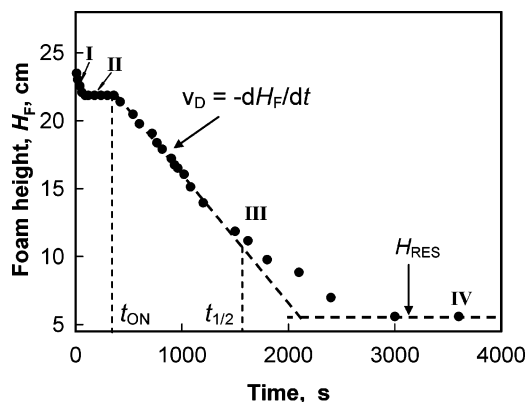


Figure 12. Foam height, $H_F(t)$, for solution containing anionic surfactant SDP3S, nonionic cosurfactant (foam booster), and 0.1 wt % silicone oil as slow antifoam. t_{ON} shows the onset of foam decay by bubble collapse; $t_{1/2}$ indicates the foam half-time. The roman numbers, associated with the curve, indicate different stages of foam evolution.¹⁴ The structural changes within the foam column, during these stages, are visualized in Figure 13.

and 20 Pa, which separates the region of the fast antifoams from the region of the slow ones. Microscope observations showed that the antifoam globules are able to enter the foam film surfaces and break the foam films when $P_C^{CR} < P_{TR}$, whereas the globules are expelled into the neighboring Plateau borders if $P_C^{CR} > P_{TR}$. These observations are described in sections 4.1–4.3 and 5.1 below.

4. Mechanism of Foam Destruction by Slow Antifoams

4.1. Stages of Foam Evolution in the Presence of Oil Drops. In the presence of slow antifoam, one can define four distinct stages in the foam evolution.^{13,14} As an illustration, we show in Figure 12 the foam height as a function of time, $H_F(t)$, for solutions containing anionic surfactant SDP3S, nonionic cosurfactant (foam booster), and 0.1 wt % of silicone oil as antifoam. The various stages are denoted in Figure 12 by roman figures I–IV. Observations by magnifying lens allowed us to identify the structural changes, within the foam column, during each of these stages.¹⁴

During period I (which took about 2 min in this particular example) the upper boundary of the foam remained still, because no coalescence of the bubbles with the uppermost air phase took place. The lower boundary of the foam rose with time (which is indicated in Figure 12 by 15–20 mL reduction of the foam volume) due to water drainage from the initially formed wet foam. Several processes were observed within the foam during this period: the foam films thinned down; the Plateau borders (PBs) and the nodes, where the PBs met, became much narrower; the smallest bubbles shrunk and disappeared due to air diffusion across the foam films (driven by the higher air pressure in the smaller bubbles); see panels A and B of Figure 13.

During stage II, the upper and lower boundaries of the foam did not change noticeably their positions (i.e., the foam volume remained practically constant), which reflected the facts that no bubble coalescence occurred and that the water drainage from the foam had become very slow. However, the optical observations were evidence of a significant restructuring of the foam cells during this period. The small bubbles disappeared due to air diffusion through the films, and as a result, the density of the PBs (i.e., their total length per unit foam volume) and of the nodes (number per unit volume) decreased several times.

Gradual accumulation of oil drops in the remaining nodes and PBs was observed with time, because the trapped drops could not escape from the foam (cf. panels B and C of Figure 13). In addition, the PBs and nodes shrunk with time—a process which led to decrease of the radius of curvature of the PB walls and, as a consequence, to gradual increase of the capillary pressure, exerted by these walls on the trapped oil drops.

When a certain critical value of the compressing capillary pressure was reached, the foam destruction started (Figure 13D), primarily through rupture of the upper layer of bubbles where the compressing capillary pressure is the highest—this was the onset of stage III, which is denoted by t_{ON} in Figure 12. The rate of foam destruction, $v_D = -dH_F/dt$, was approximately constant during the main course of period III. Afterward, v_D gradually decreased in magnitude and stage IV was reached when the foam volume remained almost constant for many hours. Only large bubbles had remained at that stage, and the process of bubble rearrangement was rather slow. Hereafter, the height of this residual, long-standing foam is denoted by H_{RES} . Note that the observed foam destruction was certainly caused by droplets of silicone oil, predispersed in the foaming solution, because no foam decay was seen in the absence of oil, in the time scale of Figure 12.

Experiments with various oils and surfactants have shown that the above scenario is rather typical for slow antifoams, though the values of t_{ON} , $t_{1/2}$, v_D , and H_{RES} can vary in very wide ranges, depending on the particular surfactant–antifoam pair. As an illustration of the various possibilities, which can be observed in the foam tests, in Figure 14 we plot the foam volume, as a function of time, for solution of the anionic surfactant SDDBS in the presence of various oils (the Ross–Miles test was used in these experiments). Additional examples are shown in Figure 20 below, in relation to the foam boosting effect of cosurfactants (section 4.4). The analysis of the results, obtained with various oil–surfactant systems, showed that the main differences between them concern the following:^{13,14,16,17,22}

(1) *Solution Foaminess.* In some systems, the addition of oil decreases the initial foam volume (i.e., the oil suppresses foam formation), whereas the opposite effect was observed in other systems; cf., for example, the effects of dodecanol and hexadecane in Figure 14. The increased foaminess in the presence of oil was explained¹⁶ with the reduced surface tension of the solutions (due to oil spreading), which facilitates the surface expansion during foaming and, thereby, promotes bubble formation. The opposite effect, the reduced foaminess in the presence of oil drops, was explained by the antifoam effect of these drops during foaming—bubble collapse was induced by the dispersed oil. The net effect could strongly depend on the type and concentration of the used oil. It was demonstrated experimentally^{16,64,65} that a given oil usually increases the foaminess when added at concentrations below and around its solubility limit (the reduced surface tension is more important than the antifoam effect at these concentrations). The same oil could significantly suppress foaming when added at higher concentrations and is present in the form of dispersed oil drops (the antifoam effect could prevail in this concentration range).

(64) Kruglyakov, P. M.; Koretskaya, T. A. Inversion of antifoam ability in the fatty alcohol series. *Kolloidn. Zh.* **1974**, *36*, 627.

(65) Kruglyakov, P. M. Equilibrium properties of free films and stability of foams and emulsions. In *Thin Liquid Films: Fundamentals and Applications*; Ivanov, I. B., Ed., Marcel Dekker: New York, 1988; Chapter 11.

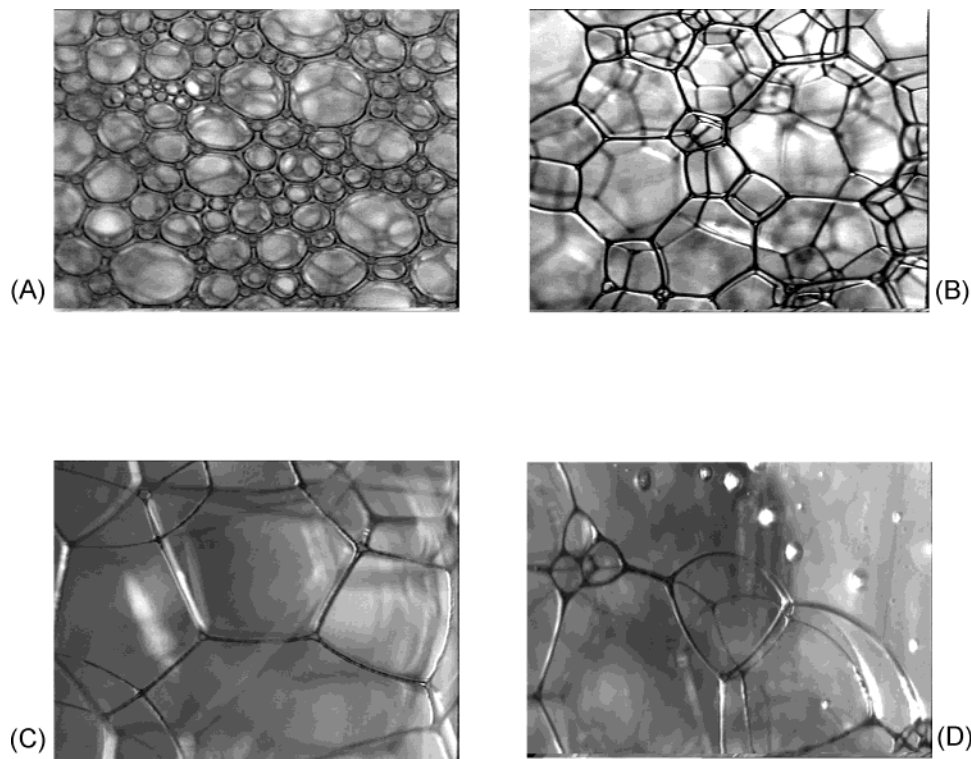


Figure 13. Photographs of foam cells, just below the top of a foam column, at different stages of the foam evolution; cf. Figure 12: (A) wet foam, stage I; (B) foam at the transition between stages I and II; (C) air diffusion from the small bubbles toward the larger ones leads to disappearance of the smallest bubbles and to gradual accumulation of oil drops in the nodes and the Plateau borders during period II. (D) When the capillary pressure at the top of the foam column exceeds the entry barrier of the oil drops, a destruction of the uppermost layers of bubbles is observed, which is the beginning of stage III.

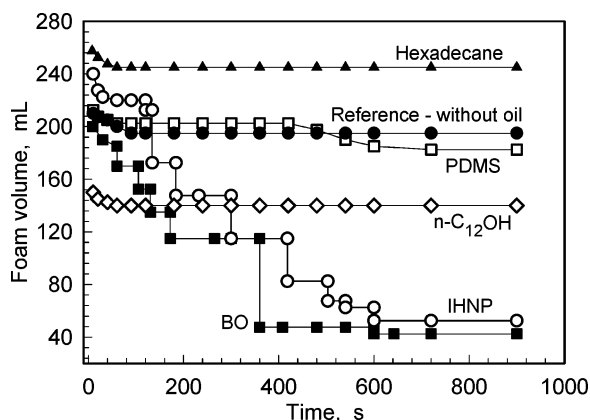


Figure 14. Comparison of the foamability and foam stability of 2.6 mM SDDBS solutions, in the presence of 0.01 wt % of different oils (Ross–Miles test).^{16,17}

(2) *Onset of Foam Destruction and Foam Half-Time.* The onset of the foam destruction, t_{ON} , and the foam half-time, $t_{1/2}$, were found^{13,14,16,17} to depend primarily on the magnitude of the entry barrier of dispersed oil drops (determined in parallel experiments by FTT) and on drop size. When the barrier was rather high and/or the oil drops were too small, the drops remained arrested in the Plateau channels without being able to destroy the foam—no antifoam effect was observed in this case (see section 4.3 for quantitative consideration). In the opposite case, low entry barriers and sufficiently large drops, the foam destruction typically started several minutes after foam formation, and several additional minutes were sufficient to reach the final foam height. The characteristic times t_{ON} and $t_{1/2}$ should depend also on the rate of water drainage from the foam (which in turn determines how rapidly the

capillary pressure increases at the top of the foam column) and on the rate of air diffusion across the foam films (which determines how rapidly the trapped oil drops concentrate in the PBs and nodes). No quantitative study of these relations has been attempted so far.

(3) *Height of the residual foam, H_{RES} .* The experiments show^{13,14} that the value of H_{RES} also depends primarily on the magnitude of entry barrier and on oil drop size. These relations are considered in section 4.3 below.

(4) In some of the systems (IHNP and BO in Figure 14) a *stepwise foam destruction* was observed¹⁶—thousands of bubbles were almost instantaneously destroyed in a process, which was probably triggered by a single drop-entry event (avalanche effect, see section 4.3).

We should note that a very clear correlation between the magnitude of the entry barrier and the antifoam activity was established in all of the studied systems.^{9–22} In contrast, no direct correlation between the antifoam activity and the magnitudes of the entry, E , spreading, S , or bridging, B , coefficient was found in our studies (see eqs 9, 24, and 31 below for definitions of these coefficients). Several examples are presented in Tables 1 and 2 (see also refs 9 and 11–22 for experimental details and for further examples). In Table 1 we present data for the E , S , and B coefficients, entry barrier, and antifoam activity of several oils in 2.6 mM SDDBS solution (Figure 14 shows the results from the respective foam tests). As seen from Table 1, the silicone oil has highest values of the E , S , and B coefficients (all of them strongly positive, except S_{EQ}) but has negligible antifoam activity, due to its high entry barrier, $P_c^{CR} > 3000$ Pa. In contrast, BO and IHNP oils have significantly smaller values of the E , S , and B coefficients, while exhibiting a pronounced antifoam effect, which can be explained by the low entry barrier of these two oils ($P_c^{CR} < 100$ Pa).

Table 1. Entry, E , Spreading, S , and Bridging, B , Coefficients, Entry Barrier, P_C^{CR} , and Relative Reduction of the Foam Volume, $V_F(t)/V_F(0)$, for Different Oils (slow antifoams; mean drop size 10–15 μm) in 2.6 mM SDDBS Solution^a

oil	E_{IN} , mN/m	E_{EQ} , mN/m	S_{IN} , mN/m	S_{EQ} , mN/m	$B_{IN}^{1/2}$, mN/m	$B_{EQ}^{1/2}$, mN/m	P_C^{CR} , Pa	$V_F(t)/V_F(0)$, $t = 15$ min
BO	7.7	4.8	0.5	-2.4	15.7	8.8	44	0.2
IHNP	8.8	3.0	5.2	-0.6	19.6	7.8	75	0.2
PDMS	17.5	10.4	6.3	-0.8	24.9	15.3	>3000	0.9
hexadecane	6.2	5.6	0.6	0.0	14.3	13.0	≈400	0.95
dodecanol	<i>b</i>	2.7	<i>b</i>	-9.3	<i>b</i>	$B_{EQ}^{1/2} < 0$	>1500	1.0

^a The subscripts IN and EQ refer to initial and equilibrium coefficients, respectively (without and with equilibrium layer of spread oil on solution surface). The accuracy of the calculated values of E , S , and $B^{1/2}$ is ± 1 mN/m. The interfacial tensions, from which the E , S , and B coefficients are calculated, are given in the original paper.¹⁶ The foam data are from Ross–Miles test with 0.01 wt % oil. ^b Cannot be measured, due to high solubility of dodecanol in the surfactant solution.

Table 2. Entry, E , Spreading, S , and Bridging, B , Coefficients, Entry Barrier, P_C^{CR} , and Relative Reduction of the Foam Volume, $V_F(t)/V_F(0)$, for Silicone Oil PDMS (slow antifoam; mean drop size 10–15 μM) in Various Surfactant Solutions^a

surfactant	E_{IN} , mN/m	E_{EQ} , mN/m	S_{IN} , mN/m	S_{EQ} , mN/m	$B_{IN}^{1/2}$, mN/m	$B_{EQ}^{1/2}$, mN/m	P_C^{CR} , Pa	$V_F(t)/V_F(0)$, $t = 15$ min	$V_F(t)/V_F(0)$, $t = 90$ min
10 mM AOT	12.1	9.6	2.5	-0.2	19.4	15.7	19	0.05	0.05
0.45 mM APG	12.6	8.4	3.4	-0.8	20.4	13.9	>1250	0.95	0.9
100 mM SDP3S	20.2	12.8	6.6	-0.8	27.5	17.9	180	0.3	0.25
80 mM SDP3S	16.0	9.6	5.2	-1.2	23.7	14.6	850	1.0	0.6
+ 20 mM CAPB									
100 mM CAPB	19.0	13.7	4.6	-0.7	25.7	18.7	>7000	1.0	0.95
2.6 mM SDDBS	17.5	10.4	6.3	-0.8	24.9	15.3	>3000	0.9	<i>b</i>

^a The subscripts IN and EQ refer to initial and equilibrium coefficients, respectively. The accuracy of the calculated values of E , S , and $B^{1/2}$ is ± 1 mN/m. The interfacial tensions, from which the E , S , and B coefficients are calculated, are given in the original papers.^{9,13,15–17} The foam data are from the Bartsch test for AOT and APG, and from the Ross–Miles test for the other solutions. The oil concentration is 0.01 wt % in AOT, APG, and SDDBS solutions, and 0.1 wt % in the other solutions. ^b Not measured.

In Table 2 we compare the E , S , and B coefficients, entry barriers, and antifoam activity of silicone oil in several surfactant solutions. One sees from Table 2 that the silicone oil has strongly positive values of all coefficients (except S_{EQ} , which is virtually zero for all solutions), while the antifoam activity of the oil varies significantly. In all cases, the antifoam activity correlates with the entry barrier. Compare, for example, the data for AOT and APG solutions (the first two lines in Table 2), which exhibit very close values of the E , S , and B coefficients, while the entry barrier and, hence, the antifoam activity are very different for these two solutions—the oil is much more active in AOT, as compared to APG solutions.

4.2. Stages of Foam Film Thinning. In this section we describe briefly the main stages of foam film thinning, with an emphasis on the film thickness evolution and on the presence of antifoam globules in the film. A capillary cell (section 2.2.1) was used for observation of small foam films with diameter ≈ 1 mm. As a typical example, we describe the results obtained with 0.1 M (4.2 wt %) solution of the anionic surfactant SDP3S in the presence of 0.1 wt % silicone oil.^{13,22} Similar results were obtained with other anionic (AOT, SDS) and nonionic (Triton X-100) surfactants of similar weight concentration. The following five stages in the process of film thinning were observed:

Dimple ($t \approx 0$ –2 s; $h \approx 5$ –1 μm). A convex-lens-shaped film, with larger thickness in its center (called “dimple” in the literature⁶⁶), was initially formed upon the mutual approach of the two film surfaces; see Figure 15A. The thickness in the dimple center was about 3–5 μm , while the thinner region at the film periphery was about 1 μm thick. Several antifoam globules were usually trapped in the central part of the dimple. The dimple was hydrodynamically unstable—an asymmetric outflow of liquid from the film was observed about a second after film formation, and the dimple disappeared. The remaining foam film

was about 1 μm thick and contained several channels (dynamic regions with thickness 200–500 nm larger than the remaining planar portions of the film). The biggest antifoam globules left the foam film with the liquid outflow, which caused dimple disappearance, but some smaller globules, with diameters comparable to film thickness, were still observed in the thicker channels at this stage of film evolution.

Drainage of Relatively Thick Planar Film Containing Channels ($t \approx 2$ –30 s; $h \approx 1$ –0.1 μm). During this stage, the films gradually thinned down. The thicker channels were well seen, Figure 15B, but gradually disappeared with the film thinning process. Small antifoam globules were initially seen in the channels, but all these globules were eventually expelled from the foam film into the neighboring meniscus region, where the aqueous layer was thicker than the film.

Drainage of Thin Plane-Parallel Film ($t \approx 30$ –60 s; $h \approx 100$ –60 nm). The films had rather uniform thickness during this stage and were too thin to contain any antifoam globules inside.

Film Stratification ($t \approx 1$ –3 min; $h \approx 60$ –10 nm; Figure 15C). Stepwise film thinning was observed at thicknesses below ca. 60 nm, due to the so-called “colloidal structural forces”, caused by the layering of micelles in the foam film.^{24,47,67,68} Each stepwise transition in the film thickness corresponds to reduction of the number of micelle layers (five to four, four to three, etc.). The arrows in Figure 15C depict film areas of different thickness, and the integers indicate the number of micelle layers in the film, at the respective film thickness.

Equilibrium Black Film ($t > 3$ min; $h \approx 10$ nm). This was the last stage, when the film was in equilibrium with the surrounding meniscus region. The film thickness was around 10–15 nm, so that such films did not contain any

(66) Ivanov, I. B.; Dimitrov, D. S. Thin film drainage. In *Thin Liquid Films: Fundamentals and Applications*, Ivanov, I. B., Ed.; Marcel Dekker: New York, 1988; Chapter 7.

(67) Bergeron, V.; Radke, C. J. Equilibrium measurements of oscillatory disjoining pressures in aqueous foam films. *Langmuir* **1992**, *8*, 3020.

(68) Kralchevsky, P. A.; Denkov, N. D. Analytical expression for the oscillatory structural surface forces. *Chem. Phys. Lett.* **1995**, *240*, 385.

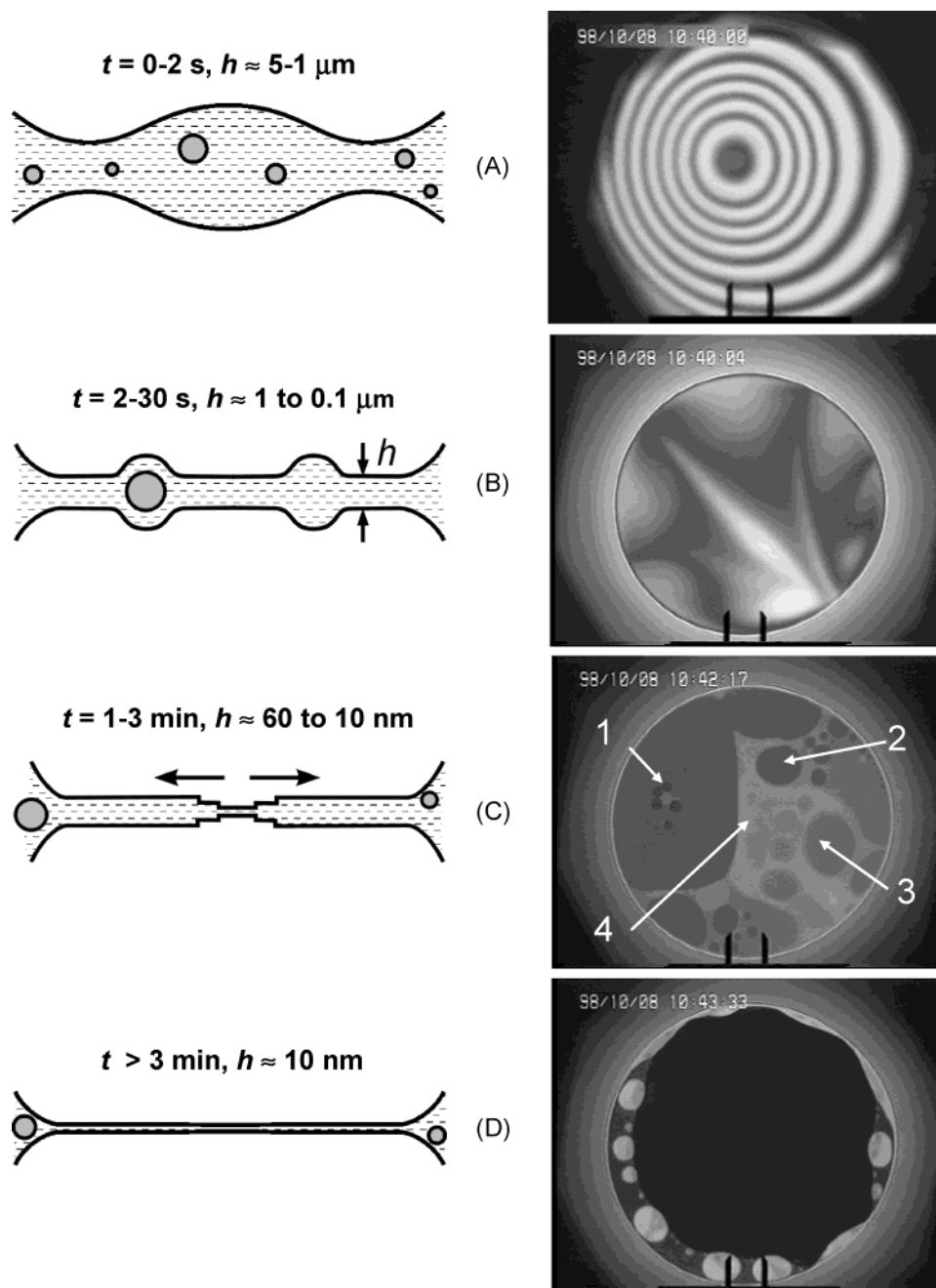


Figure 15. Stages of foam film thinning, as observed in the capillary cell: (A) dimple, lens-shaped film with larger thickness in its center; (B) planar film containing thicker channels; (C) stratification, stepwise film thinning through formation and expansion of thinner (darker) spots, the arrows show film areas containing different numbers of micelle layers, indicated by integers; (D) black film, which does not contain micelles, is finally formed (the mark is 100 μm). The film is formed from 0.1 M SDP3S solution, containing 0.1 wt % predispersed silicone oil.

oil droplets. Figure 15D represents the moment just before the complete occupation of the film area by the final black film (which was stable in the absence of antifoam or in the presence of slow antifoam).

The experiments with large, centimeter-sized vertical foam films (section 2.2.2) also showed⁹ that the initial stage of dimple formation was followed by hydrodynamic instability, which led to liquid outflow and reduction of film thickness down to 1–2 μm within several seconds after film formation. In fact, all experiments, performed with solutions of low molecular mass surfactants of concentration around and below several weight percent, showed that the foam films always thinned very rapidly (within 30 s) to thickness which was smaller than the diameter of the antifoam globules.^{9–16,22} Therefore, the

antifoam globules, trapped in the foam films immediately after film formation, either should break the films at the early stages of their thinning (as the fast antifoams do, Figure 10) or should leave the films soon after film formation with the draining water (slow antifoams; see for illustration Figure 16). The fact that the foams are stable for many minutes in the presence of slow antifoams is a clear indication that the foam destruction in these systems occurs through drop entry in the Plateau channels (see Figure 17 as an illustration of such drop entry event).

4.3. Relation between Entry Barrier, Drop Size, and Height of the Final (Residual) Foam. As explained above, very soon after the foaming agitation stops, the antifoam globules of slow antifoams are expelled from the

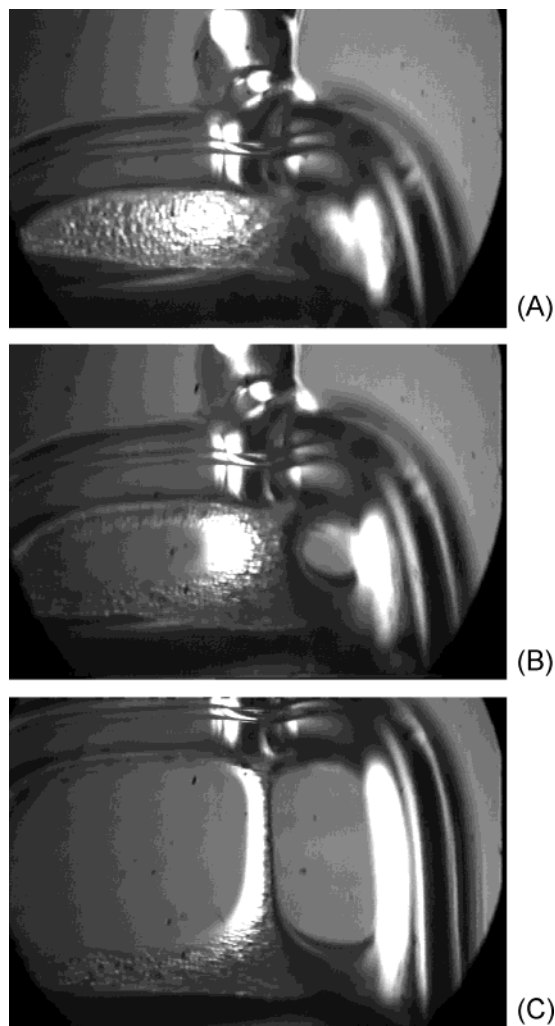


Figure 16. Consecutive images of vertical foam film in the presence of dispersed oil drops: (A) Many oil drops are captured in the film, just after its formation, which is evidenced by the grainy appearance of the film surface. (B) The oil drops leave the foam film and enter into the Plateau channel. (C) The Plateau channel narrows, as a result of water drainage, and traps some of the oil drops. The further evolution of this system is shown in Figure 17. The films are formed on a three-leg frame (Figure 6B), which is withdrawn from 0.1 M SDP3S solution, containing 0.1 wt % predispersed silicone oil.

foam films into the neighboring PBs. As the water drains from the foam, the oil drops are compressed by the PB walls; see Figure 18 for a schematic illustration of these processes. The compressing capillary pressure, P_C^{PB} , gradually increases with time in the upper part of the foam column. When P_C^{PB} becomes higher than the barrier opposing drop entry, the oil drops are forced to enter the PB wall. As illustrated in Figure 17, such an entry can be followed by rupture of the neighboring foam films. The foam would decay, under the antifoam action, until P_C^{PB} , at the top of the shrinking foam, becomes lower than the drop entry barrier or/and until the cross section of the Plateau channels, in the upper part of the foam, becomes larger than the drop diameter. In the current section we apply these ideas to explain and quantify theoretically the height of the residual foam, H_{RES} , observed in the experiments with slow antifoams.^{14,16}

The water drainage from the foam is governed by the interplay between the hydrostatic pressure (which is the driving force for drainage) and the capillary pressure of the walls of the Plateau channels, P_C^{PB} (the latter causes water suction from the surfactant solution into the

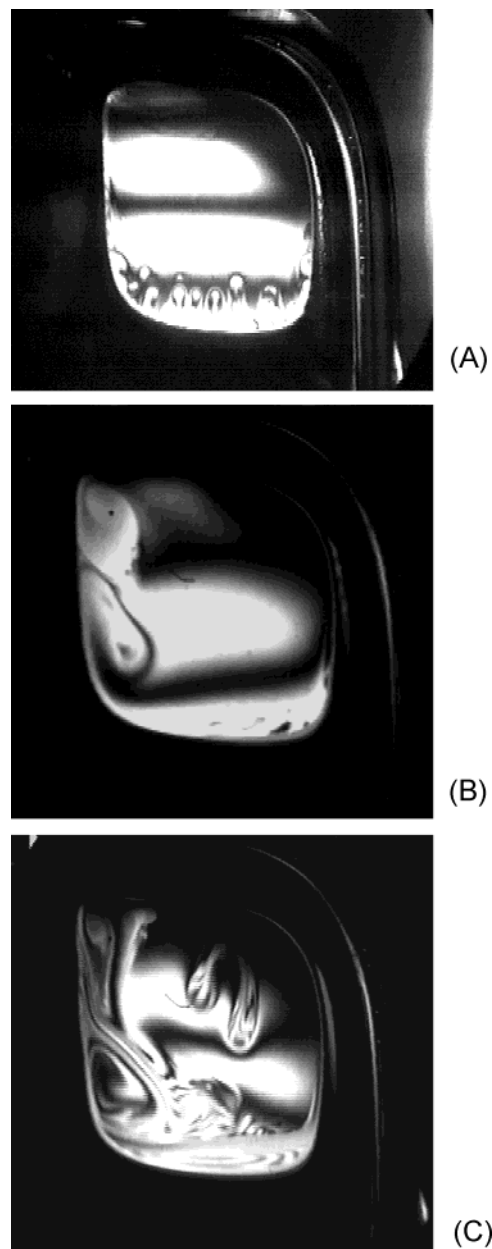


Figure 17. Drainage of a vertical foam film. The experimental conditions are the same, as in Figure 16, except for light illumination, which is adjusted to see the interference pattern of the film here, whereas the oil drops and the Plateau channel are seen in Figure 16. (A) Regular drainage of the foam film. (B) Oil drop enters the air–water interface in the Plateau channel. The spreading oil causes capillary waves with large amplitude and wavelength; note the change in the interference pattern in the left-hand side of the film. (C) The capillary waves develop with time and occupy almost the entire film area; the film ruptures several seconds later. Only one of the three films formed is seen bright in reflected light. The Plateau channel (not well seen, because it appears dark under this illumination), is situated on the left-hand side of the bright film.

foam).^{6,69} A mechanical equilibrium is established when the hydrostatic pressure is counterbalanced by P_C^{PB} . At the top of the foam column, the relationship between P_C^{PB} and the hydrostatic pressure, $\rho g H_F$, can be expressed as^{6,13,22,69}

$$P_C^{PB}(H_F) = \frac{\sigma_{AW}}{R_B} + \rho g H_F \quad (3)$$

where H_F is the foam height, σ_{AW} is the solution surface

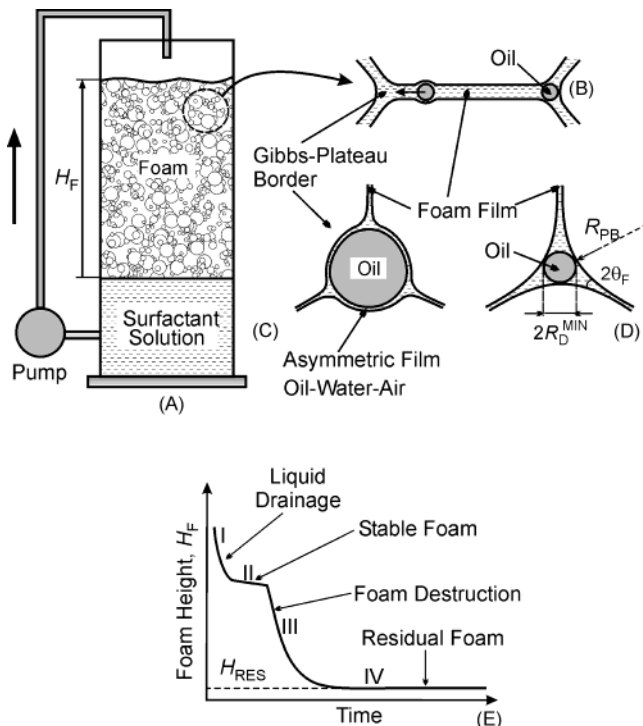


Figure 18. Schematic presentation of foam destruction by the globules of slow antifoams. (A, B) The oily globules rapidly leave the foam films and enter the neighboring Plateau borders (PBs) soon after foam agitation is stopped. (C) Water drainage from the foam leads to gradual narrowing of the PBs. The large drops are compressed by the PB walls, and asymmetric oil–water–air films are formed. When the compressing capillary pressure exceeds the drop entry barrier, P_C^{CR} , the asymmetric film ruptures and the drop enters the PB wall and causes rupture of the neighboring foam films, section 4.3. (D) Drops of radius smaller than R_D^{MIN} remain uncompressed and cannot induce foam destruction. (E) Stages of foam evolution in the presence of slow antifoam, section 4.1.

tension, R_B is the radius of the bubbles at the bottom of the foam column (in contact with the bulk solution), ρ is the mass density of the aqueous phase, and g is the acceleration of gravity. In relatively dry foam, the capillary pressure is related to the radius of curvature of the wall of the Plateau channel, R_{PB} , by the formula^{6,69}

$$R_{PB} = \frac{\sigma_{AW}}{P_C^{PB}} \approx \frac{\sigma_{AW}}{\rho g H_F} \quad (4)$$

Equation 4 predicts that, at equilibrium, $R_{PB} \approx 30 \mu\text{m}$ for foam column with height $H_F = 10 \text{ cm}$, and $R_{PB} \approx 300 \mu\text{m}$ for $H_F = 1 \text{ cm}$ ($\sigma_{AW} = 30 \text{ mN/m}$ and $\rho \approx 10^3 \text{ kg/m}^3$ are used for these estimates).

The radius of a sphere, inscribed in a Plateau channel (i.e., touching its walls, Figure 18D), can be found from geometrical considerations^{13,16}

$$R_D^{MIN}(H_F) = R_{PB}(H_F) \left[\frac{3^{1/2}}{3} \sin\left(\frac{\pi}{6} - \theta_F\right) + \cos\left(\frac{\pi}{6} - \theta_F\right) - 1 \right] \approx R_{PB} [0.155 - 0.577\theta_F^2] \quad (5)$$

where θ_F (expressed in radians) is the half of the contact angle film meniscus (see Figure 18D). Since the foam film thickness, h , is orders of magnitude smaller than R_{PB} , the film is considered as infinitely thin in the derivation of eq 5. In most cases, θ_F is well below $\pi/15 = 12^\circ$, which means that its contribution to eq 5 can be neglected, and a reasonable estimate of R_D^{MIN} is given by the expression^{13,22}

$$R_D^{MIN}(H_F) = \left(\frac{2(3^{1/2})}{3} - 1 \right) R_{PB} \approx 0.155 \frac{\sigma_{AW}}{\rho g H_F} \quad (6)$$

Equation 6 predicts $R_D^{MIN} \approx 5 \mu\text{m}$ for foam column with height $H_F = 10 \text{ cm}$, and $R_D^{MIN} \approx 50 \mu\text{m}$ for $H_F = 1 \text{ cm}$. The notation $R_D^{MIN}(H_F)$ is used in eqs 5 and 6, because this is the minimal radius of a drop, which can be compressed by the walls of the Plateau channels, in a foam column of height H_F .

One sees from eqs 3 and 6 that the compressing capillary pressure P_C^{PB} is higher and R_D^{MIN} is smaller, for taller foam columns. If the oil drops, trapped in the PBs, have entry barrier $P_C^{CR} < P_C^{PB}(H_F)$ and radius $R_D > R_D^{MIN}(H_F)$, then the foam destruction would begin after a certain period of water drainage, because the asymmetric oil–water–air films, formed between the trapped drops and the walls of the Plateau channels, would be unable to resist the compressing pressure (Figure 18C). The foam destruction would continue until the foam height, H_F , becomes so small that $P_C^{PB}(H_F) \approx P_C^{CR}$ (i.e., the asymmetric films become stable) or until the cross section of the Plateau channels becomes larger than the drop size, $R_D^{MIN}(H_F) \approx R_D$ (i.e., the oil drops are not compressed anymore by the PB walls). Therefore, the height of the residual foam, H_{RES} , reached as a result of the foam destruction by antifoam globules (Figure 18E), must be close to the larger of the two estimates

$$H_{RES} = \max\{H_P, H_R\} \quad (7)$$

$$H_P = \frac{P_C^{CR}}{\rho g} \quad (8a)$$

$$H_R = 0.155 \frac{\sigma_{AW}}{\rho g} \frac{1}{R_D} \quad (8b)$$

One can conclude from this analysis that the dimensionless ratio

$$\frac{H_P}{H_R} = \frac{P_C^{CR} R_D}{0.155 \sigma_{AW}} \quad (8c)$$

determines whether H_{RES} is governed by the entry barrier or by the oil drop size. If $(H_P/H_R) > 1$, H_{RES} is determined by the entry barrier—in this case, the oil drops are still compressed, but the asymmetric films are stable. In contrast, if $(H_P/H_R) < 1$, the final foam height is determined by the drop size (the oil drops are too small to be compressed at the end of the foam destruction process), while the entry barrier is of secondary importance.

The relevance of the above estimates to real foams was verified by comparing the predictions of eqs 7 and 8 to experimental results, obtained with a series of surfactant–antifoam pairs.²² The entry barrier, P_C^{CR} , was measured by FTT, H_{RES} was measured in the Ross–Miles test, and the size of the oil drops was determined by optical microscopy. As one can see from Figure 19, the experimental data for H_{RES} vs P_C^{CR} comply very well with the theoretical linear relationship between P_C^{CR} and H_P for

(69) Narsimhan, G.; Ruckenstein, E. Structure, drainage, and coalescence of foams and concentrated emulsions. In *Foams: Theory, Measurements, and Applications*; Surfactant Science Series 57; Prud'homme, R. K., Khan, S. A., Eds.; Marcel Dekker: New York, 1996; Chapter 2.

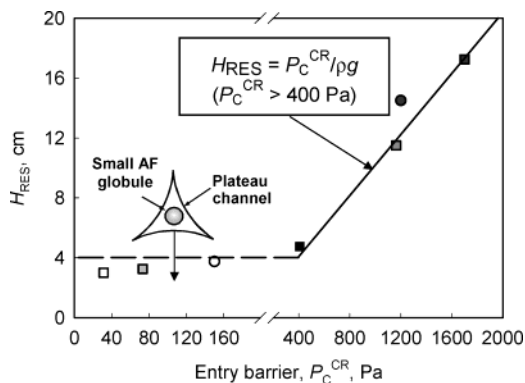


Figure 19. The symbols represent experimental results for the height of the residual foam, H_{RES} (from Ross–Miles test), versus the entry barrier, P_C^{CR} (measured by FTT), with different surfactant–cosurfactant mixtures, containing 0.1 wt % silicone oil as slow antifoam (adapted from ref 22). The continuous line is a theoretical estimate by eq 8a.

$P_C^{CR} \geq 400$ Pa; see the continuous line that is drawn according to eq 8a without any adjustable parameter. This comparison shows that the height of the entry barrier, P_C^{CR} , governs the foam stability for taller foams ($H_F > 5$ cm), in which the PBs are relatively narrow.

On the other hand, at lower entry barriers, the final foam height H_{RES} was almost the same, around 3–4 cm, irrespective of the particular value of P_C^{CR} (see the experimental points below the horizontal dashed line in Figure 19). For these systems, the Plateau channels were too wide to compress the emulsified oil drops in the short foam columns, obtained at the end of the foam destruction process (viz., eq 8b is relevant). Indeed, $R_D \approx 15 \mu\text{m}$ can be estimated from eq 8b for these systems ($H_{RES} \approx 3$ cm), which agrees well with the actual drop size distribution, determined by optical microscopy (between 2 and 20 μm). By comparing the theoretical prediction of eq 8b, $R_D \approx 15 \mu\text{m}$, with the various mean drop radii, determined from the measured size-distribution curves, we found that the volume averaged, geometric mean drop size ($R_{33} \approx 16 \mu\text{m}$ in these experiments) and the volume–surface radius ($R_{32} \approx 12 \mu\text{m}$) can be used as reasonable estimates of R_D in eq 8b. The mean number radius, $\approx 5 \mu\text{m}$, was about three times smaller than R_D , which shows that R_D in eq 8b represents the typical size of the larger oil drops in the size distribution curve, because these drops are most active as antifoam entities.

Equations 7 and 8 predict that one can vary the entry barrier and/or the oil drop size, to control the final foam height in the presence of slow antifoams. Indeed, FTT measurements showed^{13,14,22} that the addition of different cosurfactants, such as dodecanol, betaines, and others, to the main surfactant (SDS or SDP3S) led to significant increase of entry barrier, at fixed total surfactant concentration. In agreement with eq 8a, enhanced foam stability was found in the foam tests.^{13,14} In parallel experiments, the foam stability was found to be higher when the oil was dispersed into smaller drops (at fixed composition of the surfactant solution), just as predicted by eq 8b; see Figure 20 for illustrative results. Further discussion of the foam boosting effect of various cosurfactants is presented in the subsequent section 4.4.

Note that the detailed mechanism of foam destruction, after the globule entry, still remains unclear for slow antifoams. It might be either the bridging- or spreading-aided mechanisms discussed in the literature (see sections 5.1–5.3 below). Furthermore, the entry of a strongly compressed drop in one PB, and the subsequent rupture of the neighboring foam films, could create a strong

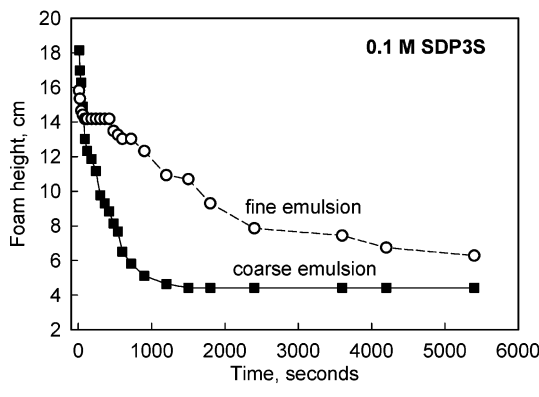
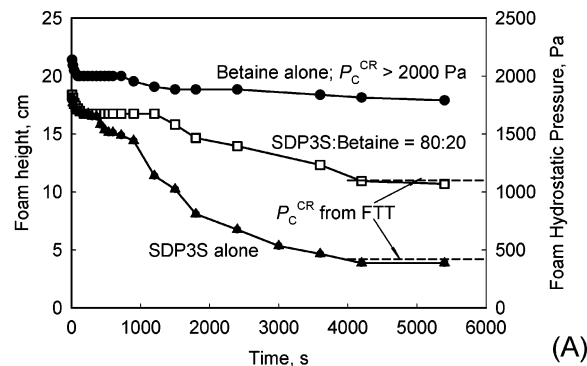


Figure 20. (A) Effect of CAPB (foam booster) on foam stability, in the presence of 0.1 wt % silicone oil as slow antifoam. The basic surfactant is SDP3S, with total surfactant concentration of SDP3S + betaine equal to 0.1 M. The main role of the foam booster is to increase the drop entry barrier, P_C^{CR} , as indicated by FTT measurements. (B) Effect of oil drop size on foam stability for 0.1 M SDP3S solution; the volume-averaged drop diameter was 6 μm in the fine emulsion and about 19 μm in the coarse emulsion (adapted from ref 13).

mechanical shock on the more distant foam films and PBs. This instant release of surface energy can induce entry of other antifoam globules and rupture of other foam films, as a result of the propagating mechanical stress through the foam (avalanche effect). Indications for such an avalanche effect are seen in Figure 14 for BO and IHNP oils, for which we observed a sudden and virtually instantaneous destruction of thousands of bubbles in a single “shot”, apparently triggered by a single drop entry event. Optical observations of the process of drop entry and foam destruction by means of a high-speed camera could be very useful for revealing further details in the action mode of slow antifoams.

4.4. Foam Boosting Effect of Cosurfactants in the Presence of Oil Drops. Amphoteric and nonionic cosurfactants are usually added to the main anionic surfactant in practical formulations, such as detergents, hair/body care, household, and many other surfactant-based products.^{70–75} These additives, called “foam boosters”, can

(70) *Mixed Surfactant Systems*, Surfactant Science Series 46; Ogino, K., Abe, M., Eds.; Marcel Dekker: New York, 1992.

(71) Rosen, M. J. *Surfactants and Interfacial Phenomena*, 2nd ed.; Wiley-Interscience Publication: New York, 1989; Chapter 11. Rosen, M. J.; Hua, X. Y. *J. Colloid Interface Sci.* **1982**, *86*, 164. Rosen, M. J.; Hua, X. Y. *J. Colloid Interface Sci.* **1982**, *90*, 212.

(72) Lomax, E. G., Ed. *Amphoteric Surfactants*; Surfactant Science Series 59; Marcel Dekker: New York, 1996.

(73) Tsujii, K. *Surface Activity: Principles, Phenomena, and Applications*; Academic Press: New York, 1998.

(74) Motomura, K. Thermodynamics of interfacial monolayers. *Adv. Colloid Interface Sci.* **1980**, *12*, 1.

(75) Zoller, U.; Broze, G., Eds. *Handbook of Detergents. Part A: Properties*; Surfactant Science Series 82; Marcel Dekker: New York, 1999.

significantly improve the foaminess, foam stability, and rheological properties of the foam.

In many cases, the foaming solutions contain dispersed oil drops. For example, lanolin, silicone oil, or triglyceride oils are widely used in shampoos, hair conditioners, and some soaps to improve their conditioning properties. The washed grease from the human body, hair or machines, could also get dispersed in the washing solution in the form of oily drops. These oil droplets can significantly deteriorate the foaminess and foam stability, which is a very undesirable effect in many of these systems.

It was shown, in refs 13 and 14, that one of the major roles of foam boosters in solutions, containing oily drops, is to suppress the “antifoam” effect of the oil. By using a combination of several experimental methods (foam tests, optical observations of foams and foam films, film trapping technique, surface tension measurements, and several others) it was demonstrated for SDP3S solutions that:

(1) One can distinguish foam boosters improving mainly solution foaminess (e.g., lauryl acid diethanol amide), foam stability (e.g., lauryl alcohol), or both (e.g., cocoylamide propyl betaine, CAPB).

(2) The obtained very stable foams, in the presence of lauryl alcohol and betaine, were explained with the increased entry barriers of the oil drops by these two cosurfactants.

(3) No correlation was observed between antifoam activity and the values of entry, E , spreading, S , and bridging, B , coefficients; see, e.g., the data for SDP3S, CAPB, and their mixture in Table 2.

(4) The size of the oil drops had an important effect. For example, a significant amount of silicone oil was introduced in the studied foaming solutions without deteriorating foam stability, when the drop diameter was below $5 \mu\text{m}$.^{13,14}

(5) In most of the studied systems, the introduction of foam booster was found to accelerate the foam film thinning, which means that the boosting effect cannot be explained by slower film thinning and water drainage. Lauryl alcohol was the only exception among the studied foam boosters, as it was found to decelerate the final stage of the film thinning process, which was explained by the high surface viscosity of the respective solutions.^{76,77}

All these results could be explained by (and strongly support) the picture of the foam destruction process, described in section 4.3, and the respective estimates of H_{RES} . Further experimental results, which support qualitatively this picture, can be found in the preceding paper by Koczo et al.⁷⁸

One interesting conclusion from these studies^{13,14} was that the choice of an appropriate foam booster, for particular application, strongly depends on the ratio between the onset of foam destruction, t_{ON} , and the time scale of interest. If the time scale of interest is shorter or close to t_{ON} , the foaminess is the most important factor. On the contrary, if the time scale is much longer than t_{ON} , the foam stability is the relevant characteristic (the foaminess being of secondary importance). Since the time scales of interest in the various applications can vary by orders of magnitude (from seconds to hours), appropriate

foam tests and optimization criteria should be chosen in each case to obtain best results from a practical viewpoint.

To illustrate the importance of t_{ON} , we recall the data from the foam tests of SDDBS solutions, in the presence of dodecanol and IHNP, Figure 14. If one is interested in the foam volume at short times, $t < 3$ min, then the conclusion is that IHNP has a foam boosting effect, while dodecanol has a foam suppressing effect, in comparison with the reference surfactant solution without additive. However, if slightly longer times are of interest, $t > 5$ min, then the conclusion is that IHNP has much stronger foam suppressing effect, as compared to dodecanol. Further examples can be found in ref 14.

5. Mechanisms of Foam Film Rupture by Fast Antifoams

5.1. “Bridging–Stretching” Mechanism. The experiments with foam films, in the presence of fast antifoams, showed that practically all films ruptured within several seconds after their formation at a relatively large film thickness.⁹ The millimeter-sized films, observed in the capillary cell, ruptured in the first two stages of film thinning, dimple or thick film with channels (see section 4.2 and Figure 15 for the stages of foam film thinning). The large, centimeter-sized films ruptured almost immediately after their formation, due to the higher probability for trapping large antifoam globules in these films. The foam films, formed from the same surfactant solutions, in the absence of antifoam, thinned down to their final equilibrium thickness and were stable. Therefore, the observed rapid rupture of the foam films was certainly caused by the globules of fast antifoams. As explained in section 3.2, this rapid foam film rupture is related to an ultralow entry barrier of these globules ($P_{\text{C}}^{\text{CR}} < P_{\text{TR}} \approx 15$ Pa). This low entry barrier makes possible the formation of oil bridges, between the foam film surfaces, at the early stages of film thinning.

The shape of the oil bridges was visualized⁹ by using the method of Dippenaar²⁸ (Figure 5B). These observations showed that a biconcave oil bridge was formed in the foam lamella, with the thinnest region being in the bridge center; see Figure 21. The stretching of this bridge in a radial direction, as a result of uncompensated capillary pressures at the oil–water and oil–air interfaces, led to the eventual formation of a thin, unstable oil film in the bridge center. The rupture of this oil film resulted in the perforation of the entire foam lamella. This mode of foam film rupture was termed the “bridging–stretching mechanism”.⁹ An important requirement for realization of this mechanism is the possibility for deformation of the antifoam globule. That is why this mechanism cannot be realized with hydrophobic solid particles. The conditions for having stable or unstable oil bridges in foam films are discussed in section 7 below.

The optical observations of small foam films in reflected light (Figure 5A) revealed⁹ the formation of a characteristic interference pattern, just before the film rupture; see Figure 10A. This characteristic pattern (termed “fisheye”⁹ for brevity) indicated a local reduction of the foam film thickness by 100–300 nm, which was caused by the formation of an oil bridge from an antifoam globule or oil lens. Typically, the foam film ruptured for less than a second after the appearance of the first fish-eye. In most cases, one could unambiguously point out the antifoam globule or the oil lens, which transformed into a bridge, in a certain moment of the film thinning process.

The optical observations showed that the perturbed film region (the fisheye) was localized, 10 to $50 \mu\text{m}$ in diameter,

(76) Poskanzer, A. M.; Goodrich, F. C. Surface viscosity of sodium dodecyl sulfate solutions with and without added dodecanol. *J. Chem. Phys.* **1975**, *79*, 2122.

(77) Patist, A.; Axelberd, T.; Shah, D. O. Effect of long chain alcohols on micellar relaxation Time and foaming properties of sodium dodecyl sulfate solutions. *J. Colloid Interface Sci.* **1998**, *208*, 259.

(78) Koczo, K.; Lobo, L.; Wasan, D. T. J. Effect of oils on foam stability: Aqueous foams stabilized by emulsions. *J. Colloid Interface Sci.* **1992**, *150*, 492.

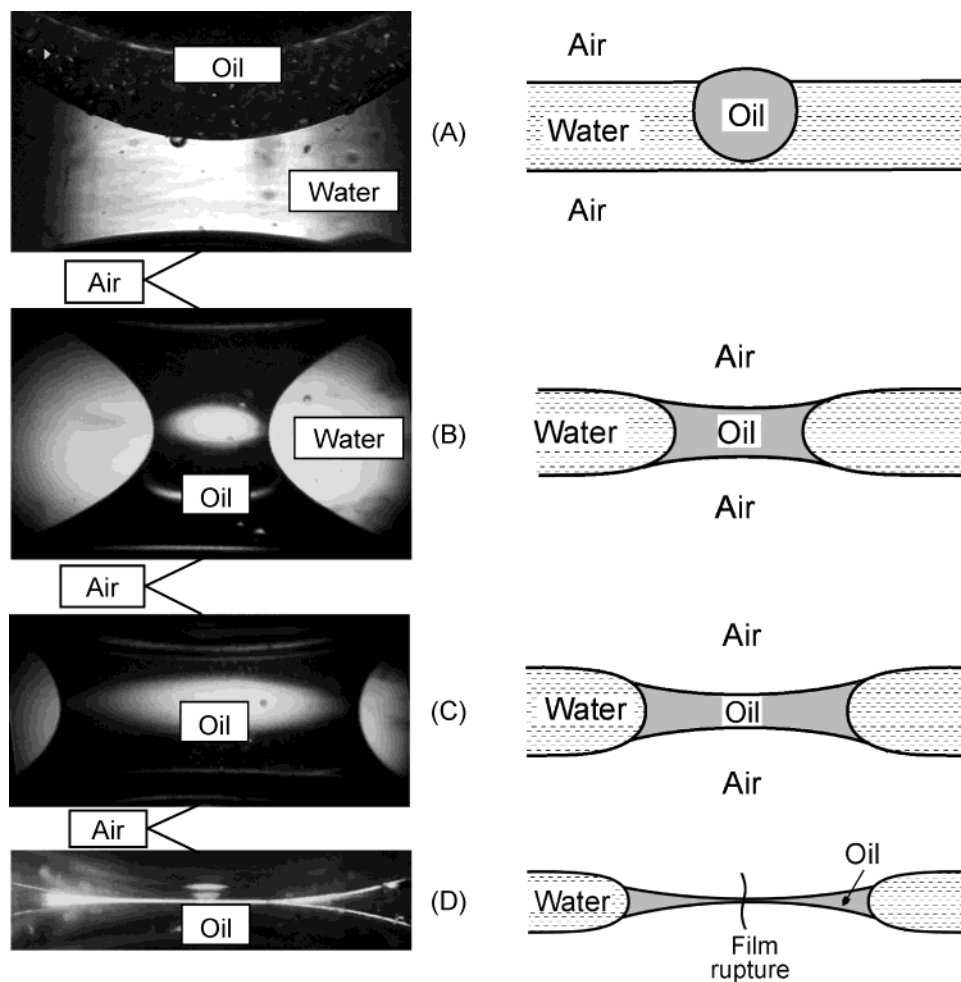


Figure 21. Bridging–stretching mechanism of foam film rupture by fast antifoams—visualization by the Dippenaar method (left-hand side) and schematic presentation (right-hand side). (A–B) Bridging of the foam film surfaces by antifoam globule leads to an oil bridge with nonbalanced capillary pressures at the oil–water and air–water interfaces. (C–D) The bridge stretches with time until a thin, unstable oil film is formed in the bridge center. The rupture of this oil film leads to destruction of the entire foam lamella.

and the rest of the foam film thinned without being noticeably affected by its presence. Note that the perturbed film region was much larger than the actual oil bridge (several micrometers). This means that the fisheye, as seen in the microscope, includes the oil bridge and the deformed surfaces of the foam film around the bridge. The shape of the perturbed film region and the related capillary pressure across the air–water interface were theoretically studied in ref 10 and will not be discussed here.

The optical observations of the foam film rupture, by fast antifoams, revealed an important role of the prespread layer of silicone oil (being only few nanometers thick) on the stability of the foam films.⁹ In the absence of spread oil, most of the antifoam globules left the foam films without making bridges. Even when bridges were formed, they were rather stable. On the contrary, in the presence of the prespread oil layer, the globules readily entered and made unstable bridges, which ruptured the foam films. These experiments showed that the spread oil facilitated the globule entry, by a mechanism explained in section 6.4.2, and destabilized the bridges by a mechanism explained in section 7.4.

5.2. “Bridging–Dewetting” Mechanism. This mechanism implies that once an oil bridge is formed between the two surfaces of the foam film, this bridge is “dewetted” by the aqueous phase, due to the hydrophobic surface of the oily globule (Figure 22C–E). This idea was sug-

gested^{1,36} in analogy with the bridging–dewetting mechanism, which was observed²⁸ with hydrophobic solid particles (section 1.5). One should note, however, that the contact angle solid–water–air (α_{SA} in Figure 3) is smaller than 90° , even for very hydrophobic particles, in the typical surfactant solutions of concentration around and above the cmc.^{25,30–34,52} That is why, a dewetting of hydrophobic particle of *spherical shape* (solid particle or nondeformable oil–solid globule) is improbable in such solutions. In contrast, when the antifoam globule is *deformable* (oil drop or oil–solid mixture with a large excess of oil), it acquires a lens shape after the first entry on one of the film surfaces, Figure 22C. Simple geometrical consideration shows¹ that such a lens can be dewetted by the opposite foam film surface, in the moment of bridge formation, if no significant change of the lens shape takes place during dewetting, Figure 22D,E.

Note that the bridging–dewetting mechanism poses two, somewhat contradictory requirements to the oily globule: the globule should be able to deform after the entry on the first film surface (to acquire the lens shape needed for dewetting), but it should not deform in the time scale of the actual dewetting process. Indeed, if the drop were able to deform in the time scale of the dewetting process (in an attempt to acquire the equilibrium three-phase-contact angles of the antifoam globule with the film surfaces), the dewetting could not be realized, because

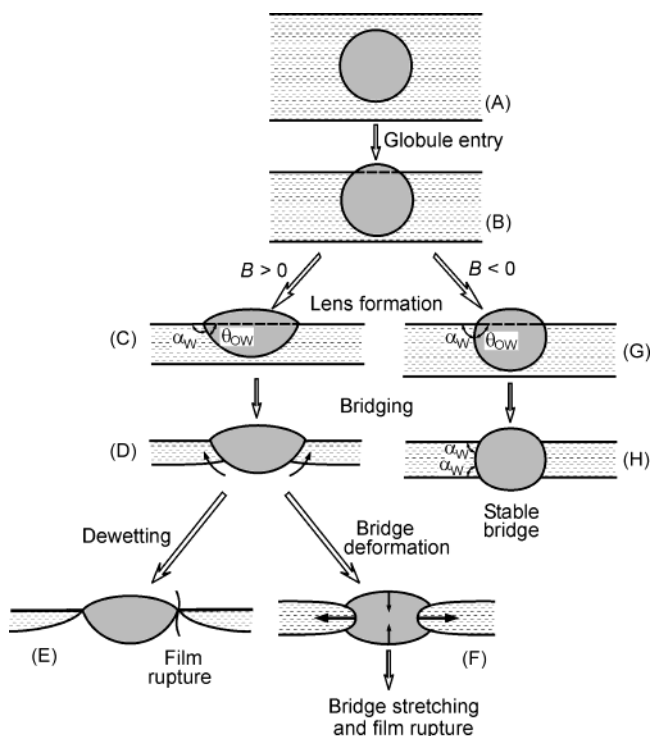


Figure 22. Schematic presentation of the possibilities for foam film destabilization, after bridging the film surfaces by oily globule. If the bridging coefficient $B < 0$, the bridge is stable and no film rupture is effected ($B \rightarrow G \rightarrow H$). If $B > 0$, two different scenarios of foam film rupture are possible: if the process of bridge dewetting is faster than bridge deformation, a bridging–dewetting mechanism could be realized ($C \rightarrow D \rightarrow E$); if the bridge deformation is faster, a bridging–stretching mechanism is realized ($C \rightarrow D \rightarrow F$).

the configuration typical for the bridging–stretching mechanism will occur, Figures 21 and 22F.

In other words, both mechanisms, bridging–stretching and bridging–dewetting, are in principle possible, if the so-called²⁷ “bridging coefficient” B is positive (see section 7.2), and which of these mechanisms would be realized, in a given system, depends on the relative velocities of lens dewetting and lens deformation. At the present time, there is no theoretical model that allows one to predict which of these mechanisms would occur in a system with known physicochemical properties, such as interfacial tensions, oil viscosity, etc. Therefore, only the experiment could answer the question whether bridging–stretching or bridging–dewetting mechanism is realized in a given system.

The bridging–dewetting mechanism has been very often considered in the literature as operative for oil-based antifoams (e.g., refs 5, 30, 32–34, 49, 50). However, the author is not aware of any unambiguous evidence that this mechanism is really responsible for foam film rupture in the case of oil-based antifoams. To a large extent, the popularity of the bridging–dewetting mechanism in the antifoam literature was created by the beautiful and convincing experiments of Dipenaar,²⁸ who demonstrated that hydrophobic *solid* particles (without oil) are indeed able to rupture foam films by this mechanism, in the absence of strong surfactants. However, no analogous experiments with oil-based antifoams have been published. My own attempts to reproduce the Dipenaar experiment, with silicone oil-based antifoams, always resulted in bridging–stretching type of instability (section 5.1 and refs 9 and 10). Therefore, a proof that the bridging–dewetting mechanism is indeed realized in the case of oil-based antifoams is still missing.

On the other hand, there is no any argument to rule out the possibility that this mechanism could be operative in some systems. Systematic experiments with different oils could demonstrate, in the future, realization of a bridging–dewetting mechanism. One of the main experimental difficulties in this aspect is that the process of bridge dewetting is probably much faster than the process of bridge stretching, so that a high-speed camera of superior quality might be needed for such observations.

Note that a bridging–dewetting mechanism is more probable for viscous oils, because the low oil viscosity favors the lens deformation, that is, the configuration corresponding to bridge stretching, Figure 21. Furthermore, if prespread oil layers are present on the two opposite surfaces of the foam film, then the oil bridge would connect these spread layers. In this case, the bridging–stretching mechanism should be operative, because one cannot expect that a spread oil layer will dewet a lens of the same oil. Therefore, the bridging–dewetting mechanism is expected to occur only in the case of viscous, nonspreading oils. In the case of silicone oils, which spread well on the surface of the typical surfactant solutions, the bridging–stretching mechanism is much more probable and is the only one proven so far.

5.3. “Spreading-Fluid Entrainment” and “Spreading-Wave Generation” Mechanisms. The “spreading-fluid entrainment” mechanism was also intensively discussed in the antifoam literature.^{31,52,79–85} According to this mechanism, the effective antifoam contains oil that spreads rapidly over the foam film surface. The oil spreading from the entered antifoam globule/lens is assumed to cause a Marangoni-driven flow of liquid in the foam film (fluid entrainment), resulting in local film thinning and subsequent rupture—see Figure 23. In relation to this mechanism, and following the original works of Ross⁸¹ and Robinson and Woods,⁸⁶ the antifoam efficiency has been often related to the so-called “spreading coefficient”, S (see section 8 below).

Our optical observations, with various systems,^{9–17,20} have never revealed a spreading-fluid entrainment type of foam film destabilization, as drawn in Figure 23. In the experiments with silicone oil-based compounds,⁹ the main observations were in a clear contradiction with this mechanism: We observed rapid rupture of the foam films, when the film surfaces were covered with a prespread layer of oil (hence, spreading and fluid entrainment in the moment of globule entry did not occur). Furthermore, when the film surfaces were free of prespread oil, spreading was indeed observed from the antifoam globules after their entry, but no intensive fluid entrainment was seen and the foam films were very stable. As proven experimentally by Garrett et al.,²⁹ the oil spreading is not a necessary

(79) Aveyard, R.; Binks, B. P.; Fletcher, P. D. I.; Peck, T.-G.; Garrett, P. R. Entry and spreading of alkane drops at the air/surfactant solution interface in relation to foam and soap film stability. *J. Chem. Soc., Faraday Trans.* **1993**, *89*, 4313.

(80) Garrett, P. R.; Moor, P. R. Foam and dynamic surface properties of micellar alkyl benzene sulphonates. *J. Colloid Interface Sci.* **1993**, *159*, 214.

(81) Ross, S. Inhibition of foaming. II. A mechanism for the rupture of liquid films by antifoam agents. *J. Phys. Colloid Chem.* **1950**, *54*, 429.

(82) Ewers, W. E.; Sutherland, K. L. *Aust. J. Sci. Res.* **1952**, *5*, 697.

(83) Shearer, L. T.; Akers, W. W. *J. Phys. Chem.* **1958**, *62*, 1264, 1269.

(84) Prins, A. Theory and practice of formation and stability of food foams. In *Food Emulsions and Foams*; Dickinson, E., Ed.; Royal Society of Chemistry Special Publication 58; Royal Society of Chemistry: London, 1986; p 30.

(85) Jha, B. K.; Christiano, S. P.; Shah, D. O. Silicone antifoams performance: Correlation with spreading and surfactant monolayer packing. *Langmuir* **2000**, *16*, 9947.

(86) Robinson, J. V.; Woods, W. W. *J. Soc. Chem. Ind.* **1948**, *67*, 361.

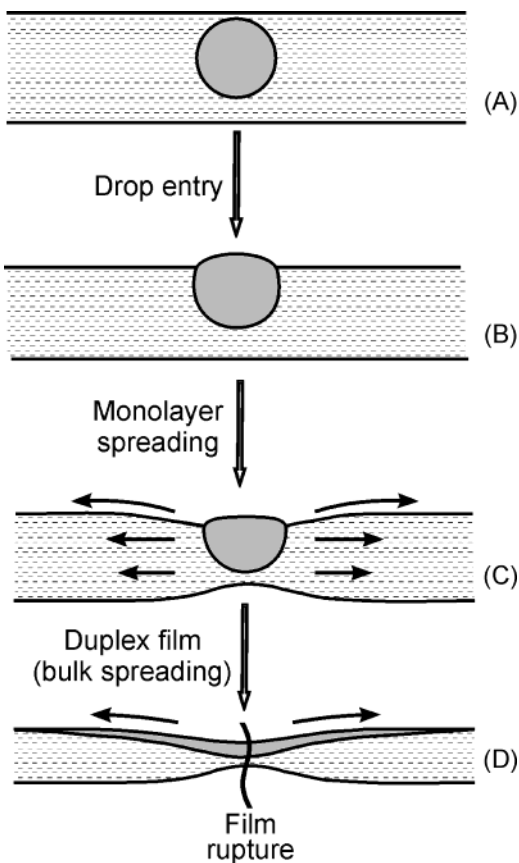


Figure 23. Schematic presentation of the spreading-fluid entrainment mechanism of foam film rupture: an antifoam globule enters the foam film surface (A–B). The oil spreading is assumed to cause a Marangoni-driven flow of water, directed radially from the oil lens, which leads to local thinning of the foam film and its eventual rupture (C–D).

condition for having antifoam activity. Therefore, the spreading-fluid entrainment mechanism, as sketched in Figure 23, remains unproven, though oil spreading can indeed enhance the antifoam activity of oils and compounds, for reasons discussed in section 8 below.

It is worthwhile mentioning that we did observe¹³ foam film rupture, after drop entry and oil spreading, in the experiments with pure silicone oil (no solid particles, slow antifoam) and centimeter-sized foam films; see Figure 17 as example. However, the observed interference pattern in the period between drop entry and film rupture, which lasted several seconds, indicated that the spreading oil created surface waves of large amplitude (hundreds of nanometers) and wavelength (ca. millimeters), which covered almost the entire film surface, rather than local film thinning around the entry spot, Figure 17. These waves eventually led to the observed foam film rupture at relatively large average film thickness, $\approx 1 \mu\text{m}$. No similar phenomena were observed with small, millimeter sized foam films. This process of capillary wave generation on the foam films surfaces, and the respective destabilization mechanism, deserve a detailed theoretical consideration (not attempted so far), because this might be a typical mechanism for rupture of large foam films, in the case of slow antifoam with spreading oil.

It is rather possible that, in these experiments,¹³ the spreading oil partially “sweeps” the adsorbed surfactant from the foam film surfaces, reducing in this way surface elasticity (known to damp the surface waves¹) and creating film regions vulnerable to thinning and rupture, due to lack of sufficiently dense adsorption layer; see Figure 24.

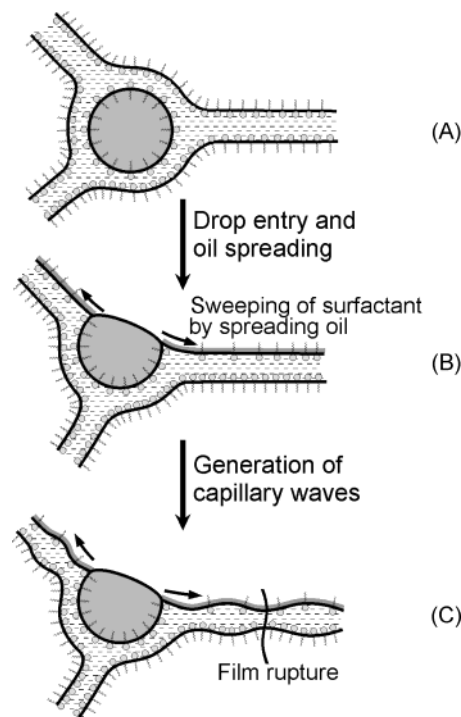


Figure 24. Schematic presentation of the “spreading-wave generation” mechanism, section 5.3. (A, B) Entry of an oil drop in the region of the Plateau channel leads to oil spreading on the surfaces of the neighboring foam films. (B, C) The spreading oil partially sweeps the surfactant from one of the film surfaces, which leads to appearance of capillary waves (cf. Figure 17B,C). The local thinning of the foam film and the loose adsorption layer lead to foam film rupture. The processes of wave generation and film rupture could be facilitated by the asymmetric surfactant and oil distribution on the film surfaces,³⁰ which might lead to surfactant transfer across the film (see section 6.4.1 for the role of mass transfer on film stability).

Therefore, there are at least two interrelated aspects of the effect of oil spreading on foam film destabilization. First, the created capillary waves lead to locally thin regions in the film, so that the film rupture becomes possible at relatively large average thickness of the foam film. Second, the diluted surfactant layers cannot stabilize the local thin spots against rupture, e.g., because of reduced surface charge density on the film surfaces (and, hence, suppressed electrostatic repulsion) and/or due to appearance of attractive hydrophobic forces. An additional factor for foam film destabilization could be the asymmetric surfactant distribution, which appears after oil spreading on only one of the foam film surfaces (see Figure 24B,C and ref 30). Such a mechanism of foam film rupture, mediated by capillary waves, can be more adequately described with the term “spreading-wave generation”, rather than “spreading-fluid entrainment”.

Let us note at the end of this overview of the various possible mechanisms of foam film rupture that the knowledge of the actual mechanism is very important from a practical viewpoint, because the different mechanisms suggest different ways for improving antifoam efficiency. For example, the spreading-aided mechanisms require easy and fast oil spreading (without any apparent requirement for the three-phase contact angle oil–water–air), while the bridging–dewetting mechanism calls for an appropriate three-phase contact angle (without any obvious requirement for oil spreading). In its own turn, the bridging–stretching mechanism requires deformability of the antifoam globules, which means appropriate rheological properties of the antifoam compounds (e.g., low yield stress, optimal viscosity).

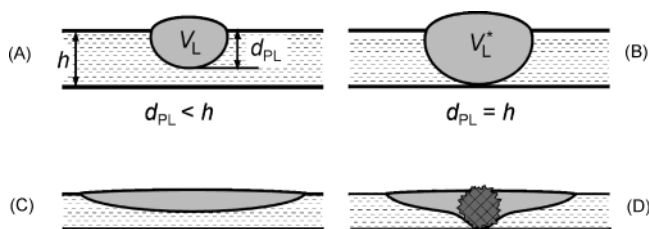


Figure 25. (A) Schematic presentation of an oil lens, with volume V_L , floating on the surface of aqueous film of thickness h . (B) Material contact between the bottom of the lens and the opposite film surface (necessary for bridge formation) is possible when the “penetration depth” of the lens, d_{PL} , is equal to h . The volume of the respective lens is denoted by V_L^* . (C, D) The lens penetration depth can be significantly increased (at the same oil volume) by a solid silica agglomerate, if such is present in the lens.

5.4. Synergistic Effect between Solid Particles and Oil in Antifoam Compounds. One remarkable feature of the fast antifoams is the established strong synergistic effect between oils and hydrophobic particles—properly formulated compounds have much higher efficiency than the individual components taken separately.^{1–6,15,17,21,29,87} Here we briefly outline the main aspects of this synergistic effect; further discussion can be found in sections 6.3 and 7.5.

It is now widely accepted^{1,3,15,18–23,29–33,48,52,80,88} that the main role of solid particles in antifoam compounds is to destabilize the asymmetric oil–water–air films, facilitating in this way drop entry (“pin-effect”). This idea was originally proposed by Garrett¹ and found direct confirmation in the experiments by Koczko et al.⁵³ and Bergeron et al.,⁵² who studied the stability of asymmetric films, formed between a relatively large drop of oil/compound and air–water interface, Figure 7. The experiments demonstrated a substantial barrier, preventing drop entry, when the oil drop contained no solid particles. In contrast, the entry barrier was much lower when the oil drop contained hydrophobized silica particles.

Precise quantification of the effect of solid particles on the entry barrier of real antifoam globules, of micrometer size, was recently achieved²² by using the film trapping technique (FTT). The results confirmed the original idea of Garrett about the pin-effect of solid particles, revealing several additional aspects of the oil particles synergy; see sections 6.2 to 6.4.

Another role of the solid particles, especially in silicone-based antifoams, is to increase the so-called “penetration depth”, d_{PL} , of the oil lenses floating on foam film surfaces (see Figure 25).^{10,36,53} Obviously, material contact between the bottom of the lens and the opposite film surface is a necessary condition for formation of an oil bridge. This contact could occur when the film thickness, h , becomes equal to d_{PL} . Therefore, an increase of d_{PL} would facilitate bridge formation in the early stages of the film thinning process. The presence of silica in the oil lenses can lead to much larger penetration depth (as compared to the lens without silica), especially for silicone oils—this aspect is discussed in more detail in section 7.5.

In some earlier studies it was hypothesized^{36,87} that the main role of the oil in compounds is to modify the surface of the solid particles, rendering it more hydrophobic. This

explanation may be relevant to systems encountered in mineral flotation, because no strong surfactants are used there, and the solid particles are usually in excess with respect to the oil phase. However, this explanation is inappropriate for typical compounds, used in detergency, due to several reasons: (1) The compounds contain only several wt % of solid particles and the oil is in a big excess. Therefore, the typical antifoam globules present oil drops, covered by a loose skin of adsorbed solid particles, rather than solid particles covered by an oil layer. (2) The experiments with silicone oil–silica compounds showed that the antifoams, containing solid particles with concentration above ca. 15 wt %, are inactive because the antifoam globules are nondeformable at such high solid content.^{19,23} Therefore, one very important role of the oil in the antifoaming process is to ensure deformability of the mixed antifoam globules. (3) The contact angles solid–water–air of the particles, used in mixed antifoams, are well below 90° in solutions of typical strong surfactants (like those used in detergency), even when the particles are very well hydrophobized by treatment with silicone oils or silazane reagents.^{8,20,52} One cannot expect that the coating of the particles with thin oil layer would produce significantly larger contact angles (in comparison with those obtained by the currently used procedures of particle hydrophobization) and transform these solid particles into highly active antifoam entities.

In conclusion, the main role of solid particles in compounds is to facilitate the entry of the antifoam globules and to increase the penetration depth of oil lenses, whereas the main role of the oil is to render the antifoam globules deformable (so that the bridging-mediated mechanisms become possible). In addition, the oil spreading may result in reduced entry barriers, via the mechanism explained in section 6.4.2.

5.5. Optimal Globule Size in Emulsions of Fast Antifoams. With respect to antifoam activity, the optimal size of the fast antifoam globules should correspond to the foam film thickness, at which the film rupture is desired.⁹ From this viewpoint, antifoam globules with number mean diameter, d_N , approximately equal to the film thickness several seconds after film formation ($h \approx 2–3 \mu\text{m}$ for typical solutions of low-molecular mass surfactants) are expected to be most active. In addition, the globules should be of sufficiently high number concentration (e.g., 5–10 particles captured in a millimeter-sized foam film) and should have a low entry barrier, $P_C^{CR} < P_{TR} \approx 15 \text{ Pa}$, to destroy efficiently the foam films.

Note that it is not recommended to use particles of much larger diameter (above ca. 30 μm), because the gain in bridging the film surfaces at somewhat earlier stages of film thinning could be overwhelmed by the reduced number concentration of antifoam globules.^{9,3,89} Indeed, if the total antifoam concentration, Φ_A (volume fraction of antifoam in the solution) is fixed, the number concentration of globules, $C_N \approx (6\Phi_A/\pi d_N^3)$, rapidly decreases with the increase of the mean globule diameter, d_N . On the other hand, using particles of smaller diameter (e.g., below 1 μm for typical detergent solutions) would also lead to slower destruction of the foam, because a longer time for film thinning would be required before the antifoam globules could bridge the film surfaces.^{1,52,89,90} Therefore, with respect to the *initial antifoam activity*, the optimal size range of the globules of fast antifoams,

(87) Birtley, R. D. N.; Burton, J. S.; Kellett, D. N.; Oswald, B. J.; Pennington, J. C. The effect of free silica on the mucosal protective and antiflatulent properties of poly(dimethylsiloxane). *J. Pharm. Pharmacol.* **1973**, *25*, 859.

(88) Zhang, H.; Miller, C. A.; Garrett, P. R.; Raney, K. H. Mechanism for defoaming by oils and calcium soap in aqueous systems. *J. Colloid Interface Sci.* **2003**, *263*, 633.

(89) Garrett, P. R. A simple statistical theory for the effect of changes in antifoam concentration on foamability. *Langmuir* **1995**, *11*, 3576.

(90) Pelton, R. A model of foam growth in the presence of antifoam emulsion. *Chem. Eng. Sci.* **1996**, *51*, 4437.

for application in detergency, is expected to be on the order of several micrometers.

One should note, however, that the *antifoam durability* is a much bigger challenge to the antifoam producers in most cases. As explained in refs 9, 11, and 23, the compound exhaustion, in the course of foam destruction, is related to a process of partial segregation of the oil from the silica particles, so that two inactive populations (silica-enriched and silica deprived) are formed. A similar process of oil–silica segregation could occur during compound emulsification (in the process of manufacturing the antifoam emulsion), if the diameter of the antifoam globules becomes comparable to the size of silica agglomerates in the compound (typically ~ 0.1 to several μm). Therefore, the fabrication of antifoam emulsions containing small droplets (1 to several μm) is not recommended, because significant fractions of the antifoam activity and durability are lost during emulsification.⁸ Practical experience shows that the optimal globule size, in antifoam emulsions, is between ca. 5 and 30 μm , which seems to be a good compromise for having both high initial activity and reasonable durability of the antifoam emulsions.

Let us specify that, in the above consideration, the characteristic size of the pre-dispersed antifoam globules is their diameter. However, if the film destruction is caused primarily by lenses of antifoam compound, floating on the foam film surfaces, then the relevant characteristic size is the penetration depth of these lenses, d_{PL} , see section 7.5 for further discussion of this point.

Note that the foam-film thinning could be much slower and the equilibrium film thickness could be much larger, if the foams are stabilized by surface active polymers, such as PVA, di-block copolymers, proteins.^{91–95} Model experiments with single foam films (section 2.2.1) can be used to monitor the film thinning process, and to determine its characteristic time-scale and the equilibrium film thickness. This information can be afterward used to evaluate the optimal size of the antifoam globules in such polymer-stabilized foams.

6. Factors Affecting the Entry Barrier of Antifoam Globules

As explained in sections 3–5, the antifoam activity strongly depends on the magnitude of the entry barrier, which prevents the emergence of pre-emulsified antifoam globules on the air–water interface (viz., the foam film surface or the wall of the Plateau channel). The same barrier is important also for the formation of an oil bridge from a lens, which initially floats on one of the film surfaces. In the current section we introduce the various definitions of the entry barrier, discussed in the literature, and summarize the main experimental and theoretical results, related to the effects of various factors on its magnitude.

6.1. Entry Coefficient. For a long period of time, the antifoam activity was discussed in relation to the so-called

(91) Bergeron, V.; Langevin, D.; Asnacios, A. Thin film forces in foam films containing anionic polyelectrolyte and charged surfactants. *Langmuir* **1996**, *12*, 1550.

(92) Monteux, C.; Williams, C. E.; Meunier, J.; Anthony, O.; Bergeron, V. Adsorption of oppositely charged polyelectrolyte/surfactant complexes at the air/water interface: formation of interfacial gels. *Langmuir* **2004**, *20*, 57.

(93) Stubenrauch, C.; von Klitzing, R. Disjoining pressure in thin liquid foam and emulsion films—new concepts and perspectives. *J. Phys.: Condens. Matter* **2003**, *15*, R1197.

(94) Sedev, R.; Exerowa, D. DLVO and non-DLVO surface forces in foam films from amphiphilic block copolymers. *Adv. Colloid Interface Sci.* **1999**, *83*, 111.

“entry coefficient” (see, e.g., the literature review in ref 1)

$$E = \sigma_{\text{AW}} + \sigma_{\text{OW}} - \sigma_{\text{OA}} \quad (9)$$

The thermodynamic analysis shows^{1,32,79} that negative values of E correspond to complete wetting of the oil drop by the aqueous phase. This means that, even if the oil drop has appeared on the solution surface in some way (e.g., as a result of deposition from the air phase), the drop would spontaneously immerse into the aqueous phase, because this is the thermodynamically favored configuration. Therefore, oil drops with negative E are expected to remain entirely immersed inside the aqueous phase of the foam, rather than to form oil bridges between the surfaces of the foam films or Plateau borders. As a result, oil with negative E (or compound prepared with such oil) is expected to be rather inactive as antifoam.^{1,32,79} In contrast, positive values of E correspond to a well-defined equilibrium position of the oil drop (lens), once the latter appears on the air–water interface. Hence, stable or unstable oil bridges can be formed, when the oil has positive E and the entry barrier is not too high.^{1,31,34}

Critical analysis of the available experimental data, made by Garrett,¹ has shown that positive values of E indeed appear to be a necessary condition for having an effective antifoam, in the sense that negative values of E definitely mean poor (if any) antifoam activity. However, positive values of E do not guarantee high antifoam performance, which is evidence that other factors are of critical importance as well, the entry barrier being one of the most important among them.^{1,3,6,22,32,65,78}

One could make an illustrative analogy of the relation between the entry coefficient, E , and the entry barrier, P_{C}^{CR} , on one side, with the concepts used in chemical kinetics, on the other side. A positive value of E is a thermodynamic condition for existence of an equilibrium position of the oil drop at the air–water interface (and subsequent bridge formation). The entry barrier plays the role of a kinetic barrier, which (if sufficiently high) can preclude the realization of the thermodynamically favored configuration; that is, the drop can remain arrested in the aqueous phase for kinetic reasons.

6.2. Definitions of the Entry Barrier Discussed in Literature. Several quantities were suggested in the literature as measures of the entry barrier for oil drops. Lobo and Wasan⁹⁶ suggested the use of the interaction energy per unit area in the asymmetric oil–water–air film, f_{AS} , as a criterion of its stability

$$f_{\text{AS}} = - \int_{h_{\text{AS}}^{\infty}}^{h_{\text{AE}}} \Pi_{\text{AS}}(h_{\text{AS}}) dh_{\text{AS}} \quad (10)$$

$\Pi_{\text{AS}}(h_{\text{AS}})$ is the disjoining pressure of the asymmetric film and h_{AE} is its equilibrium thickness, at a certain capillary pressure, which has to be specified. In a parallel study, Bergeron et al.⁹⁷ suggested the so-called generalized entry coefficient

$$E_{\text{g}} = - \int_0^{\Pi_{\text{AS}}(h_{\text{AE}})} h_{\text{AS}} d\Pi_{\text{AS}} \quad (11)$$

where the lower limit of the integral corresponds to Π_{AS}^-

(95) Dimitrova, T. D.; Leal-Calderon, F.; Gurkov, T. D.; Campbell, B. Disjoining pressure vs thickness isotherms of thin emulsion films stabilized by proteins. *Langmuir* **2001**, *17*, 8069.

(96) Lobo, L.; Wasan, D. T. Mechanisms of aqueous foams stability in the presence of emulsified nonaqueous-phase liquids: Structure and stability of the pseudoemulsion film. *Langmuir* **1993**, *9*, 1668.

(97) Bergeron, V.; Fagan, M. E.; Radke, C. J. Generalized entering coefficients: A criterion for foam stability against oil in porous media. *Langmuir* **1993**, *9*, 1704.

$(h_{AS} \rightarrow \infty) = 0$. As shown by Bergeron et al.,⁹⁷ the classical entry coefficient, E , can be obtained as a particular case of E_g in the limit $h_{AE} \rightarrow 0$. As seen from their integral definitions, eqs 10 and 11, f_{AS} and E_g are interrelated

$$E_g(h_{AE}) + f(h_{AE}) = -h_{AE} \Pi_{AS}(h_{AE}) \quad (12)$$

Equation 12 can be obtained, for example, by taking the integral in the right-hand-side of eq 10 by parts and comparing the result with eq 11.

The determination of the values of f_{AS} and E_g for real systems, and their comparison with the antifoam efficiency of different oils, is a very difficult task, because one needs to know the disjoining pressure isotherms, $\Pi_{AS}(h_{AS})$. The most thorough analysis of this type was carried out by Bergeron et al.,⁹⁷ who measured the disjoining pressure isotherms of planar foam and asymmetric oil–water–air films, for several surfactant–oil pairs. Bergeron et al.^{97–100} established a good correlation between the asymmetric film stability and the foam stability in the presence of oil. Furthermore, these authors proved that the destabilizing effect of the oil was indeed caused by lower stability of the asymmetric oil–water–air films, as compared to the stability of the foam films.

In our recent studies,^{13–23} we found that the capillary pressure of the air–water interface in the moment of oil drop entry, P_C^{CR} , can be precisely measured by the FTT (section 2.3.2) and used as a quantitative characteristic of the entry barrier in relation to antifoam efficiency. For brevity, we often term P_C^{CR} as the “entry barrier” of given oil or compound. The *critical capillary pressure* of drop entry is indeed a relevant measure of asymmetric film stability, because the capillary pressure is the actual external variable that compresses the film surfaces against each other, against the repulsive surface forces (disjoining pressure) which stabilize the film.

A similar idea had been used before by Khristov et al.,^{6,39,40} to explain the foam collapse in the absence of oil: As shown in refs 39 and 40, the measured foam collapse pressure (which acts as to suck liquid from the foam, Figure 4) was close in magnitude to the capillary pressure for rupture of single foam films, measured by the porous plate method.^{6,67,101–105} One should emphasize that, in the case of *planar* foam or asymmetric films, the capillary pressure in equilibrium is exactly counterbalanced by the disjoining pressure,^{106,107} $P_C = \Pi(h_E)$. That is why the concept of critical capillary pressure, P_C^{CR} , is equivalent to the

concept of critical disjoining pressure, Π^{CR} , for planar films. In contrast, the values of P_C and Π may differ by many orders of magnitude for the asymmetric films, formed between micrometer-sized antifoam droplets and the air–water interface, due to the *curvature* of these asymmetric films.¹⁷ Hence, in the antifoam studies, one can use either of the two quantities, P_C^{CR} or Π_{AS}^{CR} , to characterize the entry barrier, and different information can be obtained by considering one or the other (see section 6.6 below for further discussion of this point).

We found²² that the application of P_C^{CR} as a measure of the entry barrier (determined by the FTT) provides several important advantages in comparison with all other definitions:

(a) P_C^{CR} has clear physical interpretation with respect to the action of antifoam globules—it corresponds to the capillary pressure, which compresses these globules against the air–water interface (foam film surface or wall of Plateau channel) in the actual foams, in the moment of drop entry. Therefore, the value of P_C^{CR} can be easily related to those foam properties (foam height, bubble size, rate of water drainage, etc.), which affect the capillary pressure in real foams. Examples for such relations are presented in sections 3.2 and 4.3.

(b) P_C^{CR} can be measured by FTT for antifoam globules of micrometer size, possibly containing solid particles, like those encountered in practice. Therefore, there is no need of additional hypotheses (often rather speculative) to transfer the conclusions from model experiments to real systems.

(c) A large number of important factors, influencing P_C^{CR} , can be studied by various modifications of the FTT. Numerous examples, such as globule size, oil spreading, hydrophobicity, and concentration of solid particles in the compound, and many others, are discussed in sections 6.2 to 6.5 below (see also refs 17–20, 22, and 23).

(d) Along with the measurements of P_C^{CR} , the visual observation of the antifoam globules in the FTT allows one to study globule morphology (e.g., silica content and position in the globules) and to evaluate globule deformability. These properties are important for realization of the bridging–stretching mechanism (examples for such applications of FTT are described in ref 23).

(e) Last but not least, P_C^{CR} can be measured relatively easy, by using inexpensive equipment, which allows one to obtain a large set of data for a reasonably short period of time.

Note that the interpretation of the experimental data from FTT experiments, in terms of the surface forces stabilizing the asymmetric oil–water–air film (i.e., in terms of Π_{AS}), requires one to calculate first the critical disjoining pressure, Π_{AS}^{CR} , from the measured value of P_C^{CR} . Such calculations can be accomplished, as explained in refs 17, 54, and 108 (see section 6.6 below for illustrative results).

6.3. Effect of the Solid Particles on the Entry Barrier of Compound Globules. 6.3.1. The Pin Effect.

As mentioned in section 5.4, the main role of the solid particles, in mixed antifoams, is to destabilize the oil–water–air films, facilitating in this way the drop entry (“pin effect”).^{1,52,53} The FTT allowed us to quantify precisely the effect of solid particles on the entry barrier and to relate it to antifoam activity.^{18–22}

Some illustrative results, obtained with drops of silicone oil and with globules of silicone oil–silica compounds, are

(98) Aronson, A. S.; Bergeron, V.; Fagan, M. E.; Radke, C. J. The influence of disjoining pressure on foam stability and flow in porous media. *Colloids Surf. A* **1994**, *83*, 109.

(99) Bergeron, V.; Radke, C. J. Disjoining pressure and stratification in asymmetric thin-liquid films. *Colloid Polym Sci.* **1995**, *273*, 165.

(100) Bergeron, V.; Hanssen, J. E.; Shoghl, F. N. Thin-film forces in hydrocarbon foam films and their application to gas-blocking foams in enhanced oil recovery. *Colloids Surf., A* **1997**, *123–124*, 609.

(101) Mysels, K. J. Soap films and some problems in surface and colloid chemistry. *J. Phys. Chem.* **1964**, *68*, 3441.

(102) Mysels, K. J.; Jones, M. N. Direct measurement of the variation of double-layer repulsion with distance. *Discuss. Faraday Soc.* **1966**, *42*, 42.

(103) Exerowa, D.; Kolarov, T.; Khristov, K. Direct measurement of disjoining pressure in black foam films. I. Films from an ionic surfactant. *Colloids Surf.* **1987**, *22*, 171.

(104) Bergeron, V. Forces and structure in surfactant-laden thin-liquid films. Ph.D. Thesis, University of California, Berkeley, 1993.

(105) Claesson, P. M.; Ederth, T.; Bergeron, V.; Rutland, M. W. Techniques for measuring surface forces. *Adv. Colloid Interface Sci.* **1996**, *67*, 119.

(106) Toshev, B. V.; Ivanov, I. B. Thermodynamics of thin liquid films. 1. Basic relations and conditions of equilibrium. *Colloid Polym. Sci.* **1975**, *253*, 558.

(107) De Feijter, J. Thermodynamics of thin liquid films. In *Thin Liquid Films: Fundamentals and Applications*; Ivanov, I. B., Ed.; Marcel Dekker: New York, 1988; Chapter 1.

(108) Hadjiiski, A., Technique for trapping of microscopic particles in liquid films: development and application. Ph.D. Thesis, University of Sofia, Sofia, 2001.

Table 3. Entry Barriers, P_C^{CR} , of Different Antifoams in 10 mM AOT and 1 mM Triton Solutions in the Presence and in the Absence of a Prespread Layer of Silicone Oil^{20,a}

antifoam	spread layer	P_C^{CR} , Pa	
		AOT	Triton
silicone oil	no	28 ± 1	200
	yes	19 ± 2	>200
compound A	no	8 ± 1	30 ± 1
	yes	3 ± 2	5 ± 2
compound B	no	20 ± 5	22 ± 1
	yes	4 ± 1	7 ± 1

^a In foam tests, both compounds (silicone oil–silica mixtures) behave as fast antifoams, the silicone oil acts as slow antifoam, whereas the foam from the reference surfactant solutions (without antifoam) are stable.

presented in Table 3. Two types of experiment were performed—in the presence and in the absence of a prespread layer of silicone oil. The so-called “two-tip procedure”⁹ was used to create solution surface free of spread oil. We consider first the results obtained *with a prespread layer of oil*, because this is the typical case in the foam tests.^{9,11,15,20} As seen from Table 3, the presence of hydrophobic solid particles in the antifoam results in lower entry barriers, as compared to those of pure oil drops. For pure silicone oil in AOT solutions, $P_C^{CR} = 19 \pm 2$ Pa, whereas for the two studied compounds, containing silica, the values are 3 ± 2 Pa and 4 ± 1 Pa, respectively. For Triton X-100 solutions this difference is even larger: the entry barrier for silicone oil is above 200 Pa, whereas it is 5 ± 2 and 7 ± 1 Pa for the two compounds. Note that all values for the studied silica-containing compounds, in the presence of spread oil, are well below 15 Pa, which agrees with their high antifoam activity observed in the foam tests (these compounds acted as fast antifoams in both AOT and Triton solutions).²⁰ In the *absence of the prespread oil layer*, the solid particles also reduce the entry barrier (as compared to pure oil drops), but to a lesser extent; see Table 3. The effect of spread oil on entry barrier is discussed in section 6.4 below.

The mechanistic explanation of the “pin effect” (both in the presence and in the absence of spread oil) has two aspects. First, the sharp edges of the solid particles, adsorbed on the surface of the oil globule, can come in a direct contact with the foam film surface much easier than the drop surface itself, because a repulsive force of lower magnitude has to be overcome.¹ This statement can be illustrated by using Derjaguin’s approximation.¹⁰⁹ According to this approximation, the force between spherical particle and planar surface, F_{PS} , can be expressed by the formula

$$F_{PS}(\delta) = 2\pi R_p \int_{\delta}^{\infty} \Pi_{PS}(H) dH \quad (13)$$

where R_p is the particle radius and $\Pi_{PS}(H)$ is the force per unit area (the disjoining pressure) that would act between two planar surfaces, one of them being the foam film surface and the other one having the same properties as the particle surface, see Figure 26, δ is the distance between the particle forehead and the planar surface, and H is a running variable.

As seen from eq 13, the interaction force is proportional to the particle radius and is, therefore, low in magnitude for small particles. If the solid particle is nonspherical, eq 13 is still applicable, with R_p being the radius of curvature of the particle forehead, which is very small for sharp edges. For typical silica agglomerates of fractal shape, used in antifoam compounds, one can approximate R_p by

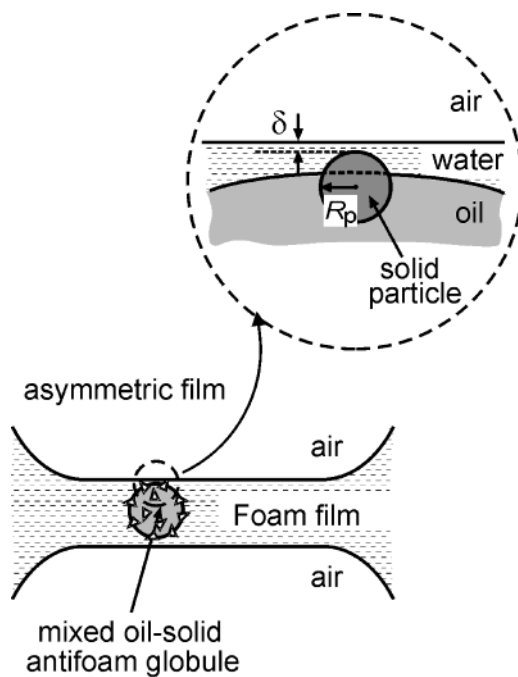


Figure 26. Schematic presentation of the asymmetric oil–water–air film in the presence of solid particle with radius R_p . The interaction force between the solid particle and the foam film surface can be estimated by Derjaguin’s approximation,¹⁰⁹ eq 13.

the radius of the primary silica particles, ~ 5 nm, which is 3 orders of magnitude smaller than the typical size of the antifoam globules, $\sim 5 \mu\text{m}$. Hence, if an antifoam globule is pushed against the film surface by a certain hydrodynamic or gravitation force, the solid particles would come in a direct contact with the foam film surface and will form solid bridges, at much lower in magnitude force, as compared to the entry of the respective oil drop in absence of solids. As explained in the subsequent section 6.3.2, the solid bridges, formed between the oil globule and the foam film surface, can significantly facilitate the oil emergence on the foam film surface (viz., the oil globule entry), if the solid particles have appropriate hydrophobicity.

6.3.2. Role of Particle Hydrophobicity. In recent studies^{18,19} we used the FTT to test how the entry barrier of mixed silicone oil–silica globules depends on the hydrophobicity of the incorporated silica particles. The following procedure was used to gradually increase silica hydrophobicity: initially hydrophilic silica particles were mixed with silicone oil (PDMS), at room temperature, and this mixture was stored for months. Mild stirring at 50 rpm was applied for 4 h every day. Under these conditions, PDMS molecules slowly adsorbed on the silica surface, rendering it more hydrophobic with time. The typical time scale of this hydrophobization process is weeks and months, which makes this system very convenient for studying the effect of silica hydrophobicity on various properties of the antifoam compounds (such as antifoam activity, entry barrier, rheological properties, oil spreading, etc.).^{18,19}

FTT experiments showed^{18,19} a pronounced minimums in the entry barrier of such compounds, as a function of particle hydrophobicity, for solutions of several surfactants; see Figure 27. The observed minimums in P_C^{CR} corresponded to maximums in the compound durability for the respective surfactant solutions (Figure 27), which is another illustration of the important role of the entry

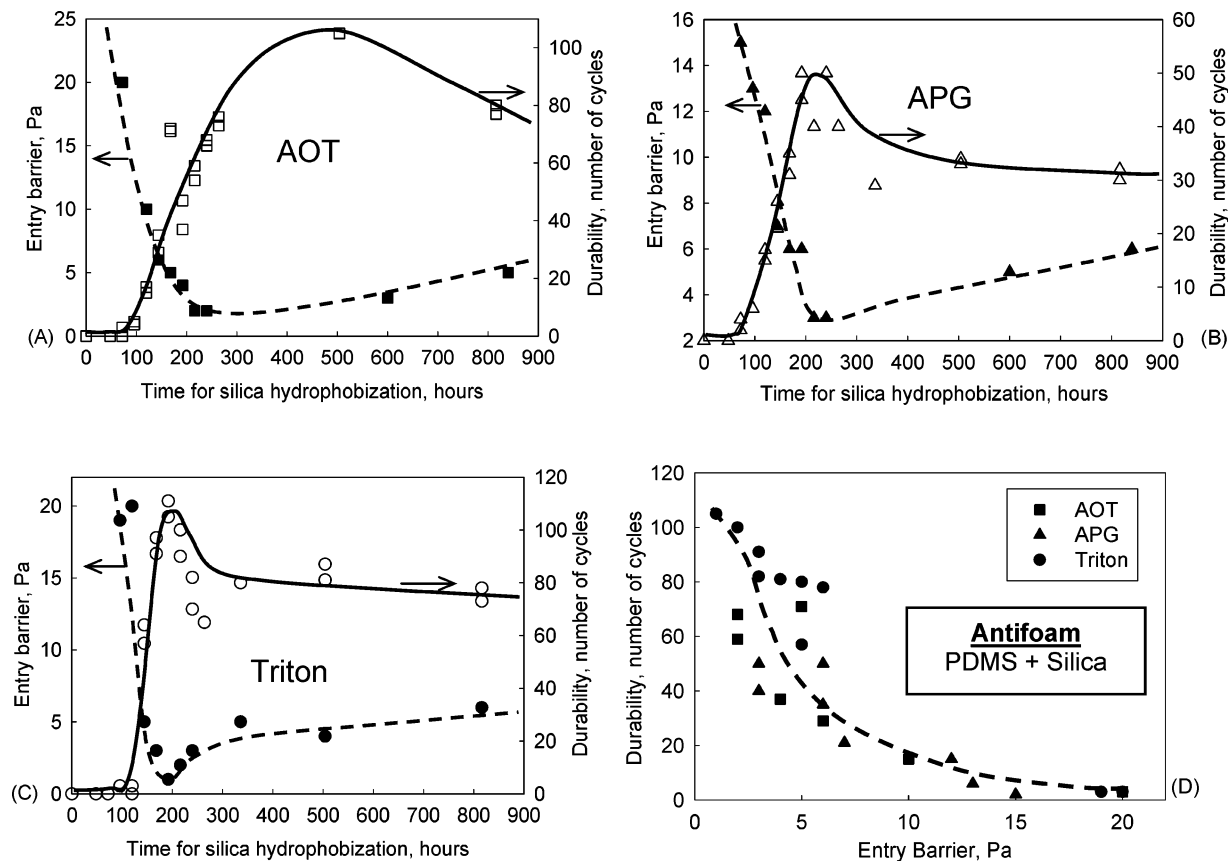


Figure 27. Entry barrier, P_C^{CR} (full symbols), and durability of silicone oil–silica compound (empty symbols), as functions of the time allowed for silica hydrophobization, section 6.3.2. The foam tests and FTT experiments are performed with (A) 10 mM AOT, (B) 0.6 mM APG, and (C) 1 mM Triton X-100 solutions. (D) Summary of these results as a dependence of antifoam durability on entry barrier, P_C^{CR} , for the studied surfactants.¹⁹ The curves are guides to the eye.

barrier in antifoam performance. The automatic shake test (AST) was used in these experiments to evaluate the antifoam durability.

The observed minimum in P_C^{CR} was explained¹⁸ as a result of two requirements, stemming from the main role of the silica particles, namely, to assist the globule entry by rupturing the asymmetric oil–water–air films. The first requirement is that the solid particles should protrude sufficiently deep into the aqueous phase to bridge the surfaces of the asymmetric oil–water–air film; Figure 28. This requirement is better satisfied by more hydrophilic particles.

On the other hand, as shown by Garrett¹ and by Aveyard and Clint,³² the particles should be sufficiently hydrophobic to be dewetted by the oil–water and air–water interfaces and to induce globule entry. These authors^{1,32} considered theoretically the equilibrium configuration of a solid sphere of radius R_p , which bridges the surfaces of the asymmetric oil–water–air film, formed when an antifoam globule approaches the foam film surface, Figure 28. Once such a solid bridge is formed, it might be capillary stable or unstable depending on the hydrophobicity of particle surface. If the three-phase contact angles solid–water–oil, α_{SO} , and solid–water–air, α_{SA} , satisfy the condition

$$\alpha_{SO} + \alpha_{SA} > 180^\circ \Rightarrow \text{complete dewetting of the solid particle (14)} \\ \text{(unstable asymmetric film)}$$

there are no separate equilibrium positions of the three-phase contact lines oil–solid–water and air–solid–water on the particle surface, because these contact lines cannot

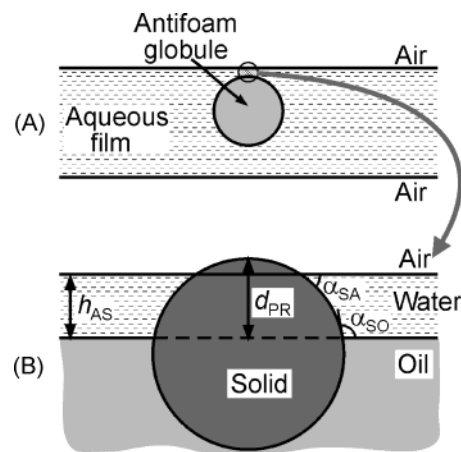


Figure 28. (A) When an antifoam globule approaches the foam film surface, asymmetric oil–water–air film is formed. (B) If the protrusion depth, d_{PR} , of the solid particle is larger than the thickness of the asymmetric film, h_{AS} , and the condition for dewetting, in eq 14, is satisfied, the solid particle pierces the air–water interface and induces asymmetric film rupture (i.e., the particle assists the oil globule entry).

satisfy simultaneously the Young equation (eq 23 below). In this case, the contact lines slide along the particle surface until they coincide, and the solid particle is dewetted by the aqueous phase.¹ In other words, the oil from the drop “uses” the particle as a solid bridge to come in a direct contact with the foam film surface.

On the contrary, if

$$\alpha_{SO} + \alpha_{SA} < 180^\circ \Rightarrow \text{stable asymmetric film (15)}$$

there are well-defined equilibrium positions of the three-phase contact lines,³² which correspond to a certain positive thickness of the asymmetric film, Figure 28B

$$h_{\text{ASP}} = R_{\text{P}}(\cos \alpha_{\text{SO}} + \cos \alpha_{\text{SA}}) \quad (16)$$

In the latter case, the particle facilitates the thinning of the asymmetric oil–water–air film only until the film thickness decreases to h_{ASP} . This means that the solid particle does not induce oil emergence on the surface of the foam film (under quasi-equilibrium conditions) and could even stabilize the asymmetric film by capillary forces, similar to those in particle-stabilized emulsions (the so-called “Pickering emulsions”¹¹⁰). A discussion of the capillary forces, in relation to film stability, can be found in refs 111 and 112.

Equations 14 and 15 suggest that the solid particles, in mixed compounds, should be sufficiently hydrophobic. This idea was sometimes reinforced into the hypothesis that more hydrophobic solid particles should necessarily correspond to more active antifoam compounds.¹¹³ However, as explained above, the particles that are too hydrophobic might have insufficient protrusion depth into the aqueous phase and, hence, the particle-aided globule entry might be impeded (example for such system is described in section 9.2 below and in ref 15). Therefore, an optimal hydrophobicity of the solid particles is expected, at which both requirements, deep protrusion and sufficient hydrophobicity, are satisfied and the entry barrier is the lowest. This theoretical prediction is in good agreement with the experimental results shown in Figure 27.^{18,19}

For spherical particles, one can express the optimal hydrophobicity in terms of an optimal three-phase contact angle solid–water–oil. For this purpose, one can assume that the optimal contact angle is achieved when the protrusion depth of the solid particle, $d_{\text{PR}} = R_{\text{P}}(1 + \cos \alpha_{\text{SO}})$, is equal to the equilibrium thickness of the asymmetric oil–water–air film, h_{AE} . Thus, the optimal contact angle can be estimated to be¹⁸

$$\cos \alpha_{\text{SO}} \approx h_{\text{AE}}/R_{\text{P}} - 1 \quad (17)$$

The above approach to the analysis of the effect of particle hydrophobicity, on the entry barrier of compound globules, was further developed to include the case with spread oil layer on the film surface—section 6.4.2 below.

6.4. Effect of Oil Spreading on Entry Barrier. 6.4.1. Oil Drops. FTT experiments show that, in most systems, the entry barrier of oil drops (free of solid particles) is moderately reduced by the presence of prespread oil.^{17,20,22} An example is presented in Table 3 for the system silicone oil in 10 mM AOT solution—the entry barrier is lower by $\approx 30\%$ in the presence of spread oil. Further examples are presented in Table 4 for drops of decane and dodecane in 2.6 mM solution of the anionic surfactant SDDBS.¹⁷ The data in Table 4 show that the spread oil reduces P_{C}^{CR} at least two times for these oils. However, in the same series of experiments,¹⁷ we observed a 5-fold increase of P_{C}^{CR} for

Table 4. Entry Barriers, P_{C}^{CR} , of Different Oils in 2.6 mM SDDBS Solutions, with and without Prespread Oil Layer on the Solution Surface^{17,22}

oil	P_{C}^{CR} , Pa	
	without spread oil	with spread oil
octane	<i>a</i>	30 ± 2
decane	> 70	35 ± 5
dodecane	96 ± 5	48 ± 5
hexadecane	80 ± 5	400 ± 10

^a Not measured.

hexadecane, when a monomolecular hexadecane layer was spread on the solution surface; see Table 4. These experimental results indicate that there is no general rule about the effect of oil spreading on entry barrier of oil drops, deprived of solid particles.

The molecular mechanism by which the spread oil changes the entry barrier is still poorly understood. One plausible hypothesis for the reduction of the entry barrier in the presence of *multimolecular* spread layer (silicone oil in Table 3, decane and dodecane in Table 4, see also ref 17) is that the surfactant adsorption on the solution surface is reduced. Indeed, if the solution surface is covered with a multilayer of oil molecules, the surfactant adsorption is expected to become similar to that at the oil–water interface. Several studies^{114–116} showed that the surfactant adsorption at the oil–water interfaces is lower in comparison with that at the air–water interface, at equivalent other conditions. Since the film stability depends strongly on the density of surfactant adsorption layers,^{6,66,117,118} one may expect that more dilute adsorption layers, possibly formed on the surface covered with spread oil, should lead to lower stability of the asymmetric film. Though rather reasonable, this hypothesis remains unproven so far.

If the oil spreads by forming a mixed *monolayer* with the surfactant (which is the case with hexadecane in Table 4), then the changes in the adsorption density and film stability are difficult to predict. As shown in a series of papers by Aveyard and co-workers,^{119–121} the density of such mixed oil–surfactant monolayers depends on various factors, such as the chain lengths and the chemical structures of the surfactant and oil molecules. One can speculate that a dense, mixed hexadecane–surfactant monolayer, with higher surface elasticity and/or viscosity, was formed in our system,¹⁷ which resulted in more stable asymmetric films. This hypothesis is also unproven (though being plausible).

(114) Todorova, D. T.; Marinova, K. G.; Gurkov, T. D.; Ivanov, I. B. Dynamic and equilibrium adsorption of ionic surfactant at liquid interfaces. Role of the hydrophobic phase and the salt concentration. *Langmuir*, in press.

(115) Kutschmann, E.-M.; Findenegg, G. H.; Nickel, D.; von Rybinski, W. Interfacial tension of alkylglucosides in different APG/oil/water systems. *Colloid Polym. Sci.* **1995**, *273*, 565.

(116) Gobel, J. G.; Joppien, G. R. Dynamic interfacial tensions of aqueous Triton X-100 solutions in contact with air, cyclohexane, *n*-heptane, and *n*-hexadecane. *J. Colloid Interface Sci.* **1997**, *191*, 30.

(117) Tcholakova, S.; Denkov, N. D.; Ivanov, I. B.; Campbell, B. Coalescence in protein stabilized Emulsions. In *Proceedings 3rd World Congress on Emulsions*, 24–27 September, 2002, Lyon, France.

(118) Tcholakova, S.; Denkov, N. D.; Sidzhakova, D.; Ivanov, I. B.; Campbell, B. Interrelation between drop size and protein adsorption at various emulsification conditions. *Langmuir* **2003**, *19*, 5640.

(119) Aveyard, R.; Cooper, P.; Fletcher, P. D. I. Solubilisation of hydrocarbons in surfactant monolayers. *J. Chem. Soc., Faraday Trans.* **1990**, *86*, 3623.

(120) Aveyard, R.; Binks, B. P.; Fletcher, P. D. I.; MacNab, J. R. Interaction of alkanes with monolayers of nonionic surfactants. *Langmuir* **1995**, *11*, 2515.

(121) Binks, B. P.; Crichton, D.; Fletcher, P. D. I.; MacNab, J. R.; Li, Z. X.; Thomas, R. K.; Penfold, J. Adsorption of oil into surfactant monolayers and structure of mixed surfactant + oil films. *Colloids Surf.* **A 1999**, *146*, 299.

(109) Derjaguin, B. V. *Theory of Stability of Colloids and Thin Liquid Films*; Plenum/Consultants Bureau: New York, 1989.

(110) Aveyard, R.; Binks, B. P.; Clint, J. H. Emulsions stabilised solely by colloidal particles. *Adv. Colloid Interface Sci.* **2003**, *100–102*, 503.

(111) Denkov, N. D.; Kralchevsky, P. A.; Ivanov, I. B.; Wasan, D. T. A possible mechanism of stabilization of emulsions by solid particles. *J. Colloid Interface Sci.* **1992**, *150*, 589.

(112) Nushtaeva A. V.; Kruglyakov, P. M. Capillary pressure in thinning emulsion film stabilized with solid spherical particles. *Kolloidn. Zh.* **2003**, *65*, 341.

(113) Lichtman, I. A.; Sinka, J. V.; Evans, D. W. *Assoc. Mex. Tec. Ind. Celul. Pap. (Bol.)* **1975**, *15*, 2632.

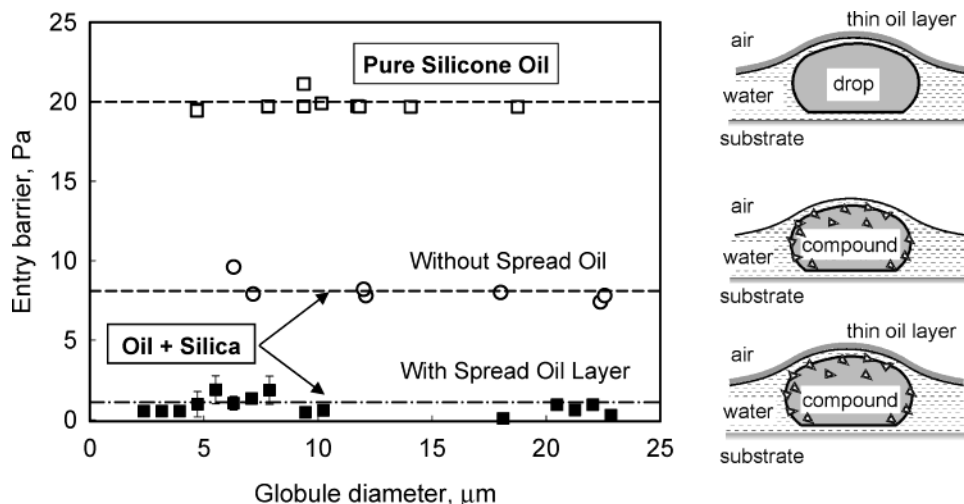


Figure 29. Entry barrier, P_C^{CR} , versus globule diameter for 10 mM AOT solution, containing either drops of silicone oil or globules of PDMS–silica compound. Two types of experiments, with and without spread oil layer, were performed. See Table 3 for additional results and sections 6.3.1, 6.4.2, and 6.5.1 for explanations.

Another possible explanation for the increase of entry barrier, in the presence of spread oil, was suggested in ref 122. The authors assume that the rupture of asymmetric films, in some antifoam systems, is induced by molecular transfer of oil molecules, from the oil drop toward the solution surface, which is supposedly undersaturated with oil. By making a theoretical analysis of the hydrodynamic equations, describing film evolution, Valkovska et al.¹²² showed that such a molecular transfer could indeed destabilize asymmetric films, if the oil has partial solubility in the aqueous phase. A similar idea was used before by Ivanov and collaborators^{123,124} to explain the observed reduced stability of emulsion films, in the presence of surfactant mass-transfer across the film surfaces. In the framework of these concepts,¹²² the higher entry barrier, in the presence of spread oil on the solution surface, is explained by the suppressed mass transfer of oil across the film (no driving force for mass transfer exists when the solution surface is saturated with oil). This mechanism cannot be excluded for some oils and deserves a more detailed experimental check. However, it contradicts the reduction of the entry barrier by the spread oil, which was observed in most of the studied systems.^{17,20} Also, this mechanism is not relevant to oils, which have very low solubility in the aqueous phase, such as the typical silicone oils, used in antifoam formulations.

6.4.2. Compound Globules. Let us compare now the data obtained with and without a prespread oil layer for mixed antifoams (silicone oil plus silica) in AOT and Triton solutions; see Table 3 and Figure 29. For all studied surfactant–compound pairs, the removal of the spread oil resulted in higher entry barriers of the antifoam globules. This increase was particularly important for Triton solutions, because the measured barriers of the studied compounds, in the absence of spread oil, $P_C^{CR} = 30 \pm 1$ Pa and $P_C^{CR} = 22 \pm 1$ Pa, were higher than the boundary separating fast from slow antifoams ($P_{TR} \approx 15$

Pa). Therefore, one could expect that, if the silicone oil did not spread on the surface of Triton solutions, both compounds would not be able to rupture the foam films and, hence, would behave as slow antifoams. Similar is the case with compound B in AOT solutions—this compound has a barrier $P_C^{CR} \approx 20$ Pa without spread oil, which would place it in the group of slow antifoams. For compound A in AOT solution, the barrier differs about three times, 3 ± 2 and 8 ± 1 Pa, but in both cases the barrier is sufficiently low to render this compound very active (fast antifoam).

An interesting conclusion from the above results is that, in many systems, the presence of solid particles is insufficient to reduce the entry barrier below the threshold value, $P_{TR} \approx 15$ Pa, which separates the fast from slow antifoams, unless an oil layer is prespread on solution surface. In other words, many compounds and their emulsions act as fast antifoams, because of the synergistic action of the solid particles, included in the antifoam globules, and the spread oil layer on solution surface. A mechanistic explanation of the observed significant reduction of the entry barrier by spread oil (for compound globules) was given in ref 20 and is briefly reproduced here.

On one hand, the interaction of the solid particles with the foam film surface is expected to depend on a number of factors, which change upon oil spreading (density of surfactant adsorption layer, surface charge density, Hamaker constant characterizing the van der Waals interaction, etc.). However, because the magnitude of the interaction force between the particle and the surface, F_{PS} , is typically small (due to the multiplier R_p in eq 13), one may expect that this effect is unsubstantial and that the formation of solid bridges by small particles does not depend on the presence of spread oil.

On the other hand, as shown in ref 20, the presence of spread oil, on the foam film surface, changes the condition for dewetting of the solid bridges. The optical observations showed that, once the solid particle comes in a direct contact with the air–water interface, oil from the spread layer starts to accumulate in the area of the contact line, forming an oil collar; see Figure 30. The driving force of this process is related to particle hydrophobicity—the displacement of the aqueous phase by oil, on the particle surface, is the energetically favored process. The oil collar acquires an equilibrium shape with contact angle α_{SO} ,

(122) Valkovska, D. S.; Kralchevsky, P. A.; Danov, K. D.; Broze, G.; Mehreteab, A. The effect of oil solubility on the oil drop entry at water–air interface. *Langmuir* **2000**, *16*, 8892.

(123) Dimitrova, B.; Ivanov, I. B.; Nakache, E. Mass transport effects on the stability of emulsion films with acetic acid and acetone diffusing across the interface. *J. Dispersion Sci. Technol.* **1988**, *9*, 321.

(124) Danov, K.; Ivanov, I. B.; Zapryanov, Z. Z.; Nakache, E.; Raharimalala, S. Marginal stability of emulsion thin films. In *Synergetics, Order and Chaos*; Velarde, M. G., Ed.; World Scientific: London, 1988; p 178.

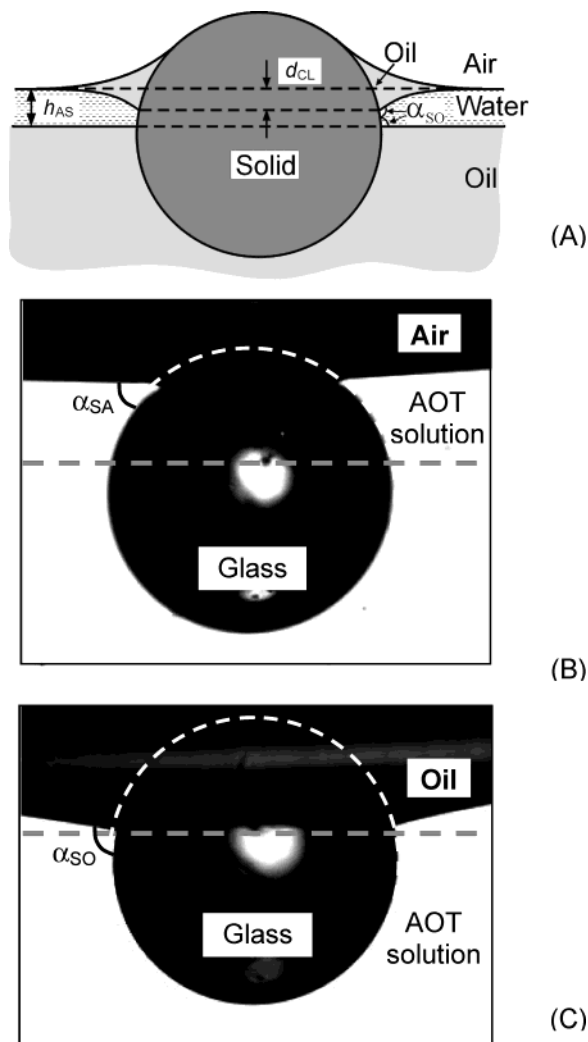


Figure 30. (A) Schematic presentation of the formation of an oil collar after a hydrophobic solid particle pierces the air–water interface, which is covered by a layer of spread oil. The entry of the oil from the antifoam globule depends on the contact angle, α_{SO} (see eq 18), and on the volume of the oil collar. (B) Photograph of a hydrophobic glass sphere, attached to air–water interface in the absence of spread oil. (C) Photograph of the same particles after spreading of silicone oil on the solution surface. Note the formation of the oil collar and the subsequent change of the three-phase contact angle on the particle surface.²⁰ The horizontal dashed lines in (B) and (C) indicate where would be the position of flat oil–water and air–water interfaces, as shown in Figure 28B.

and the lower end of the collar slides along the particle surface with the oil accumulation.²⁰

The penetration depth of the collar below the level of the air–water interface, d_{CL} , can be calculated by using the Laplace equation of capillarity, if the three-phase contact angles and the volume of the oil collar are known. Such detailed calculations have not been made so far, but one can predict, on the basis of simple scaling arguments, that d_{CL} is larger when the contact angle, α_{SO} , and the collar volume are larger. Note that the fluid surfaces of the oil collar are concave, which means that the pressure (and thereby the chemical potential) in the oil collar is reduced, as compared to the pressure in a bulk oil phase. Therefore, the collar can “suck in” oil (and, hence, increase in size) from the spread oil layer and/or from distant oil lenses, by the mechanism described in section 7.4 in relation to the effect of spread oil on oil bridge stability.

From geometrical consideration it is obvious that when d_{CL} becomes larger than h_{ASP} (defined by eq 16) the two separated oil phases, in the antifoam globule and on the solution surface, should coalesce and a globule entry would be effected.²⁰ A necessary condition for realization of this process is

$$\alpha_{SO} > 90 \Rightarrow \text{complete dewetting in the presence of spread oil (unstable asymmetric film)} \quad (18)$$

In other words, the condition for oil entry, mediated by solid particles, is eq 18 in the presence of spread oil (at sufficiently large volume of the oil collar), instead of eq 14, which is applicable in the absence of spread oil.

Experiments with hydrophobized glass particles in the presence of strong surfactants, above the cmc, showed^{20,25,52} that, typically, $\alpha_{SO} \approx 130\text{--}150^\circ > 90^\circ$, while $\alpha_{SA} \approx 30\text{--}70^\circ < 90^\circ$. This means that eq 18 is always satisfied with hydrophobic particles, whereas eq 14 might be unsatisfied for typical antifoams in detergent solutions. Therefore, in the latter systems, the presence of spread oil on the foam film surfaces should lead to strong reduction of the entry barrier, at other equivalent conditions. This theoretical conclusion agrees very well with the experimental results shown in Table 3.²⁰

6.5. Effect of Other Factors on the Magnitude of Entry Barrier. 6.5.1. Globule Size. FTT experiments with various systems showed²² that, in general, P_C^{CR} monotonically decreases with the increase of drop size. In many systems this trend is very weak (e.g., the results shown in Figure 29) and can be neglected for the size range of typical antifoam globules, whereas in some systems this effect is very pronounced. The results, obtained so far, suggest that the drop-size effect is more significant at higher surfactant concentration and in the absence of solid particles; see Figure 31 for illustration. A clear explanation of these experimental trends is still missing. The observed differences between the various systems are certainly related to the different types of surface forces, which stabilize the asymmetric films and, possibly, to different mechanisms of asymmetric film rupture. For example, in the absence of solid particles, the electrostatic and van der Waals forces between the film surfaces are expected to dominate at surfactant concentrations around and slightly above the cmc, whereas the oscillatory structural forces (created by surfactant micelles) prevail at higher surfactant concentrations.^{3,24,47,67,68,96} In the presence of solid particles, the film stability is probably governed by capillary forces.^{110–112} No theoretical approaches are available to analyze the effect of film size on film stability for most of these interactions. One exception is the case of oscillatory structure forces, for which Kralchevsky et al.¹²⁵ showed theoretically that larger in diameter films should be less stable with respect to thinning, which is in qualitative agreement with the experimental results (e.g., the upper curve in Figure 31).

6.5.2. Surfactant Concentration. The effect of surfactant concentration on the magnitude of entry barrier was studied by FTT for hexadecane drops in SDDBS solutions.¹⁷ As expected, the entry barrier was found to increase with the surfactant concentration; see Figure 32. At concentrations well below the cmc, the entry barrier

(125) Kralchevsky, P. A.; Nikolov, A. D.; Wasan, D. T.; Ivanov, I. B. Interaction of colloid particles in thinning foam films. Formation and expansion of dark spots. *Langmuir* **1990**, *6*, 1180.

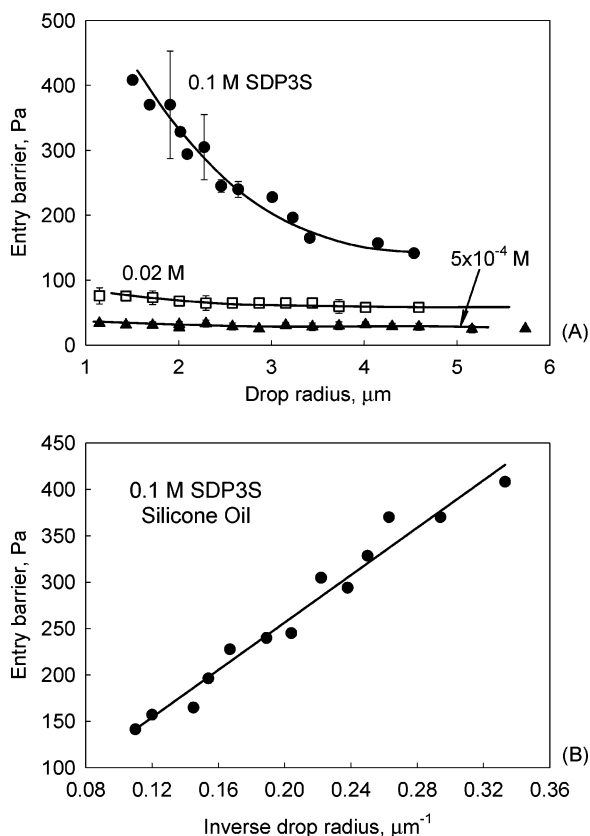


Figure 31. (A) Entry barrier of silicone oil drops, as a function of drop radius, R_D , at three different SDP3S concentrations. (B) The data for 0.1 M SDP3S, plotted versus the inverse drop radius, $1/R_D$.

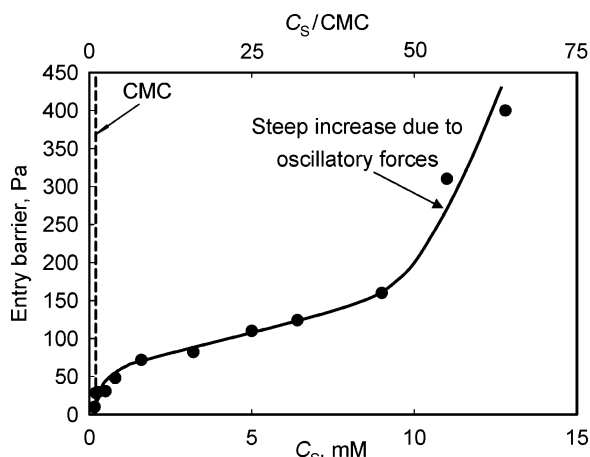


Figure 32. Entry barrier of hexadecane drops, P_C^{CR} , as a function of SDDBS concentration, C_S . P_C^{CR} was measured by FTT, with drops having approximately the same equatorial radius, $R_E = 2.25 \pm 0.25 \mu\text{m}$. The two-tip procedure⁹ was used to create surface without spread oil before starting the FTT experiment (adapted from ref 22).

was extremely low and could not be measured, because the oil droplets spontaneously entered the solution surface before starting the actual FTT experiment. Around the cmc, the entry barrier increased in a stepwise manner, reflecting the saturation of the surfactant adsorption layers at the air–water and oil–water interfaces. Slow increase of P_C^{CR} was observed with the surfactant concentration in the range between the cmc and ca. $40 \times \text{cmc}$, followed by a much steeper increase at higher surfactant concentrations, where the oscillatory structural forces were operative. A more detailed discussion of these results

is presented in ref 17. Further experimental and theoretical studies of this effect could be of significant help to better understand the forces, which control the stability of the asymmetric films, and the mechanisms of asymmetric film rupture.

6.5.3. Chemical Nature of the Oil. The entry barrier of oil drops, free of solid particles, was found to depend very strongly on the chemical nature of the oil phase (at equivalent other conditions). Comparative experiments were performed¹⁷ with solutions containing 2.6 mM SDDBS and eight different oils: octane, decane, dodecane, hexadecane, dodecanol, silicone oil, 2-butyltolanol (BO), and isohexyl neopentanoate (IHNP); see Tables 1 and 4. Only the results in the presence of spread oil are discussed here, because this is usually the case in the actual foaming systems (except upon intensive agitation during foaming, when the rate of surface generation could be faster than the rate of oil spreading).

The experimental results demonstrate that the entry barrier increases with the molecular mass of *n*-alkanes: for octane $P_C^{\text{CR}} = 30 \pm 2$ Pa, for decane 35 ± 5 Pa, for dodecane 48 ± 5 Pa, and for hexadecane it is 400 ± 10 Pa. Such a significant increase of the entry barrier with the alkane chain length is certainly important for the antifoam action, but systematic foam tests, aimed to clarify the relation between entry barrier and the antifoam activity of alkanes, are missing. The explanation for the observed difference in the entry barriers of the studied *n*-alkanes is also missing. It could be related to different densities of the surfactant adsorption layers on the surface of the oil drops and/or to different spreading behavior of these oils (and, hence, to different structure and density of the adsorption layers on the air–water interface). No experimental results are available, at the present moment, to support or reject any of these hypotheses.

Experiments with drops of 1-dodecanol and silicone oil revealed¹⁷ very high entry barriers, above 1500 Pa (Table 1). Not surprisingly, the foam tests showed¹⁶ that these oils did not destroy the foam, although the entry, spreading, and bridging coefficients were strongly positive for the silicone oil (cf. the data in Table 1 with the results from the foam tests, shown in Figure 14). In contrast, the entry barriers of BO and IHNP were relatively low and, in agreement, these two oils had a pronounced antifoam effect in the studied solutions. More detailed discussion of these results, along with some possible explanations for the different entry barriers of these oils, are presented in ref 17.

6.6. Critical Disjoining Pressure for Rupture of the Asymmetric Oil–Water–Air Film. The *critical capillary pressure*, P_C^{CR} , is a very convenient quantity for characterization of the entry barrier from a practical viewpoint (see section 6.2). However, for analysis of the entry barrier, with respect to the surface forces stabilizing the asymmetric oil–water–air film, one should consider the *critical disjoining pressure*, $\Pi_{\text{AS}}^{\text{CR}}$. In this section, we briefly present some results about the dependence of $\Pi_{\text{AS}}^{\text{CR}}$ on the size of the asymmetric films and discuss this dependence in relation to the mechanism of film rupture.^{17,22}

By definition, the disjoining pressure, Π_{AS} , accounts for the interactions between the film surfaces (van der Waals, electrostatic, steric, etc.) and is conventionally defined as a surface force per unit area.^{24,109,126} Positive disjoining pressure corresponds to prevailing repulsive surface forces (i.e., to film stabilization) and vice versa. Explicit expressions for the various components of the disjoining pressure

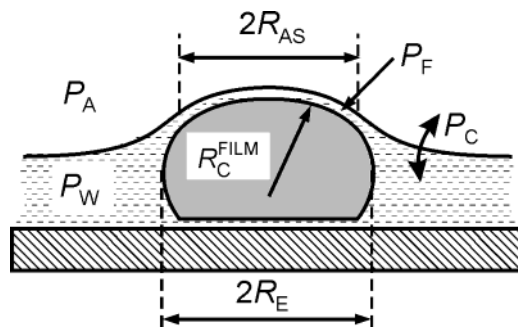


Figure 33. Schematic presentation of an oil globule, trapped in wetting film (FTT). This scheme introduces the different film radii, R_{AS} and R_C^{FILM} , used in section 6.6.

can be found in the literature^{24,109,126,127} and will not be reproduced here.

In the case of *planar* liquid films, the condition for mechanical equilibrium (corresponding to certain equilibrium film thickness, h_{AE}) requires the capillary sucking pressure to be exactly counterbalanced by the disjoining pressure. However, in the case of micrometer oil drops, compressed against an air–water interface, the thin films are *strongly curved* and the condition for mechanical equilibrium is more complex, because it accounts for the capillary pressure jumps across the curved film surfaces. The relevant theoretical approach to this configuration was developed by Ivanov et al.,^{54,128} who showed that the disjoining pressure, Π_{AS} , is related to the capillary pressure across the water–air interface, P_C , by the expression

$$\Pi_{AS} \equiv P_F - P_W = (P_F - P_A) + (P_A - P_W) = \frac{2\sigma_{AW}}{R_C^{FILM}} + P_C \quad (19)$$

where P_F is the pressure in the asymmetric oil–water–air film and R_C^{FILM} is its radius of curvature (see Figure 33).

For micrometer-sized drops, R_C^{FILM} is of the order of the drop radius and, hence, the term $(2\sigma_{AW}/R_C^{FILM}) > 10^4$ Pa. In most of our systems $P_C \leq 10^3$ Pa, which means that P_C can be neglected in the right-hand side of eq 19. Thus only the radius of film curvature, R_C^{FILM} , would be sufficient to calculate Π_{AS} , because σ_{AW} is known. Note that R_C^{FILM} depends on drop deformation, which in its own turn is affected by the applied capillary pressure, P_C . For large drops or bubbles, one can measure R_C^{FILM} by using the method of differential interferometry.¹²⁹ However, this method cannot be applied to micrometer-sized films. That is why, an indirect method was used in ref 17 to estimate the magnitude of Π_{AS} from the accessible experimental data and to study how the critical disjoining pressure for drop entry, Π_{AS}^{CR} , depends on the size of the asymmetric films. Briefly, a numerical procedure was used to reconstruct the shape of the trapped oil drop and of the contiguous water–air meniscus from the accessible experimental data (capillary pressure P_C , equatorial drop radius R_E , and interfacial tensions σ_{AW} and σ_{OW}). From

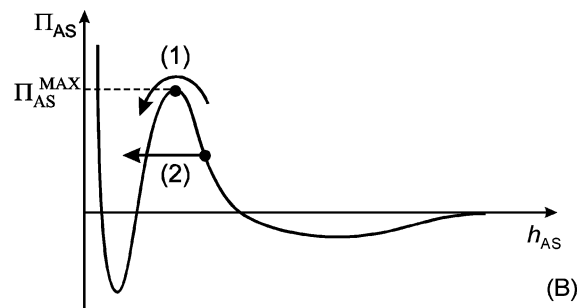
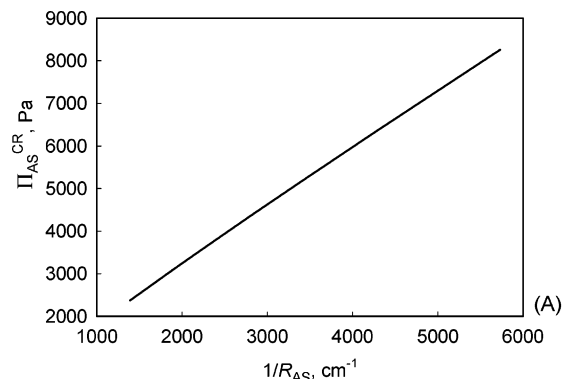


Figure 34. (A) Dependence of the critical disjoining pressure, Π_{AS}^{CR} , on the inverse radius of the asymmetric film, $1/R_{AS}$, as determined by FTT with hexadecane drops in 3.2 mM SDDBS solution.¹⁷ (B) Schematic presentation of the disjoining pressure isotherm $\Pi_{AS}(h_{AS})$. Two possible ways for overcoming the barrier and possible film rupture are indicated: (1) The film surfaces are compressed against each other by capillary pressure, which drives the system to surmount the barrier Π_{AS}^{MAX} —in this case the critical disjoining pressure Π_{AS}^{CR} should be equal to Π_{AS}^{MAX} and independent of film radius. (2) Local fluctuation in the film leads to formation of an unstable spot and film rupture. In this case, the film rupture may occur at a critical disjoining pressure $\Pi_{AS}^{CR} < \Pi_{AS}^{MAX}$ and Π_{AS}^{CR} could depend on film radius.

the drop shape, Π_{AS}^{CR} and the radius of the asymmetric film, R_{AS} , in the moment of film rupture, were calculated.¹⁷

The data interpretation for different systems showed an almost linear dependence of Π_{AS}^{CR} on the inverse radius of the asymmetric film, R_{AS} . As an illustration, we show this dependence in Figure 34 for hexadecane drops in 3.2 mM SDDBS solutions. Similar linear dependence of Π_{AS}^{CR} vs $1/R_{AS}$ was obtained with variety of systems, like protein stabilized oil drops and antifoam globules comprising silicone oil and silica (unpublished results).

The observed dependence of Π_{AS}^{CR} on $1/R_{AS}$ is by no means a trivial fact. Indeed, the disjoining pressure $\Pi_{AS}(h_{AS})$ is not expected to depend on either the film diameter or film curvature, because the film thickness, h_{AS} , is at least 2 orders of magnitude smaller than both R_{AS} and R_C^{FILM} . Therefore, if the film rupture were accomplished by surmounting a maximum in the isotherm $\Pi_{AS}(h_{AS})$ (e.g., over an electrostatic barrier, as in the classical DLVO theory¹⁰⁹), then the rupture event would be expected to occur always at $\Pi_{AS}^{CR} = \Pi_{AS}^{MAX}$ for a given system, independently of drop size.

The most probable explanation of the experimentally observed dependence of Π_{AS}^{CR} vs R_{AS} is that the film rupture occurs by passing below the barrier Π_{MAX} (Figure 34B). Such a possibility was demonstrated experimentally by Bergeron¹³⁰ for planar foam films. He showed with millimeter-sized films that, in some systems, the measured Π^{CR} was approximately equal to the calculated height of

(126) Ivanov, I. B., Ed.; *Thin Liquid Films: Fundamentals and Applications*; Marcel Dekker: New York, 1988.

(127) Israelachvili, J. N. *Intermolecular and Surface Forces*, 2nd ed.; Academic Press: London, 1992.

(128) Ivanov, I. B.; Kralchevsky, P. A. Mechanics and thermodynamics of curved thin films. In *Thin Liquid Films: Fundamentals and Applications*; Ivanov, I. B., Ed.; Marcel Dekker: New York; Chapter 2.

(129) Nikolov, A. D.; Kralchevsky, P. A.; Ivanov, I. B. Film and line tension effects on the attachment of particles to an interface. III. A differential interferometric method for determination of the shapes of fluid surfaces. *J. Colloid Interface Sci.* **1986**, *112*, 122

(130) Bergeron, V. Disjoining pressures and film stability of alkyltrimethylammonium bromide foam films. *Langmuir* **1997**, *13*, 3474.

the electrostatic barrier in the curve $\Pi(h)$, while in other systems Π^{CR} was well below the maximum of the theoretical curve. Bergeron¹³⁰ assumed that, in the latter case, the film ruptured as a result of lateral fluctuations in the adsorption surfactant layers, which led to formation of unstable spots in the foam films. The possibility for film rupture through fluctuations, without overcoming the barrier in the $\Pi(h)$ curve, was discussed also in other theoretical models,^{125,131} but no explicit expressions are available to describe the experimentally observed dependence of $\Pi_{\text{AS}}^{\text{CR}}$ on film size. Further experimental and theoretical work is needed to reveal the actual mechanism of asymmetric film rupture and to develop an adequate model for theoretical calculation of $\Pi_{\text{AS}}^{\text{CR}}$.

7. Stability of Oil Bridges in Foam Films

As explained in section 5, the foam film destruction by fast antifoams involves formation and rupture of oil bridges; see Figures 21 and 22. In sections 7.1–7.3 we consider the stability of these oil bridges, by using the theory of capillarity. The effects of the solid particles (possibly present in the oil phase) and of the spread oil layer are discussed in sections 7.4 and 7.5, respectively.

7.1. The Laplace Equation of Capillarity, the Neumann Vectorial Triangle, and the Young Equation. According to theory of capillarity (see, e.g., refs 7, 24, and 132), the equilibrium shape of fluid interfaces obeys the Laplace equation, which relates the capillary pressure across the interface, P_C , with the interfacial curvature

$$P_C = \sigma(1/R_1 + 1/R_2) \quad (20)$$

Here σ is interfacial tension (oil–air, oil–water, or water–air), while R_1 and R_2 are the two principle (local) radii of curvature of the respective interface. Note that, in principle, R_1 and R_2 could be negative, or positive, or have different signs, at a given point of the interface. In the case of axi-symmetric systems (e.g., an idealized oil bridge in foam film)

$$1/R_1 = d \sin \varphi / dr; \quad 1/R_2 = \sin \varphi / r \quad (21)$$

where $\varphi(r)$ is the running slope angle of the interface and r is the distance to the axis of symmetry; see Figure 35A. For axi-symmetric systems, the Laplace equation can be represented by a set of two ordinary differential equations, whose solution $z(r)$ describes the interfacial shape.^{7,24,132} The effect of gravity is neglected in eq 20, because the oil bridges are of micrometer size, and the estimate shows that gravity pressure, $P_G \sim \rho g d_B \sim 0.1$ Pa, is much smaller than the capillary pressure, $P_{OW} \sim \sigma_{OW} / d_B \sim 10^3$ Pa (d_B is the bridge size taken $\sim 10 \mu\text{m}$ in this estimate).

The mechanical equilibrium of the system requires also a balance of the surface tensions, acting on the three-phase contact lines; see Figure 35B. For fluid phases, this requirement is represented by the Neumann vectorial triangle

$$\sigma_{\text{AW}} + \sigma_{\text{OW}} + \sigma_{\text{OA}} = 0 \quad (22)$$

where the vectors σ_{AW} , σ_{OW} , and σ_{OA} have magnitudes equal

(131) Kaschiev, D.; Exerowa, D. Nucleation mechanism of rupture of newtonian black films. I. Theory. *J. Colloid Interface Sci.* **1980**, *77*, 501.

(132) Princen, H. M. The equilibrium shape of interfaces, drops and bubbles. Rigid and deformable particles at interfaces. In *Surface and Colloid Science*, Matijevic, E., Ed.; Wiley-Interscience: New York, 1969; Vol. 2, p 1.

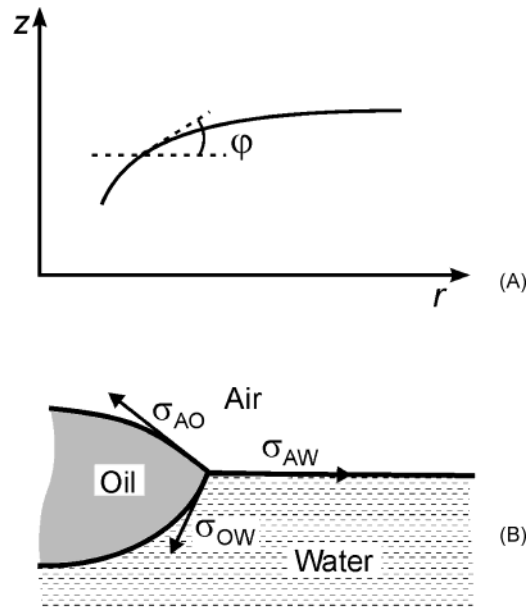


Figure 35. (A) Notation used to describe the shape of an interface with axial symmetry: $\varphi(r)$ is the running slope angle and r is the distance to the axis of symmetry. (B) Schematic presentation of a three-phase contact line oil–water–air. The mechanical equilibrium of the system requires a vector balance of the interfacial tensions, acting on the three-phase contact line.

to the respective scalar interfacial tensions. These vectors are oriented to be simultaneously tangential to the respective interface and perpendicular to the three-phase contact line. The Neumann triangle relates the magnitudes of the interfacial tensions with the three-phase contact angles, at the contact line. From a mathematical viewpoint, the Neumann triangle provides the boundary conditions for solving the Laplace equation of capillarity for the various fluid interfaces.

In the general case, at negligible gravity, the fluid interfaces could be planar ($\Delta P = 0$; $1/R_1 = 1/R_2 = 0$), spherical ($R_1 = R_2 \neq 0$), cylindrical ($1/R_1 = 0$, $R_2 \neq 0$), or the surface generatrix could be part of catenoid ($\Delta P = 0$, $R_1 = -R_2 \neq 0$), nodoid, or unduloid.^{7,132} Explicit expressions for these functions can be found in refs 7, 24, and 132. Theoretical analysis, made in ref 10, shows that the interfacial shape, in the case of oil bridges (deprived of solid particles) in foam films, is spherical for the oil–air interface and planar or nodoid for the air–water interface. Various shapes are possible for the oil–water interface (sphere, catenoid, nodoid, or unduloid) depending on the three-phase contact angles, foam film thickness, and bridge volume; see Figure 36.

If one of the surfaces is solid (e.g., the surface of solid particle), one should use the Young equation, instead of the Neumann vectorial triangle, to describe the mechanical equilibrium at the three-phase contact line. For solid particle, attached to the air–water or oil–water interface, the respective Young equations read (see Figure 37)

$$\sigma_{\text{SA}} = \sigma_{\text{SW}} + \sigma_{\text{AW}} \cos \alpha_{\text{SA}} \quad (23a)$$

$$\sigma_{\text{SO}} = \sigma_{\text{SW}} + \sigma_{\text{OW}} \cos \alpha_{\text{SO}} \quad (23b)$$

where the angles α_{SA} and α_{SO} are defined through the aqueous phase.

7.2. Garrett's Model. Bridging Coefficient. The analysis of film destabilization by oil bridges is much more difficult, as compared to the case of solid particles (section

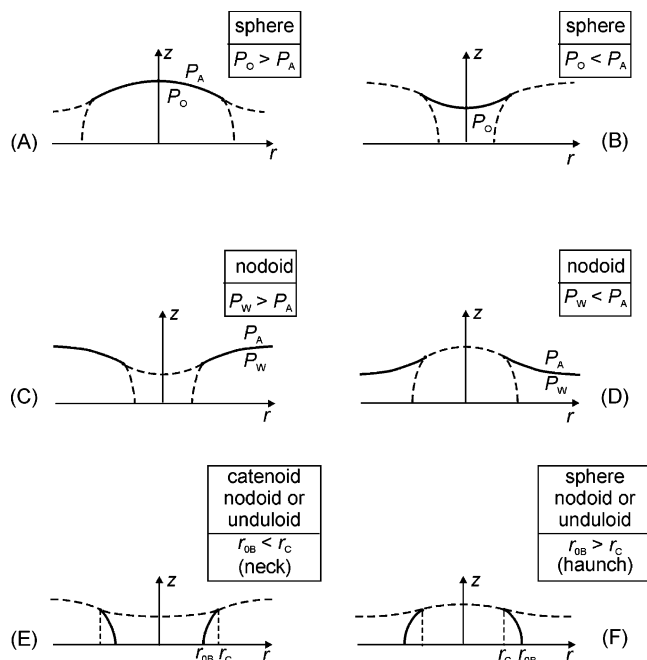


Figure 36. Schematic presentation of the different possible shapes of the oil–air (A and B), air–water (C and D), and oil–water (E and F) interfaces, for oil bridges in foam films.¹⁰

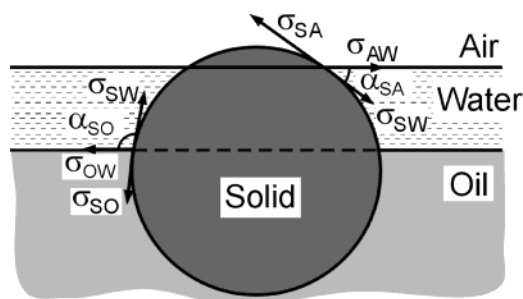


Figure 37. Schematic presentation of solid particle, bridging the surfaces of the asymmetric oil–water–air film. The respective contact angles and interfacial tensions are shown.

1.5), due to the variety of possible shapes of the fluid interfaces. Garrett^{1,27} was the first who made a detailed theoretical study of the stability of oil bridges in foam films, in relation to antifoaming. He analyzed whether an oil bridge could be in mechanical equilibrium, when placed in an imaginary foam film with perfectly planar surfaces, Figure 38. To assess the bridge stability, Garrett assumed that the Neumann triangle was satisfied at the three-phase contact lines oil–water–air and then he checked whether the capillary pressure jumps across the oil–air and oil–water interfaces, P_{OA} and P_{OW} , can be balanced.

This analysis showed that, if the contact angle oil–water–air, α_W , is larger than $\pi/2$ (which is equivalent to $\theta_{OW} \equiv \pi - \alpha_W < \pi/2$, in Garrett's notation), the capillary pressure across the oil–water interface, $P_{OW} \equiv P_O - P_W$, is always smaller than the capillary pressure across the oil–air interface, $P_{OA} \equiv P_O - P_A$. This means that it is impossible to satisfy simultaneously the Neumann triangle and the capillary pressure balance, which are both necessary conditions for mechanical equilibrium in the system. Therefore, the oil bridge was considered²⁷ as unstable and causing foam film rupture in systems with $\alpha_W > \pi/2$; Figure 38A. In contrast, Garrett found that it was possible to satisfy both the Neumann triangle and the pressure balance when $\alpha_W < \pi/2$ (equivalent to $\theta_{OW} > \pi/2$) and these bridges were considered as stable. Hence,

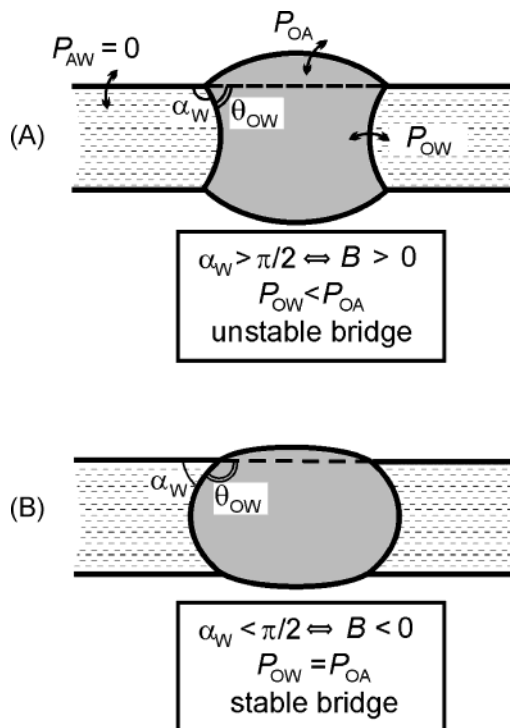


Figure 38. Schematic presentation of an oil bridge, placed in foam film with planar surfaces, according to Garrett's model:^{1,27} (A) unstable bridge with positive bridging coefficient, $B > 0$ ($\alpha_W > 90^\circ$; $\theta_{OW} < 90^\circ$); (B) stable bridge with negative bridging coefficient, $B < 0$ ($\alpha_W < 90^\circ$; $\theta_{OW} > 90^\circ$).

no significant antifoam effect of the oil is expected in these systems, even if oil bridges are formed in the foam films, Figure 38B.

Furthermore, Garrett²⁷ showed that the geometrical requirement $\alpha_W > \pi/2$ is equivalent to the condition $B > 0$, where B is the so-called *bridging coefficient*

$$B \equiv \sigma_{AW}^2 + \sigma_{OW}^2 - \sigma_{OA}^2 > 0 \quad (24)$$

which can be calculated from the respective interfacial tensions. It can be proven theoretically that positive values of the bridging coefficient, B , necessarily mean positive entry coefficient, E , while the reverse statement is not true.^{7,79}

In conclusion, Garrett's analysis predicts that positive values of B correspond to unstable bridges (i.e., to foam film rupture) and vice versa.

7.3. Further Development of Garrett's Model. An important feature of Garrett's model is that the surfaces of the foam film are assumed to be perfectly planar. As a result of this approximation, the capillary pressure across the air–water interface, $P_{AW} \equiv P_A - P_W$, is equal to zero. This assumption was dismissed in a later model, in which the foam film surfaces were considered as deformable.¹⁰ This modification made the model much more complex. The bridge shape and stability were found to depend not only on the three-phase contact angles but also on the bridge volume, V_B , and on the foam film thickness, h . To analyze this dependence, it is convenient to scale the actual bridge volume, V_B , by the volume of an imaginary oil drop, with diameter equal to film thickness¹⁰

$$V_0 = \frac{\pi}{6} h^3 \quad (25)$$

With respect to antifoaming, liquid bridges of volume V_B

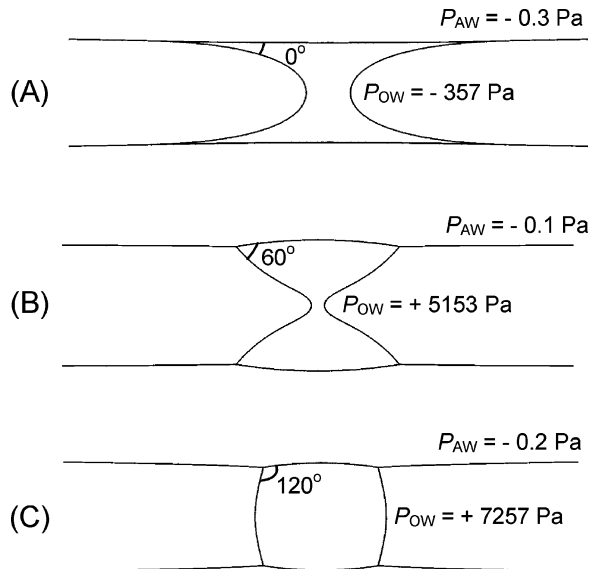


Figure 39. Equilibrium shape of oil bridges with different contact angles water–oil–air: (A) $\alpha_0 = 0^\circ$; (B) $\alpha_0 = 60^\circ$; (C) $\alpha_0 = 120^\circ$. The dimensionless bridge volume is $V_B/V_0 = 1$. Adapted from ref 10.

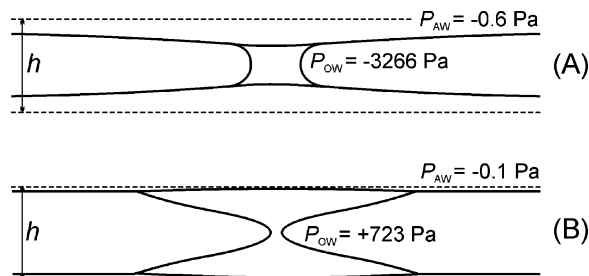


Figure 40. Shape of equilibrium oil bridges with positive bridging coefficient, $B > 0$, at different bridge volumes: (A) $V_B/V_0 = 0.3$; (B) $V_B/V_0 = 5$ (adapted from 10). The bridge in (A) is stable, whereas the bridge in (B) is in unstable equilibrium. The contact angles are $\alpha_w = 164^\circ$ and $\alpha_o = 20^\circ$ for both bridges; h indicates the thickness of the nonperturbed foam film away from the bridge.

$\geq V_0$ are of primary interest (otherwise, the oil drop is too small to make a bridge).

The theoretical analysis, performed in ref 10, showed that the oil bridges can acquire equilibrium shape, with satisfied Neumann triangle and balanced capillary pressures, for both positive and negative values of the bridging coefficient, B . These equilibrium shapes usually include a certain deformation of the air–water interface, which was neglected in the original Garrett's model (section 7.2). As an illustration, we show in Figure 39 theoretically calculated shapes of three oil bridges (along with part of the contiguous foam film) at: (A) $\alpha_w = 180^\circ$ and $\alpha_o = 0$, (B) $\alpha_w = 130^\circ$ and $\alpha_o = 60^\circ$, and (C) $\alpha_w = 73^\circ$ and $\alpha_o = 120^\circ$. Note that the values of B for the bridges shown in Figure 39A,B are positive, because $\alpha_w > 90^\circ$. The dependence of the equilibrium shape of a bridge on its volume, at fixed all remaining parameters, is illustrated in Figure 40 for $\alpha_w = 164^\circ$ and $\alpha_o = 20^\circ$.

The analysis performed in ref 10 revealed that some of the equilibrium bridge shapes correspond to stable equilibrium, whereas others correspond to equilibrium, which is unstable (i.e., corresponding to local maximum of the system energy). The stable bridges would tend to restore their equilibrium shape if subjected to small mechanical perturbations (e.g., vibrations, local change of the foam film thickness, etc.), because this shape corresponds to a

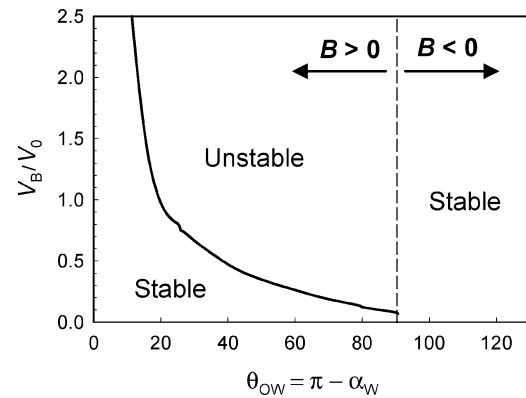


Figure 41. Map of the regions of stable and unstable bridges. V_B/V_0 is the dimensionless bridge volume (adapted from ref 10).

local minimum of the system energy.^{133,134} In contrast, the unstable configurations are in equilibrium, which is vulnerable to any small perturbation of the system, just as in the classical example of a ball placed on the top of smooth hill. Any small perturbation is able to displace the unstable bridge from the position of mechanical equilibrium and to lead to eventual destruction of the bridge and of the entire foam film. Therefore, the complete theoretical analysis of foam film stability requires one to specify the regions of stable and unstable equilibrium bridges.

The numerical analysis revealed¹⁰ that the bridge stability depends mainly on two factors: on the value of the three-phase contact angle α_w (or on the angle $\theta_{ow} = \pi - \alpha_w$ in Garrett's notation) and on the ratio V_B/V_0 ; see Figure 41. In summary, the calculations with the detailed model¹⁰ showed that, at $B > 0$, the large bridges are always in unstable mechanical equilibrium, whereas the small bridges could be in stable or unstable equilibrium, depending on the three-phase contact angles and bridge volume, Figure 41. Only stable bridges exist at $B < 0$, as predicted by the original model of Garrett.²⁷

It is important to note that Figure 41 suggests the possibility for transition of a given bridge from the region of stable bridges into the region of unstable ones, following two different pathways. First, the reference volume, V_0 , decreases with the process of film thinning, which leads to an increase of the ratio V_B/V_0 at fixed actual volume of the bridge. Second, at fixed film thickness (i.e., fixed V_0), the actual size of the bridge could increase by sucking oil, which is spread on the surfaces of the foam film (the driving force for this process is described in section 7.4 below). Thus an initially stable bridge could eventually cross the boundary separating the stable from unstable bridges and rupture the film. Experimental observations supporting these theoretical predictions are described in refs 9 and 10.

Let us explain briefly how the foam films are ruptured by unstable bridges, such as those shown in Figures 39B and 40B. Any axial contraction of an unstable bridge, along its axis of symmetry (due to local transient decrease of the foam film thickness in the bridge region), would lead to increase of the equatorial radius of the bridge. As a result, the capillary pressure across the oil–water and oil–air interfaces is violated, and a process of

(133) Myshkis, A. D.; Babskii, V. G.; Kopachevskii, N. D.; Slobozhanin, L. A.; Tyuptsov, A. D. *Low Gravity Fluid Mechanics*; Springer-Verlag: New York, 1987.

(134) Eriksson, J. C.; Ljunggren, S. Comments on the alleged formation of bridging cavities/bubbles between planar hydrophobic surfaces. *Langmuir* **1995**, *11*, 2325.

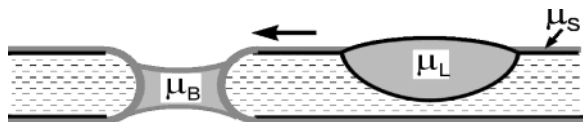


Figure 42. Schematic presentation of the surface transfer of oil from an oil lens, floating on the foam film surface, toward an oil bridge. The oil transfer is caused by the reduced pressure P_0 and, hence, the reduced chemical potential, μ_B , of the oil in the bridge, eq 26. Even if there are no lenses on the film surface, a transfer of oil from a spread oil layer toward the bridge is possible, if μ_B is lower than the oil chemical potential in the spread layer, μ_S (section 7.4).

spontaneous expansion of the equatorial radius of the bridge is induced. This expansion continues until a thin oil layer is formed in the center of the bridge (Figure 21), which eventually ruptures, perforating in this way the entire foam film. More detailed explanations about the driving pressures of this process can be found in ref 10.

7.4. Effect of Spread Oil on Bridge Stability. Let us assume that an oil bridge is initially formed from an oil drop or lens of volume, V_B , smaller than the critical one (i.e., below the curve separating stable from unstable bridges in Figure 41). As explained in section 7.3, such a bridge would be stable until the ratio V_B/V_0 reaches the critical value, as a result of the foam film thinning and/or of an actual increase of bridge volume. In the current section, we explain one possible mechanism for transformation of an initially stable into unstable oil bridge. This mechanism is related to the presence of spread oil on the foam film surfaces and has been supported by experimental observations, described in refs 9 and 10.

If oil is spread on the film surfaces, then an oil exchange between the bridge and the spread layer is possible (see Figure 42). In general, two opposite directions of oil transfer are possible: (1) spreading of oil from the bridge over the film surfaces or (2) accumulation of oil from the spread layer into the bridge. Which of these two possibilities would be realized depends on the difference between the chemical potentials of the oil in the bridge, μ_B , and in the spread layer, μ_S . If the oil phase does not contain solutes, μ_B depends only on temperature and pressure¹³⁵

$$\mu_B(T, P) = \mu_0(T) + v(P_0 - P_A) = \mu_0(T) + vP_{OA} \quad (26)$$

where $\mu_0(T)$ is the chemical potential of pure bulk oil phase, which is under ambient pressure, P_A , while v is the molar volume of the oil. Similarly, the chemical potential of the oil in the spread layer, μ_S , is a function of the disjoining pressure in the layer, Π_0 , which in turn depends on layer thickness, h_0 ^{42,107,136}

$$\mu_S(T, h_0) = \mu_0(T) - v\Pi_0(h_0) \quad (27)$$

$\Pi_0(h_0)$ accounts for the intermolecular interactions in the layer of the spread oil. At large thickness of the spread layer, $\Pi_0(h_0 \rightarrow \infty) = 0$, which corresponds to negligible interaction between the oil–air and oil–water surfaces of the spread layer (i.e., to the chemical potential in bulk oil layer). Further explanations on the role of $\Pi_0(h_0)$ in spreading can be found in refs 60, 97, and 136–138.

(135) Prigogine, I.; Defay, R. *Chemical Thermodynamics*; Longmans-Green: London, 1954.

(136) Hirasaki, G. J. Thermodynamics of thin films and three-phase contact regions. In *Interfacial Phenomena in Petroleum Recovery*; Morrow, N. R., Ed.; Marcel Dekker: New York, 1990; Chapter 2.

(137) Brochard-Wyart, F.; Di Meglio, J. M.; Quere, D., De Gennes, P. G. Spreading of nonvolatile liquids in a continuum picture. *Langmuir* **1991**, *7*, 335.

If the spread layer is in equilibrium with *macroscopic* oil lenses floating on the foam film surface (Figure 42), then the spread layer will be fully saturated with oil, $\Pi_0(h_{OE}) \approx 0$ and $\mu_S(T, h) \approx \mu_0(T)$. In this case, the oil transfer from and toward the bridge would depend primarily on the capillary pressure at the oil–air interface of the bridge, P_{OA} . If the capillary pressure P_{OA} is negative (which is the typical case¹⁰ for small bridges and strongly positive values of B), the oil chemical potential in the bridge, $\mu_B < \mu_0 \approx \mu_S$. In such a case, influx of oil is expected from the spread layer toward the bridge. This influx would increase the actual bridge size, and the bridge could eventually cross the boundary separating stable from unstable bridges (see Figure 41 and refs 9 and 10).

Note that, if the spread layer is undersaturated with oil (i.e., the layer is very thin and there are no lenses to supply oil on the film surface), the disjoining pressure $\Pi_0 > 0$ and the chemical potential in the spread layer $\mu_S < \mu_0(T)$. As a result, μ_B can be larger than μ_S , and the oil from the bridges could spread over the film surfaces. Such spreading was observed in ref 9 with silicone oil–silica antifoams, and finally the obtained bridges (composed of nondeformable silica agglomerate, impregnated with some residual oil) were stable. This interrelation between bridge stability and the presence of spread oil was found to be very important for the process of exhaustion of mixed oil–silica compounds.^{11,23}

7.5. Effect of Silica on Bridge Formation and Stability. The available experimental results suggest several possible effects of the solid particles on bridge formation and stability:

First, the solid particles can substantially facilitate the formation of oil bridges by (1) reducing the entry barrier of the oil globules,¹ see section 6.3, and (2) increasing the penetration depth of the oil lenses,³⁶ see Figure 25. The second effect is particularly important for small contact angles of water–oil–air, $\alpha_0 < 10^\circ$, which is the typical case with silicone oil and with many other oils as well. That is why, we briefly consider effect (2) below.

A necessary condition for transformation of a lens into an oil bridge is that the penetration depth, d_{PL} , should become equal to the thickness of the foam film, h , Figure 25. In the absence of solid particles, d_{PL} can be easily calculated by using the Neumann triangle, eq 22, and taking into account the fact that the lens surfaces are spherical. It is convenient to present the final result of this analysis in terms of the volume, V_L^* , of an oil lens, whose penetration depth is equal to the thickness of the foam film, Figure 25. The scaled volume, V_L^*/V_0 (where V_0 is defined by eq 25) depends only on the interfacial tensions σ_{OA} , σ_{OW} , and σ_{AW} :¹⁰

$$V_L^*/V_0 = 2 \frac{\sin^3 \theta_{OW}}{(1 - \cos \theta_{OW})^3} \left[\frac{\sin \theta_{OW}(2 + \cos \theta_{OW})}{(1 + \cos \theta_{OW})^2} + \frac{\sin \theta_{OA}(2 + \cos \theta_{OA})}{(1 + \cos \theta_{OA})^2} \right] \quad (28)$$

$$\cos \theta_{OW} = \frac{\sigma_{AW}^2 + \sigma_{OW}^2 - \sigma_{OA}^2}{2\sigma_{AW}\sigma_{OW}} \quad (29)$$

$$\cos \theta_{OA} = \frac{\sigma_{AW}^2 + \sigma_{OA}^2 - \sigma_{OW}^2}{2\sigma_{AW}\sigma_{OA}} \quad (30)$$

The physical meaning of V_L^* is the following: A lens with volume $V_L > V_L^*$ “touches” the opposite surface of the foam film, so that an oil bridge can be formed, if the entry

barrier is sufficiently low. In contrast, lens with $V_L < V_L^*$ could not make a bridge, even at a low entry barrier, because its penetration depth is too small. Numerical results for V_L^*/V_0 are presented in Figure 12 in ref 10. For our current discussion, it is sufficient to note that eq 28 predicts that excessively large lenses are needed to form a bridge, at small contact angles of the oil phase, $\alpha_0 = \theta_{OW} + \theta_{OA}$. Indeed, the term before the brackets in eq 28 shows that $V_L^* \rightarrow \infty$ as $\theta_{OW} \rightarrow 0$, which is equivalent to $\alpha_0 \rightarrow 0$.

These estimates show that the entry of an oil drop on one of the foam film surfaces would lead to formation of very flat lenses of small d_{PL} , in the absence of silica and at small angles α_0 . The contact of such a lens with the opposite film surface would require a certain period for further film thinning, until the film thickness, h , becomes comparable to d_{PL} . In contrast, the presence of solid particles inside the lens would maintain d_{PL} comparable to the size of particle agglomerates (typically $\approx 1 \mu\text{m}$), and the bridge formation would become possible soon after the globule entry on the first film surface. Microscopic observations showed⁹ that the penetration depth of the lenses of silicone oil, on the surface of AOT solutions, was determined primarily by the silica particles present in the antifoam; see Figure 1. That is why the foam films ruptured at a relatively large thickness, $h \sim 1$ to several micrometers, which would be impossible for these systems in the absence of silica, due to the very low values of $\alpha_0 \approx 0.5^\circ$. This is expected to be a typical case for silicone oil-based antifoams, because the contact angle α_0 is usually very small for silicone oil and the respective oil lenses are very flat.

On the other side, the presence of excessive silica in the oil bridges suppresses the antifoam activity of the compounds, because the bridges become nondeformable. Observations, made by FTT with silicone oil–silica compounds, showed that the bridges behave as nondeformable entities, if the silica concentration is above ca. 15 wt %, when a relatively rigid, 3D silica network is formed in the compound.^{19,23} Such nondeformable compound globules are unable to rupture the foam films by the bridging–stretching mechanism. The bridging–dewetting mechanism is also nonoperative in typical surfactant solutions due to inappropriate contact angles and, consequently, such gelled compounds have rather low activity and do not act as fast antifoams.^{5,19,23,139}

8. Role of Oil Spreading in Foam Destruction

In this section we summarize the main concepts, discussed in the literature, about the role of oil spreading for antifoam activity. Whenever possible, we briefly discuss these concepts from the viewpoint of our current understanding of the antifoam mechanisms.

Leviton and Leighton¹⁴⁰ were the first who suggested that there is a qualitative correlation between the spreading behavior of oils and their antifoam activity. Ross⁸¹ put this idea in quantitative terms by comparing the sign of the spreading coefficient, S (introduced by Harkins¹⁴¹) of various oils with their foam breaking

$$S = \sigma_{AW} - \sigma_{OW} - \sigma_{OA} \quad (31)$$

efficiency. On the basis of the data available at this time, Ross⁸¹ revealed a certain correlation, in the sense that most of the oils with antifoam activity had a positive spreading coefficient. Several exceptions, however, were noticed in the same study and, since that time, there is an ongoing debate in the literature about the role of oil spreading for the antifoam activity (e.g., refs 1–6, 9–14, 29–32, 36, 52, 65, 78, 79, 82–85, 97, 138, 142, and 143).

The discussions on the role of oil spreading are usually made in the context of the assumed mechanism of antifoam action. Ross⁸¹ speculated that the oil should first connect the two foam film surfaces, and the subsequent spreading of the oil, as a thick layer, would lead to replacement of a portion of the aqueous foam film (presumably stable) with an unstable oil bridge. This scenario of foam film rupture resembles, pictorially, the bridging–stretching mechanism, described in section 5.1. However, no oil spreading is required in the bridging–stretching mechanism, because the film rupture is explained by a different mechanism, namely, capillary instability.

In the mechanism proposed by Kulkarni et al.,^{142,143} spreading is deemed important for another reason. These authors assume that the oil acts as a carrier fluid (and as a coat), for the solid particles, which are considered as being the actual foam breaking entities. The oil spreading, after a mixed antifoam globule enters the foam film surface, leaves the surface of the solid particles uncovered, and a rapid surfactant adsorption on the particles' surface is assumed to occur. The authors^{142,143} suggest that this event leads to local depletion of surfactant and to foam film destabilization. This mechanism, however, contradicts some later observations by other authors^{3,9,11,29} and remains unproven.

In the “spreading-fluid entrainment” mechanism (section 5.3, Figure 23), the bridging of the two foam film surfaces by oil drops is not considered as necessary. The main idea is that once an oil drop enters either of the film surfaces, the oil would spread from the formed oil lens, if S is positive. The oil spreading is assumed to drag water in the foam film away from the oil lens, inducing in this way a rapid local thinning and subsequent rupture of the foam film. Discussion of some theoretical models, based on this idea, can be found in ref 1. An important conclusion from the theoretical analysis^{1,32,79} was that one should distinguish between the initial spreading coefficient, S_{IN} (defined by using σ_{AW} in the absence of spread oil) and the equilibrium spreading coefficient, S_{EQ} (σ_{AW} in the presence of spread oil). It was rigorously proven by thermodynamic analysis that S_{EQ} can be only negative or equal to zero, while S_{IN} might have an arbitrary sign—see refs 1, 31, 79, and 144 for a more detailed explanations. The spreading affinity of the oil on a bare solution surface is characterized by S_{IN} : if $S_{IN} < 0$, the oil does not spread on the solution surface and vice versa. S_{EQ} brings information about the structure of the spread layer at equilibrium. If S_{EQ} is zero, the oil spreads as a thick layer (the so-called “duplex film”). If S_{EQ} is negative, and E and S_{IN} are both positive, lenses coexist with thin oil layer on the solution surface at equilibrium. Note that many of the concepts, discussed in the literature^{1,32,52,79,60} in relation to the spreading-fluid entrainment mechanism (such as the role of spreading coefficient and of the spreading rate), can be applied after

(138) Kruglyakov, P. M.; Vilkova, N. G. The relation between stability of asymmetric films of the liquid/liquid/gas type, spreading coefficient and surface pressure. *Colloids Surf., A* **1999**, *156*, 475.

(139) Patterson, R. E. Influence of silica properties on performance of antifoams in pulp and paper applications 2. In-situ hydrophobing. *Colloids Surf., A* **1993**, *74*, 115.

(140) Leviton, A.; Leighton A. *J. Dairy Sci.* **1935**, *18*, 105.

(141) Harkins, W. D. *J. Chem. Phys.* **1941**, *9*, 552.

(142) Kulkarni, R. D.; Goddard, E. D.; Kanner, B. Mechanism of antifoaming: Role of filler particle. *Ind. Eng. Chem., Fundam.* **1977**, *16*, 472.

(143) Kulkarni, R. D.; Goddard, E. D.; Kanner, B. Mechanism of antifoam action. *J. Colloid Interface Sci.* **1977**, *59*, 468.

(144) Rowlinson, J. S.; Widom, B. *Molecular Theory of Capillarity*; Oxford University Press: Oxford, 1989; Chapter 8.

a certain adaptation to the spreading-wave generation mechanism, suggested in section 5.3 for slow antifoams. Just as an example, faster oil spreading^{52,60} is expected to sweep more efficiently the surfactant from the foam film surface (against the surfactant diffusion, which would act to restore the homogeneous surfactant adsorption throughout the film surface), facilitating in this way the foam film rupture.

It was found in many studies (e.g., refs 1, 3, 6, 9–11, 13, 14, 29, 65, 78, 97, and 138), that there is no correlation between the magnitude of the spreading coefficient for given oil and its antifoam activity. Furthermore, by selecting an appropriate oil–surfactant system, Garrett et al.²⁹ were able to show that nonspreading oils may have antifoam activity. Our observations also showed unambiguously that very active (fast) antifoams could operate without spreading-fluid entrainment.⁹ The conclusion from these studies^{9,29} was that the oil spreading is not a necessary condition for antifoam activity. Nevertheless, the observed correlation between the oil spreading ability and the antifoam efficiency for many systems (though not in all) suggest that the spreading could facilitate the foam destruction process.

Let us explain the beneficial effect of oil spreading from the viewpoint of the “bridging–stretching” and “bridging–dewetting” mechanisms for fast antifoams (Figures 21 and 22). First, we note that neither of these mechanisms requires oil spreading, as a necessary condition for foam destruction. On the other hand, microscopic observations of foam film rupture⁹ and drop entry experiments^{20,22} showed that oil spreading could significantly facilitate the foam destruction by antifoam compounds due to (1) reduced entry barriers, section 6.4, (2) supplying oil toward the oil bridges, section 7.4, and (3) facilitating the compound dispersion, section 1.2. Therefore, having a positive initial spreading coefficient, S_{IN} (which ensures a driving force for oil spreading during foaming), could be rather helpful for the antifoam action. From this viewpoint, it is not surprising that the rate of oil spreading could be an important factor for the antifoam efficiency.^{52,60} Indeed, if the creation of a new surface during foaming is faster than the rate of oil spreading, one can obtain foam films, depleted of spread oil, which could result in reduced antifoam activity for reasons 1 and 2 above. Note that less viscous silicone oils have higher spreading rate, as experimentally shown by Bergeron.^{52,60} However, compounds prepared with oils of low viscosity were found to lose rapidly their activity (i.e., their exhaustion is relatively fast), which means that an optimal oil viscosity is needed for having both active and durable antifoam.⁸

9. Examples of More Complex Antifoam Effects in Detergent Systems.

In this section we discuss several examples of antifoam action in more complex systems, which can be encountered in detergent applications. The studies, discussed below, show that the same basic principles and factors, as described in the previous sections (entry barrier, pin effect of the solid particles, etc.), play a decisive role. However, due to the complexity of the composition and of the phenomena, which occur simultaneously in real applications, it is often rather difficult to understand the interplay of the various factors without a detailed study. As illustrated below, the use of a wider set of complementary experimental methods may allow the researchers to reveal the detailed mechanism of antifoam action in complex systems and (in many cases) to suggest efficient ways for foam control.

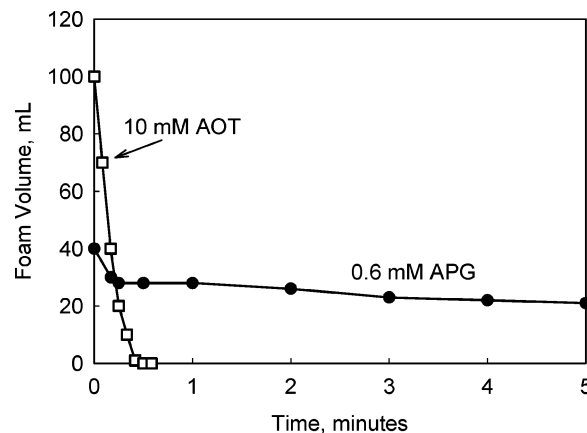


Figure 43. Foam volume vs time for two surfactant solutions, 10 mM AOT and 0.6 mM APG, containing 0.01 wt % PDMS–silica compound (Bartsch test). For comparison, in the absence of antifoam, the initial foam volume was 180 ± 10 mL for AOT and 100 ± 10 mL for APG, and the foam was stable during the time span of this experiment.

9.1. Role of Kinetics of Surfactant Adsorption for Antifoam Activity during Foaming. The foam tests have revealed systems, in which the antifoam strongly suppresses foam generation, while being rather inactive in still foams.^{15,16,88} An example for such system is shown in Figure 43, where the foaminess and foam stability of 10 mM AOT and 0.6 mM APG solutions are compared, in the presence of 0.01 wt % silicone oil–silica compound. The concentration of both surfactants corresponds to approximately $4 \times \text{cmc}$. As seen from Figure 43, the initial foam generated by shaking AOT solutions (Bartsch method) is several times larger, as compared to the foam generated from APG solutions at equivalent foaming conditions. However, after stopping the agitation, the foam completely disappears within seconds in the case of AOT, whereas the foam remains stable for hours, without complete destruction, in APG solutions. The reference samples (surfactant solutions without antifoam) show rather good foaminess and no foam destruction, in the time scale of Figure 43, for both AOT and APG.

One should note that the equilibrium values of E , S , and B coefficients are strongly positive in both systems (see Table 2 and ref 15). Hence these coefficients cannot be used to explain the observed differences in the antifoam activity. Optical observations showed¹⁵ that the APG-stabilized foams are destroyed by the same bridging–stretching mechanism of foam film rupture, which is responsible for the destruction of AOT-stabilized foams. Therefore, the difference between the antifoam performance, in these two solutions, is not related to different mechanisms of foam destruction.

The key to understand the observed differences in the antifoam performance was provided by the FTT, which showed that the entry barrier was much higher for APG solutions (above 125 Pa) in comparison with AOT (≈ 3 Pa). Note that the FTT measurements characterize the entry barriers at fully saturated surfactant adsorption layers, due to the relatively long duration of the FTT experiment (at least 15 min). These FTT results show that the antifoam globules are unable to enter the surfaces of APG-stabilized foam films, if the surfactant adsorption layers are saturated—the globule entry and the foam film rupture are possible only if the film surfaces are depleted of surfactant, i.e., during foaming. In contrast, due to the low entry barrier, globule entry and subsequent film rupture are possible in AOT solutions, even when the

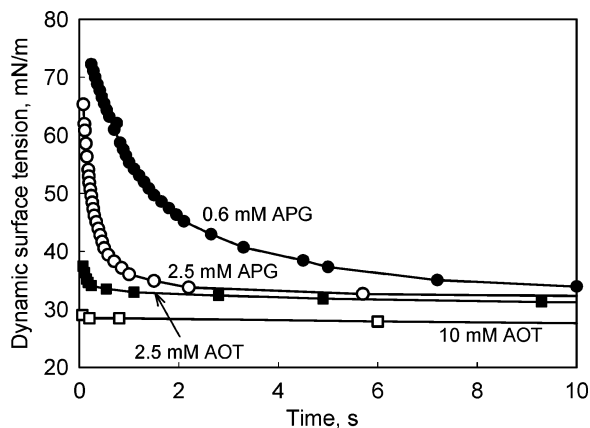


Figure 44. Dynamic surface tension of AOT and APG solutions, measured by MBPM: 10 mM AOT and 0.6 mM APG are the concentrations used in the foam tests (Figure 43). The results for equal surfactant concentrations, 2.5 mM, are also shown for comparison.

surfactant adsorption layers are fully saturated—that is why the antifoam is active even in still AOT-stabilized foams.

Furthermore, measurements of the dynamic surface tension of the studied AOT and APG solutions (by the MBPM) showed a large difference in the adsorption kinetics for these two surfactants.¹⁵ More than 10 s was needed for saturation of the adsorption layer in the working APG solution, whereas this process took less than 0.1 s in the case of AOT; see Figure 44. One can conclude from these results that the studied antifoam compound had significant activity in APG solutions, during foaming, mainly due to the slow adsorption of the APG molecules. If the kinetics of APG adsorption was so fast, as that of AOT, one could expect that the antifoam would be much less efficient in suppressing foam generation for APG solutions (at the same entry barrier, $P_{c}^{CR} > 125$ Pa).

In conclusion, an antifoam can be very active during foaming, when the adsorption layers on the foam film surfaces are not completed and the entry barrier is low. However, the same antifoam may lose a significant fraction of its activity (due to inability to enter foam film surfaces), once the agitation is stopped, saturated surfactant layers are built up, and the entry barrier becomes higher than 15 Pa. This might be a very typical case for many nonionic surfactants, because the kinetics of surfactant adsorption is known to be relatively slow in these systems, due to the low monomer concentration in the solutions and the relatively slow demicellization time.¹⁴⁵

9.2. Role of Electrostatic Repulsion in Solutions of Nonionic Surfactants. Experiments with APG-stabilized foam and asymmetric films demonstrated that the high entry barrier of silicone oil–silica compound, discussed in section 9.1, was related to excessively long-ranged electrostatic repulsion between the surfaces of the asymmetric oil–water–air film.¹⁵ This result is not very trivial, because APG is a nonionic surfactant, so that the electrical charge of the film surfaces cannot be explained by surfactant adsorption, as it is usually made for ionic surfactants. Numerous studies^{6,15,146,147} have shown that the air–water and oil–water interfaces can be negatively charged, even in the absence of any surfactant, due to the

specific adsorption of HO^- ions. The adsorption of nonionic surfactants was shown to reduce the electrical surface potential to a certain value, without necessarily eliminating it completely.^{146–153}

Measurements of the electrophoretic mobility of silicone oil drops, dispersed in 0.6 mM APG solution, showed that the magnitude of the ζ -potential of the oil–water interface is rather high in this solution, $\zeta \approx -60$ mV (unpublished results). Furthermore, due to the absence of external electrolyte, which could screen the electrostatic repulsion, the APG-stabilized foam and asymmetric films were rather thick, $h > 100$ nm.¹⁵ This large thickness of the foam films is evidence that the air–water interface is also charged. For comparison, the AOT-stabilized foam and asymmetric films had a thickness of only about 10–15 nm. Hence, the electrostatic repulsion in the case of ionic surfactants, such as AOT, is of considerably shorter range (as compared to APG) because the ionic surfactant, dissolved in the aqueous phase, acts as an electrolyte and screens the repulsion.¹⁵

In other words, the electrostatic repulsion is unusually long ranged in the case of nonionic surfactants, if the surfaces are charged and there is no external electrolyte in the solution, because the nonionic surfactants are unable to screen the electrostatic repulsion (as the ionic surfactants do). As a result, the foam and asymmetric films, stabilized by nonionic surfactants, like APG and some members of the Span and Brij series, are very thick, which could impede the antifoam activity of compounds. Indeed, microscopic observations of APG-stabilized asymmetric films showed¹⁵ that the protrusion depth of the solid silica particles present in the antifoam compound was insufficient to form solid bridges, such as those discussed in section 6.3 (i.e., d_{PR} was smaller than h_{AE}). Hence, the silica particles were unable to break the asymmetric films and to induce globule entry—this explains why the antifoam activity was very low in still, APG-stabilized foams (cf. Figure 43).

The important role of the electrostatic repulsion in APG solutions was further demonstrated by two foam tests.¹⁵ In one of these tests, 10 mM NaCl was added to APG solution. As a result, the antifoam activity of the oil–silica compound increased significantly, because the asymmetric films became thinner (~ 20 nm), and the entry barrier was strongly reduced. In the other test, less hydrophobic solid particles, which protruded deeper into the aqueous phase, were introduced in the compound, which led to great improvement of its antifoam activity, in agreement with the consideration from section 6.3.2.

Phenomena, like those discussed in sections 9.1 and 9.2, are expected to play a significant role in solutions of other nonionic surfactants and some polymers, because

(147) Marinova, K. G.; Alargova, R. G.; Denkov, N. D.; Veleev, O. D.; Petsev, D. N.; Ivanov, I. B.; Borwankar, R. P. Charging of oil/water interfaces due to spontaneous adsorption of hydroxyl ions. *Langmuir* **1996**, *12*, 2045.

(148) Walthermo, A.; Claesson, P. M.; Simonsson, S.; Manev, E.; Johansson, I.; Bergeron, V. Foam and thin-liquid-film studies of alkyl glucoside systems. *Langmuir* **1996**, *12*, 5271.

(149) Binks, B. P.; Cho, W.-G.; Fletcher, P. D. I. Disjoining pressure for oil–water–oil emulsion films. *Langmuir* **1997**, *13*, 7180.

(150) Pugh, R. G.; Yoon, R.-H. Hydrophobicity and rupture of thin aqueous films. *J. Colloid Interface Sci.* **1994**, *163*, 169.

(151) Manev, E. D.; Pugh, R. J. Drainage and equilibrium thickness of aqueous films containing nonionic frothers and xanthate flotation collector. *J. Colloid Interface Sci.* **1992**, *151*, 505.

(152) Manev, E. D.; Pugh, R. J. Diffuse layer electrostatic potential and stability of thin aqueous films containing a nonionic surfactant. *Langmuir* **1992**, *8*, 2253.

(153) Walthermo, A.; Manev, E.; Pugh, R.; Claesson, P. Foam films and surface force studies of aqueous solutions of octyl- β -glucoside. *J. Dispersion Sci. Technol.* **1994**, *15*, 273.

(145) Patist, A.; Oh, S. G.; Leung, R.; Shah, D. O. Importance of micellar kinetics in relation to technological processes. *J. Colloid Interface Sci.* **2002**, *245*, 1.

(146) Exerowa, D.; Zacharieva, M. Investigation of the isoelectric point at water/air surface. In *Research in Surface Forces*; Consultants Bureau: New York, 1975; Vol. 4.

rather often thick films (due to nonscreened electrostatic or steric repulsion between the film surfaces) and slow adsorption are observed with such systems.

9.3. Formation of Solid Particles as a Result of Chemical Reaction in the Foaming Solution. The composition of the foaming solutions can be very complex in many applications. That is why it might be rather difficult in some systems to reveal which are the main components leading to the observed antifoam effect. An illustrative example, on how one can approach such a complex system, has been presented in a recent study by Zhang et al.⁸⁸ These authors⁸⁸ performed a large systematic set of experiments (including foam tests, foam and asymmetric film observations, determination of E , S , and B coefficients) to analyze the antifoam effect of hexadecane and triolein in solutions of anionic and nonionic surfactants. A small amount of oleic acid was added to the oil phase, and Ca^{2+} ions were introduced in the aqueous phase, to promote formation of solid particles (precipitate) of Ca oleate on the surface of the oil droplets. In this way, some of the processes, which appear during detergent application in hard water, were mimicked. By careful choice of the experimental methods and conditions, the authors⁸⁸ were able to show unambiguously that the entry barrier played a significant role in the case of the anionic surfactant and that the solid particles (formed by precipitation in situ) facilitated oil drop entry. A pronounced synergistic antifoam effect of the oil and the solid particles was proven. Nontrivial temporal changes in the antifoam activity of the oil-particle globules were observed and explained by considering the kinetics of surfactant adsorption and the time, needed for Ca oleate precipitation.

9.4. Antifoam Effect of Nonionic Surfactants above Their Cloud Points. It had been known for many years^{154,155} that the foaminess of nonionic surfactant solutions sharply decreases above their cloud point. This phenomenon has important practical implications, because surfactant mixtures with good detergent properties and low foaminess can be designed by adjusting the solution cloud point to the desired temperature.^{154,156–158} This phenomenon was observed with various surfactant and polymer solutions, which indicates that it is rather general.^{155–159}

A possible explanation of this effect could be that the coacervate phase, formed above the cloud point, collects most of the surfactant and, in this way, reduces the surfactant available for adsorption and foam film stabilization. However, as shown by Koretskaya¹⁵⁴ and confirmed later in several other studies,^{156–159} the solution foaminess is almost completely recovered, if one removes the coacervate droplets from the solution (at equivalent all other conditions). This is clear evidence that the coacervate drops act as oily antifoam and destroy the foam in a manner similar to the drops of regular oils. Therefore, many of the concepts, discussed above for the antifoam action of oil drops, are applicable to these systems as well.

(154) Koretskaya, T. A. Mechanism of prevention of foam formation in solutions of nonionic surfactants, *Kolloidn. Zh.* **1977**, *39*, 571.

(155) Ross, S.; Nishioka, G. The relation of foam behavior to phase separation in polymer solutions. *Colloid Polym. Sci.* **1977**, *255*, 560.

(156) Bonfillon-Colin, A.; Langevin, D. Why do ethoxylated nonionic surfactants not foam at high temperature? *Langmuir* **1997**, *13*, 599.

(157) Colin, A.; Giermanska-Kahn, J.; Langevin, D.; Desbat, B. Foaming properties of modified ethoxylated nonionic surfactants. *Langmuir* **1997**, *13*, 2953.

(158) Nemeth, Z.; Racz, G.; Koczó, K. Foam control by silicone polyethers – mechanisms of “cloud point antifoaming”. *J. Colloid Interface Sci.* **1998**, *207*, 386.

(159) Chaisalee, R.; Soontravanich, S.; Yanumet, N.; Scamehorn, J. F. Mechanism of antifoam behavior of solutions of nonionic surfactants above the cloud point. *J. Surfactants Deterg.* **2003**, *6*, 345.

For example, Bonfillon-Colin et al.¹⁵⁶ and Chaisalee et al.¹⁵⁹ measured the E , S , and B coefficients of the coacervate phase and concluded that the foam destabilization occurs though a bridging mechanism (without being clear whether this is a bridging–stretching or bridging–dewetting mechanism). A similar conclusion was drawn by Nemeth et al.¹⁵⁸ on the basis of optical observations of foam films. The bridges are formed by micrometer sized drops and/or lenses of the coacervate phase, like those in the case of regular oils (section 1.2).

10. Conclusions

The main goal of this review is to describe the most important results obtained during the recent years, in relation to the modes of foam destruction by oil-based antifoams (with some emphasis on the studies performed in our laboratory). The following conclusions are formulated without any attempt to differentiate the results, obtained in the various research groups—such a differentiation was made, as carefully as possible, in the main text:

Two types of antifoam can be clearly distinguished, which differ in the modes of their action. The so-called “fast antifoams” rupture the foam films in seconds, at the early stages of film thinning. As a result, the fast antifoams destroy completely the foam in less than a minute (typically, between 3 and 30 s, depending on the specific foam test and antifoam concentration). In contrast, the time scale of foam destruction by slow antifoams is at least several minutes and often much longer (tens of minutes or even hours), with a long-living residual foam remaining.

The fast antifoams rupture the foam films by a “bridging–stretching” or (possibly, without being proven yet) by a “bridging–dewetting” mechanism, which involves the formation of an oil bridge between the two surfaces of the foam film. The stability/instability of the oil bridges is explained by using the theory of capillarity.

The oily globules of the slow antifoams are unable to enter the surfaces of the foam films and are first expelled into the Plateau borders (PBs). Only after being compressed by the narrowing walls of the PBs, due to water drainage from the foam, the globules of the slow antifoams enter the solution surface and destroy the adjacent foam films. The detailed mechanism of foam destruction, after the entry of the slow antifoam globules, is still unclear.

There is no direct relation between the magnitudes of the entry, E , spreading, S , and bridging, B , coefficients and the antifoam efficiency, because the entry barrier plays a decisive role in most systems of practical interest (see, for examples, Tables 1 and 2). The only requirement for having active antifoam, with respect to the bridging-mediated mechanisms, is that the value of the bridging coefficient, B , should be positive.

The entry barrier controlling the emergence of pre-emulsified oil drops on the solution surface and the bridge formation is of critical importance for the mode of foam destruction and for the antifoam efficiency. This barrier can be quantified precisely by the film trapping technique (FTT). Compounds with entry barrier below ca. 15 Pa act as fast antifoams, whereas higher barriers correspond to slow or inactive antifoams (although the E , S , and B coefficients could be strongly positive in the latter case).

The fast antifoams typically contain solid particles, whose main role is to decrease the entry barrier below the threshold value of 15 Pa. In many systems, such a low entry barrier is achieved only when having both solid particles in the antifoam globule and spread oil on the foam film surface. A mechanistic explanation of this

synergistic action of the solid particles and spread oil is described. Note that many compounds (oil–solid mixtures) behave as slow antifoams, because their entry barrier is above 15 Pa, despite the presence of solid particles in the compound globules. Another important role of the solid particles (especially in silicone oil-based antifoams) is to increase the penetration depth of the oil lenses, facilitating in this way the formation of oil bridges soon after the foam film is formed.

In the presence of slow antifoam, theoretical analysis allows one (1) to relate the capillary pressure in the PBs of the real foams with the entry barrier and the size of the antifoam globules and (2) to explain the observed stages of foam evolution. A good agreement between the theoretical model and the experimental results is established.

When oil drops are present in the surfactant solution, the foam boosting effect of many cosurfactants is due to efficient suppression of the antifoam effect of these drops. In most cases, this suppression is related to increased entry barrier of the oil drops, as a result of formation of mixed surfactant adsorption layers, which stabilize very efficiently the asymmetric oil–water–air films.

The effect of other factors, such as the size of antifoam globules, oil spreading characteristics, hydrophobicity of the solid particles in compounds, and rate of surfactant adsorption, are explained from the viewpoint of the discussed mechanisms of antifoaming.

In conclusion, significant progress has been achieved during the past decade in revealing the modes of foam destruction by oil-based antifoams. The stage of speculative ideas has been gradually displaced by a new approach, which involves a critical evaluation of various possible hypotheses, on the basis of a consistent set of experiments and careful analysis of the obtained data. One can mark the dawn of this approach by the pioneering studies of Ross and Nishioka,⁵ Dippenaar,²⁸ Kruglyakov and Koretskaya,^{64,65} Aronson,⁴⁸ and especially Garrett,¹ but it became widespread only during the past decade, mainly due to the works of Garrett et al.,^{29,80,88,89} Koczko et al.,^{53,78} Aveyard et al.,^{30–34,79} Bergeron et al.,^{52,97,99} and our group.^{8–23} This significant change in the approach of the antifoam studies has been greatly facilitated by the application of various microscope methods for observation of foams and foam films, and by the implementation of the FTT for measuring the entry barrier of antifoam globules. Still, there are very important issues, many of them mentioned throughout the text, which remain unresolved and keep the door open for further studies and discoveries.

Acknowledgment. I would like to thank my colleagues from the Laboratory of Chemical Physics & Engineering (LCPE), who contributed in many different ways to the studies, summarized in this review. Special thanks are due to Dr. K. Marinova, Dr. A. Hadjiiski, Dr. S. Tcholakova, and Dr. E. Basheva, who were deeply involved and obtained many valuable results in these studies. In addition, Dr. Marinova and Dr. Tcholakova were very kind to critically read the manuscript and to help me in its technical preparation. The critical reading of the manuscript by Dr. K. P. Ananth and Dr. M. Aronson (Unilever Research & Development, USA) is also gratefully acknowledged. I would like to express my gratitude to Dr. P. Branlard, Dr. M. Deruelle, and Dr. Y. Giraud (Rhodia Silicones Europe), and to Professor I. B. Ivanov (LCPE) for their support and for their useful comments and suggestions. In many occasions, our studies were inspired and strongly influenced by the careful, thoughtful, and convincing publications by Dr. P. Garrett (UMIST,

Manchester, U.K.). Last but not least, I would like to thank Miss M. Paraskova for the beautiful figures.

Glossary

3D	three-dimensional
AF	antifoam
AOT	sodium dioctylsulfosuccinate (anionic surfactant)
APG	alkylpolyglucoside (nonionic surfactant)
AST	automated shake test, section 2.1.3
BO	2-butyloctanol (oil)
CAPB	cocoamidopropyl betaine
cmc	critical micelle concentration
FTT	film trapping technique, section 2.3.2
IHNP	isohexyl-neopentanoate (oil)
MBPM	maximum bubble pressure method for measuring dynamic surface tension
PB	Plateau border
PDMS	poly(dimethylsiloxane) (silicone oil)
PTFE	polytetrafluorethylene
PVA	poly(vinyl alcohol) (nonionic polymer with high surface activity)
rpm	rounds per minute
SDDBS	sodium dodecyl benzenesulfonate (anionic surfactant)
SDP3S	sodium dodecyl polyoxyethylene-3 sulfate (anionic surfactant)
SDS	sodium dodecyl sulfate (anionic surfactant)

Variables

d_B	diameter of oil bridge
d_N	number-mean diameter of oil globules
d_{PR}	protrusion depth of solid particle into the aqueous phase, Figure 28
d_{PL}	penetration depth of oil lens into the aqueous phase, Figure 25
d_{CL}	penetration depth of oil collar into the aqueous phase, Figure 30
f_{AS}	interaction energy per unit area in the asymmetric oil–water–air film, eq 10
g	acceleration due to gravity
h	thickness of foam film
h_{AE}	equilibrium thickness of asymmetric oil–water–air film
h_{AS}	thickness of asymmetric oil–water–air film, Figure 28
h_{ASP}	thickness of asymmetric oil–water–air film, equal to the equilibrium distance between the two contact lines of a spherical particle with the asymmetric film surfaces, eq 16
h_E	equilibrium thickness of foam film
h_O	thickness of spread oil layer
h_{OE}	equilibrium thickness of spread oil layer
n	refractive index of surfactant solution
r	radial coordinate in cylindrical coordinate system, Figure 35
r_{OB}	equatorial radius of oil bridge, Figure 36
r_C	radius of the three-phase contact line oil–water–air of an oil bridge, Figure 36
t	time
t^*	foaming time before a fast antifoam gets exhausted, Figure 2D
$t_{1/2}$	half-time of a foam, Figure 12
t_D	defoaming time for fast antifoams, section 2.1.3
t_{ON}	onset of foam destruction for slow antifoams, Figure 12
v_D	rate of foam destruction (stage III) in the Ross–Miles test, section 4.1 and Figure 12
z	vertical coordinate in cylindrical coordinate system, Figure 35
B	bridging coefficient, eq 24
B_{EQ}	equilibrium bridging coefficient, eq 24 (with spread oil layer on solution surface)
B_{IN}	initial bridging coefficient, eq 24 (without spread oil layer)

C_N	number concentration of antifoam globules in the solution	R_{PB}	radius of curvature of the wall of Plateau channel, Figure 18
C_S	surfactant concentration in the foaming solution	R_P	radius of solid particle, Figure 26
E	entry coefficient, eq 9	S	spreading coefficient, eq 31
E_{EQ}	equilibrium entry coefficient, eq 9 (with spread oil layer on solution surface)	S_{EQ}	equilibrium spreading coefficient, section 8
E_S	generalized entry coefficient, eq 11	S_{IN}	initial spreading coefficient, section 8
E_{IN}	initial entry coefficient, eq 9 (without spread oil layer)	V_0	volume of oil drop with diameter equal to the foam film thickness, h ; eq 25
F_{PS}	force between solid particle and foam film surface, eq 13	V_B	volume of oil bridge
H	running (dummy) variable for film thickness in integrals, eq 13	V_F	foam volume
H_F	foam height, Figure 18	V_L	volume of oil lens, Figure 25
H_P	theoretical estimate of the height of residual foam by eq 8a (entry barrier is governing factor)	V_L^*	volume of oil lens with $d_{PL} = h$, Figure 25
H_R	theoretical estimate of the height of residual foam by eq 8b (drop size is governing factor)	V_{RES}	volume of residual foam in the presence of slow antifoam; section 4.3, Figure 12
H_{RES}	residual foam in the experiments with slow antifoams, section 4.3, Figure 18	Z	depth of the liquid pool in FTT experiment, Figure 8
P_A	air pressure (in general); air pressure inside the capillary of the FTT equipment, Figure 8; $\Delta P_A = (P_A - P_A^0)$	<i>Greek Letters</i>	
P_A^0	ambient atmospheric pressure (outside the capillary of the FTT equipment), Figure 8	α_O	contact angle water–oil–air
P_C	capillary pressure (in general); capillary pressure at air–water interface in the FTT experiment, Figure 8	α_W	contact angle oil–water–air, Figure 38
P_C^{CR}	critical capillary pressure leading to drop entry in FTT experiment (entry barrier), sections 2.3.2 and 6.2, Figure 8	α_{SA}	contact angle solid particle–water–air, Figures 2 and 28
P_C^{PB}	capillary pressure of the walls of Plateau channels at the top of foam column, section 4.3	α_{SO}	contact angle solid particle–water–oil, Figure 28
P_F	pressure inside the asymmetric oil–water–air film, Figure 33	δ	distance between solid particle and foam film surface, Figure 26
P_O	pressure inside oil phase	φ	running slope angle of interface, Figure 35
P_{AW}	capillary pressure at air–water interface, $P_{AW} = (P_A - P_W)$	λ	wavelength of illuminating light
P_{OA}	capillary pressure at oil–air interface, $P_{OA} = (P_O - P_A)$	μ_0	standard chemical potential of oil
P_{OW}	capillary pressure at oil–water interface, $P_{OW} = (P_O - P_W)$	μ_B	chemical potential of oil in a bridge, Figure 42
P_{TR}	threshold value of P_C^{CR} , which separates fast from slow antifoams, section 3.2 and Figure 11, $P_{TR} \approx 15$ Pa	μ_L	chemical potential of oil in a lens, Figure 42
P_W	pressure inside water phase, Figures 8 and 33	μ_S	chemical potential of oil in a spread layer
R_1, R_2	principal radii of curvature of arbitrary interface	ν	molar volume of oil
R_{32}	volume–surface mean drop radius (Sauter radius)	θ_F	half of the contact angle film–meniscus, Figure 18
R_{33}	volume averaged, geometric mean drop radius	θ_{OW}	Equation 29 and Figure 38; $\theta_{OW} = (\pi - \alpha_W)$
R_{AS}	radius of asymmetric oil–water–air film, Figure 33	θ_{OA}	defined by eq 30
R_B	bubble radius	ρ	mass density of surfactant solution
R_C^{FILM}	radius of curvature of asymmetric oil–water–air film, Figure 33	σ_{AW}	air–water interfacial tension
R_D	radius of antifoam drop (globule)	σ_{OW}	oil–water interfacial tension
R_D^{MIN}	minimal radius of oil drop, which can be compressed by the walls of Plateau channel (radius of inscribed sphere in Plateau channel), Figure 18	σ_{OA}	oil–air interfacial tension
R_E	equatorial radius of trapped drop in FTT experiment, Figure 33	σ_{SA}	solid–air interfacial tension
		σ_{SW}	solid–water interfacial tension
		σ_{SO}	solid–oil interfacial tension
		Φ_A	volume fraction of antifoam dispersed in the surfactant solution
		Π	disjoining pressure of foam film; disjoining pressure in general
		Π_{AS}	disjoining pressure of asymmetric oil–water–air film
		Π_{AS}^{CR}	critical disjoining pressure of rupture of asymmetric oil–water–air film
		Π_{AS}^{MAX}	height of the calculated barrier in the disjoining pressure isotherm of asymmetric oil–water–air film, Figure 34
		Π_O	disjoining pressure in spread oil layer
		Π_{PS}	disjoining pressure of a planar solid–water–air film
		Π^{CR}	critical disjoining pressure of foam film rupture, section 6.2

LA0496760